HALOCARBON REACTIONS OVER THE CHROMIUM (111) OXIDE (10$\underline{1}$2) SURFACE

by

Steven C. York

Dissertation submitted to the faculty of the
Virginia Polytechnic Institute and State University
In partial fulfillment of the requirements for the degree of
DOCTOR OF PHILOSOPHY

in

Chemical Engineering

David F. Cox

S. T. Oyama

Eva Marand

John G. Dillard

Brian E. Hanson

August 13, 1999
Blacksburg, VA

Key Words: chromium (III) oxide, halocarbon, haloalkane, haloalkene,
Dehalogenation, oxygen adsorption

INVESTIGATION OF HALOCARBON REACTIONS OVER Cr_2O_3 (10$\underline{1}$2)

by

Steven C. York

(Abstract)

A nearly stoichiometric, (1×1) Cr_2O_3 (10$\underline{1}$2) surface was prepared from a single crystal of α-Cr_2O_3. The five-coordinate cations exposed at the stoichiometric surface dissociatively adsorb molecular oxygen to form a (1×1), terminating chromyl (Cr=O) layer that is stable to >1100 K. TDS and AES were used to investigate the reactivity of the halo-alkanes $CFCl_2CH_2Cl$, CF_2ClCH_2Cl, CF_3CH_2Cl, and CF_3CH_2F, in addition to the halo-alkenes $CFCl{=}CH_2$ and $CF_2{=}CH_2$. The halo-alkanes $CFCl_2CH_2Cl$, CF_2ClCH_2Cl, and CF_3CH_2Cl undergo 1,2-dihalo elimination similar to the Zn-catalyzed dehalogenation of vicinal dihalides to form alkenes. Some acetylene is also formed. The halo-alkenes $CFCl{=}CH_2$ and $CF_2{=}CH_2$ decompose to yield acetylene. Halogen removed from the molecules remains bound to the surface following TDS experiments and eventually terminates the surface chemistry due to site blocking of the cations. Reactivity is directly related to the chlorine content of the molecules investigated. Only $CFCl_2CH_2Cl$ was reactive on a chromyl-terminated surface.

ACKNOWLEDGEMENTS

This project was made possible through a grant of love, money, and patience from the Francene York Foundation, thanks babe.

Each of the following played important roles in making this project a success, and each is gratefully acknowledged.

Mark Abee, Dr. Wei Li, Dr. David F. Cox, Dr. S. T. Oyama, Dr. John G. Dillard, Dr. Eva Marand,
Dr. Brian E. Hanson, Sam & Jessie York, Frank & Judy Kristoff, Dianne Canaday,
Dr. Joseph S. Merola, Dr. Anne-Claire Christiaen, Dr. William L. Conger,
Betsy Daughtry, Watt Jones, Annie & Sam, and Horace & Boo, Jeff & Greg,
John Andrews (for always being willing to argue the other side),
Slade & Lynn, Tunga, Dr. Preston Durrill, Dr. Robert Boggess,
Dr. C. W. Hickam, The Morning Glory Café, Tom-bone,
Caitlin Kirkwood, P.G.T. Beauregard, Scarlet, T.J Jackson,
Charles & Audrey Laney, Bob & June Milligan,
Robinson, Dodger, other family and
friends that have supported me
during this arduous
journey, and if
you feel forgotten
then this is
for you.
THANKS!

DEDICATED TO BOO.

TABLE OF CONTENTS

3. REACTION OF 1-CHLORO-1-FLOUROETHENE OVER THE Cr_2O_3 (10$\underline{1}$2) SURFACE

4. REACTIONS OF 1, 1, 2-TRICHLORO-1-FLUOROETHANE OVER THE Cr_2O_3 (10$\underline{1}$2) SURFACE

5. THE REACTIONS OF CF_2ClCH_2Cl AND CF_2CH_2 OVER THE Cr_2O_3 (10$\underline{1}$2) SURFACE

LIST OF FIGURES

LIST OF TABLES

Chapter 1
Introduction

1.1 Background

The catalytic properties of Cr_2O_3 have long been recognized [1,2]. The polymerization of ethylene over various oxides of chromium has motivated much of the research into the properties of Cr_2O_3 over the last 50 years [3]. More recently, interest in Cr_2O_3 has been generated due to its use as a catalyst in the manufacture of the alternative refrigerant HFC-134a [4] (see Table 1 for an explanation of halocarbon notation). The manufacture of HFC-134a (CF_3CH_2F) is more complicated than its predecessor, CFC-12, and many manufacturing schemes may be envisioned, as shown in Figure 1 [4, 5]. One of the more direct routes to HFC-134a begins with trichloroethylene (TCE) as a feedstock and uses Cr_2O_3 as a catalyst for the gas-phase reaction. HF addition across the carbon-carbon double bond to make HCFC-131a (CCl_2FCH_2Cl) is followed by a series of fluorine for chlorine exchange reactions to yield the desired product. The difficulty in manufacture is created by the many side reactions, which are also promoted by Cr_2O_3. The lack of catalyst selectivity necessitates the use of recycle reactors and expensive separation processes to obtain acceptable yields of HFC-134a [4].

Table 1.1 An explanation of halocarbon notation is given below using HCFC-XYZ as a generic example to illustrate the meaning of each symbol.

X	The number of carbon atoms minus one, omitted if zero.
Y	The number of hydrogen atoms plus one.
Z	The number of fluorine atoms.
HCFC	Designates the compound as a Hydro-Chloro-Fluoro-Carbon.
HFC	Designates the compound as a Hydro-Fluoro-Carbon.
a, b, c,	In cases where isomers exist, letters are assigned in accordance with increasing asymmetry. The most symmetric isomer is not assigned a letter.

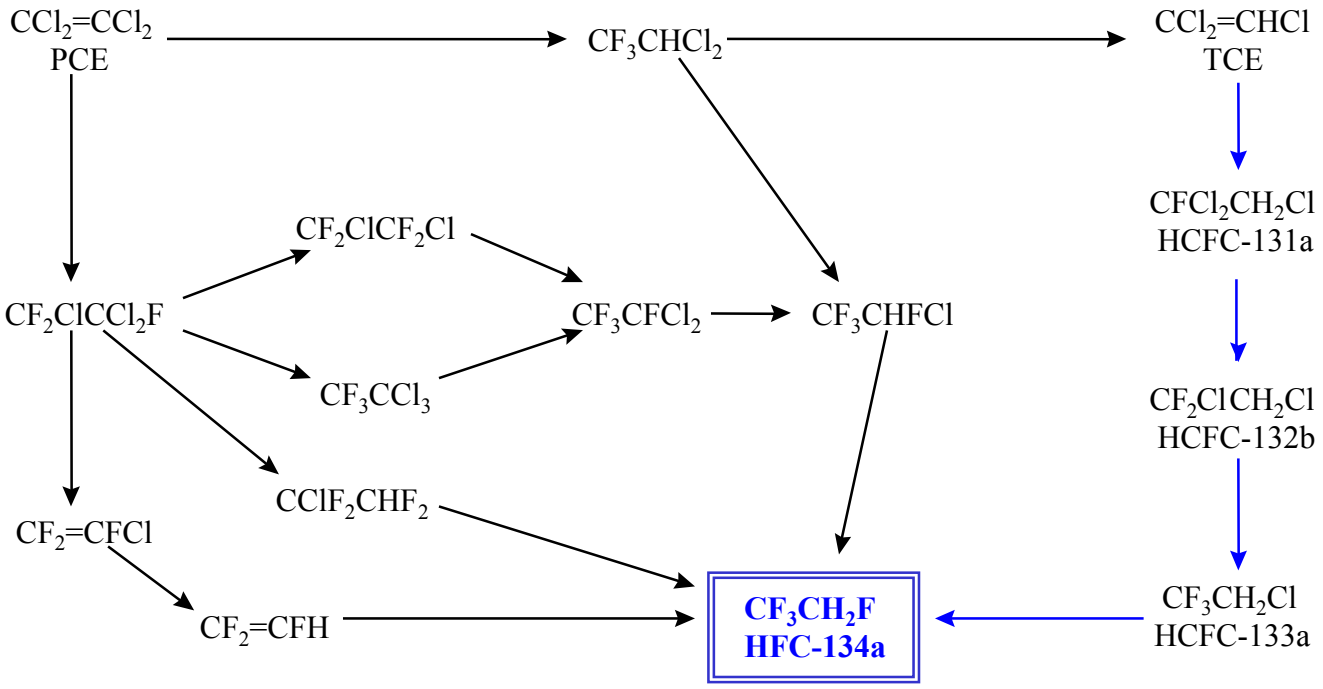

Figure 1. Manufacturing routes to HFC-134a from the unsaturated chloroethenes PCE and TCE [adapted from reference 4].

The study of reactions over single crystal surfaces to model heterogeneous catalysis is a major focus of surface science [6, 7, 8, 9, 10]. By studying reactions over a well-characterized surface, information concerning reaction site requirements, reaction pathways, and the structure sensitivity of reactions may be obtained. In this work, the Cr_2O_3 (10$\underline{1}$2) surface was investigated. The objective was twofold: (1) to characterize the Cr_2O_3 (10$\underline{1}$2) surface in terms of structure, stoichiometry, and reactivity to various probe molecules, and (2) to investigate the reaction pathway from HCFC-131a to HFC-134a over this surface.

Although Cr_2O_3 microcrystalline powders have been extensively studied [11, 12] few studies of single crystals have been reported [13, 66]. In chapter 2, studies of surface periodicity, stoichiometry, and the surface interaction with oxygen are reported for the Cr_2O_3 (10$\underline{1}$2) surface.

The reaction of HCFC-131a to HFC-134a in the presence of HF involves a sequence of halogen exchange reactions and is thought to proceed as follows [4]:

$CFCl_2CH_2Cl$	$\rightarrow$	$CClF_2CH_2Cl$	$\rightarrow$	CF_3CH_2Cl	$\rightarrow$	CF_3CH_2F
HCFC-131a		HCFC-132b		HCFC-133a		HFC-134a

The final reaction step is equilibrium limited and, therefore, the most difficult to carry out [4, 101]. The interaction of each of the above compounds with the Cr_2O_3 (10$\underline{1}$2) surface was investigated. The principal focus of these studies was to identify reaction products, determine reaction kinetics, evaluate the effects of surface treatment upon reactivity, and to identify any change in the surface caused by surface reactions. Studies of the halocarbons above, and their products on the Cr_2O_3 (10$\underline{1}$2) surface are reported in chapters 3, 4, 5 and 6. A summary and recommendations for future work are presented in chapter 7. Literature relevant to the topic is reviewed at the beginning of each chapter.

1.2 The Cr_2O_3 (10$\underline{1}$2) Surface

α-Cr_2O_3 is an electrically insulating material (band gap=3.4 eV) having the corundum structure [14, 15]. The bulk chromium coordination geometry is a distorted octahedron, while oxygen anions are coordinated in a distorted tetrahedral arrangement of cations. In the corundum structure, one third of the possible cation sites are vacant and these vacancies are located along the (10$\underline{1}$2), and other crystallographically equivalent planes [13]. A ball model representation of the ideal, stoichiometric surface is shown in Figure 2. The (10$\underline{1}$2) surface is somewhat corrugated or wavy due to the alternating tilt of incomplete octahedra relative to the macroscopic (10$\underline{1}$2) plane.

The ideal (10$\underline{1}$2) surface is non-polar and has the lowest energy of any perfect low-index surface of Cr_2O_3 [16]. The topmost atomic layer of the ideal surface is composed entirely of oxygen anions. One full stoichiometric repeating unit normal to the surface contains five atomic layers arranged as {O,Cr,O,Cr,O}. The surface has a rectangular (almost square) periodicity with a ratio of sides of a/b=0.94. At the (10$\underline{1}$2) surface, all O^{2-} (oxide) anions in the top atomic layer are three coordinate and the Cr^{3+} cations in the second atomic layer are five coordinate. Both ions have one degree of coordinate unsaturation relative to their bulk counterparts [17]. All ions below the top two atomic layers are fully coordinated.

1.3 Experimental

The Cr_2O_3 sample used throughout this work was oriented by Laue back reflection and was mechanically polished to within ±1° of the (10$\underline{1}$2) plane. The sample has an exposed surface area of approximately 77 mm^2 (≈11 mm × 7 mm) and an average thickness of 1 mm. The sample was mounted on a tantalum holder, which also acted as an indirect heating and cooling source. A type K thermocouple was attached to the rear of the sample crystal through a hole in the sample holder using AREMCO #569 ceramic cement.

All Auger electron spectroscopy (AES), low-energy electron diffraction (LEED), and thermal desorption spectroscopy (TDS) experiments were conducted in an ion-pumped, stainless steel ultrahigh vacuum (UHV) system having a nominal background pressure of 1×10^{-10} Torr. AES data were collected using a Perkin-Elmer model 15-155 single-pass cylindrical mirror analyzer (CMA). An incident electron beam of 5 keV was used for all Auger experiments. Spectra were collected in N(E) mode and differentiated numerically. Electron stimulated reduction of the surface did not occur during AES experiments. LEED observations were performed using V. G. 3-grid reverse view optics. A broad beam ion gun was used for sample cleaning (sputtering). X-ray photoelectron spectroscopy (XPS) measurements were performed in a separate vacuum system equipped with a Leybold EA-11 hemispherical analyzer a dual-anode Mg/Al X-ray source. All XPS ratios have been corrected with Leybold atomic sensitivity factors, and XPS binding energies are referenced to Ag $3d_{5/2}$ binding energy of 368.3 eV [42, 43].

Desorbing species were monitored during TDS experiments using an Inficon Quadrex 200 quadrupole mass spectrometer. A quartz skimmer was used to minimize the desorption signal detected from the sample mounting hardware. A linear heating rate of 2 K/sec was used for all thermal desorption experiments in order to avoid thermally fracturing the ceramic sample by rapid heating. Gases were introduced into the chamber by backfilling through a variable leak valve.

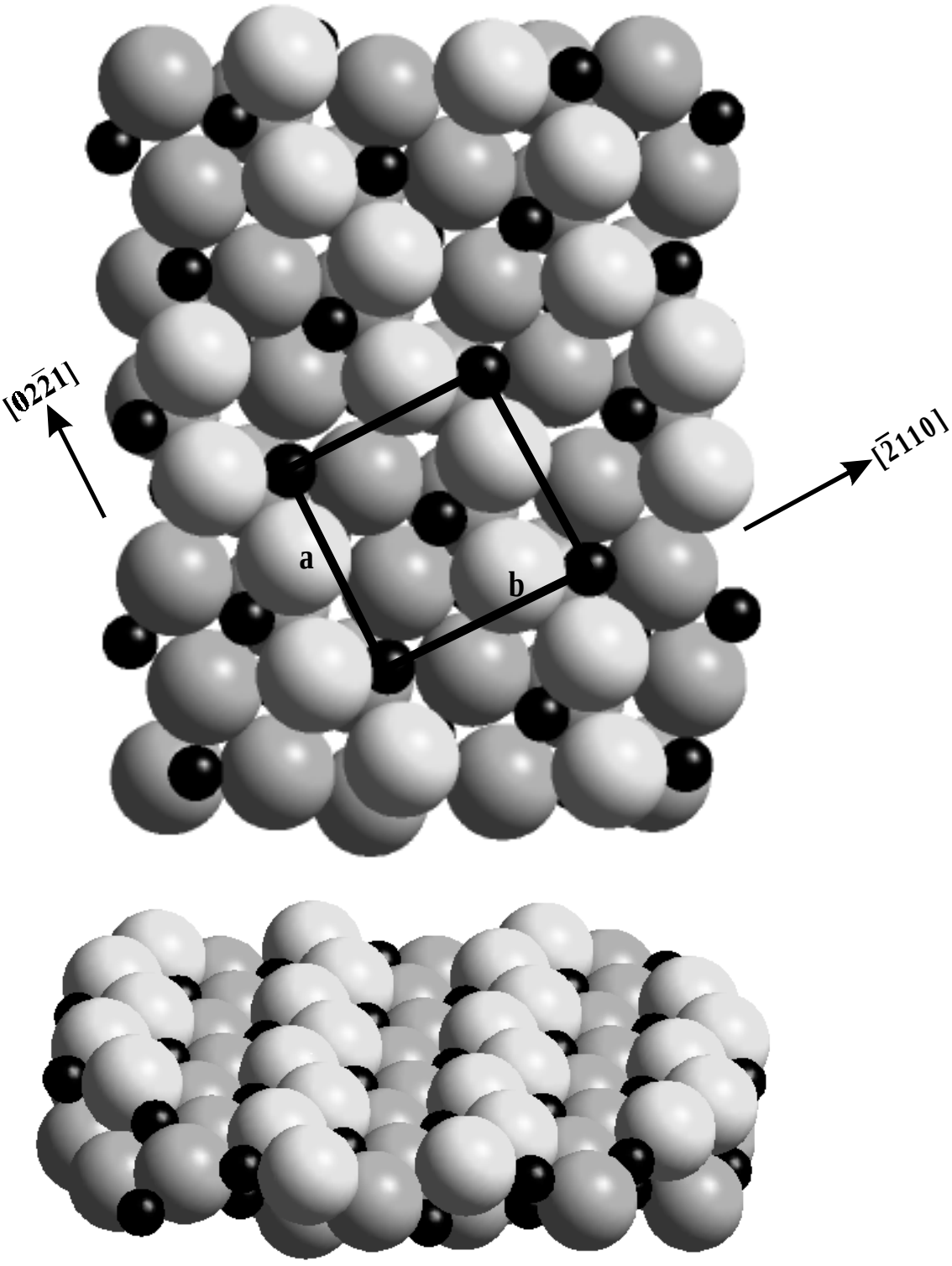

Figure 2. A ball model representation of the Cr_2O_3 (10$\underline{1}$2) surface. The top view shows the (10$\underline{1}$2) surface parallel to the plane of the page. A surface unit cell is drawn to show the periodicity. The bottom shows a side-on view of one stoichiometric repeating layer, which is tilted for perspective. Chromium cations are represented by the small black spheres and oxygen anions by the large gray spheres.

Chapter 2

Surface Characterization and Oxidation Behavior of the Cr_2O_3 (10$\underline{1}$2) Surface

2.1 Introduction

Ion bombardment is a common method of cleaning surfaces in UHV. The literature contains several studies of ion-bombarded Cr_2O_3 surfaces, but the effects of ion bombardment upon Cr_2O_3 surfaces is still uncertain [18, 19]. Traditional wisdom concerning metal oxides suggests that oxygen will be preferentially removed and the surface reduced [20, 21], but this is not the case for Cr_2O_3 [18, 21, 22]. XPS studies of Cr_2O_3 surface composition changes caused by Ar^+ ion bombardment show that oxygen and chromium are removed at a stoichiometric rate [21, 22], although models for surface ion removal rates based upon mass effects and chemical bonding fail to predict this behavior [18]. More recently, a paper by Henrich and coworkers [19] offers UPS and XPS evidence that the Cr_2O_3 surface may become more oxidized during Ar^+ ion bombardment, possibly forming Cr^{4+}, but the degree to which this process may occur was not quantified.

The interaction of oxygen with Cr_2O_3 has been studied extensively. In the classic work on the surface chemistry of Cr_2O_3, Burwell *et al.* [23] reported that oxygen is strongly chemisorbed by Cr_2O_3 microcrystalline gels. Numerous groups have since studied the adsorption of oxygen by Cr_2O_3 powders and films, but the nature of absorbed oxygen on the Cr_2O_3 surface remains a matter of debate [24, 25, 26, 38].

Zecchina and coworkers [26 - 33] used infrared (IR) spectroscopy in a broad study of adsorption on Cr_2O_3 powders that exhibited predominantly (10$\underline{1}$2) natural growth faces. They observed that oxygen was strongly adsorbed and used infrared assignments to argue that the adsorbed oxygen was linked to the surface via covalent double bonds to chromium cations (*i*.e. a Cr=O species). A similar assignment was made by Carrot and Sheppard [25], though neither study addressed the oxidation state of chromium cations. Carrot and Sheppard investigated both amorphous and crystalline Cr_2O_3 powders and reported that chemisorbed oxygen forms a Cr=O species over both

forms of the material. Both groups report a single adsorption state for oxygen, a strongly bound atomic species having a bond order of two. Neither group observed molecularly bound O_2^-.

Burwell and McDaniel also found a single adsorption state for oxygen on amorphous Cr_2O_3 powders, but disagree with the assignment of Cr=O for adsorbed oxygen [34]. They suggest that adsorbed (or "excess") oxygen exists as peroxide ions (O_2^-) that fill bridging sites between cations, an arrangement that is equivalent to Cr=O from a coverage standpoint, but requires the presence of Cr^{3+} with only a single coordination vacancy.

Davydov and coworkers [35, 36, 37] also investigated the O_2-Cr_2O_3 system using IR spectroscopy and found two states of adsorbed oxygen, one state corresponding to Cr=O and the other to Cr-O_2^--Cr bridging sites. The preferred type of oxygen adsorption was a function of the crystal faces exposed and the sample pretreatment. It is often cited in the literature on Cr_2O_3 powders that lower oxidation and coordination numbers for surface cations cause a stronger chromium-oxygen interaction [23, 26, 36].

Davydov and coworkers [35, 36, 37] argue that the (10$\underline{1}$2) family of planes adsorbs molecular oxygen in a bridging configuration, while the (0001) family of basal planes is responsible for the formation of surface Cr=O. Davydov proposed that dissociative oxygen adsorption may only occur at Cr^{4+} sites while adsorption at Cr^{3+} sites results in the formation of Cr^{4+}-O_2^- complexes. They were able to selectively prepare samples to obtain either dissociative or molecular oxygen adsorption.

Interestingly, Davydov [35] proposed that five-coordinate surface Cr^{3+} cations are unreactive towards oxygen. Five-coordinate Cr^{3+} is the predominant cation at the stoichiometric Cr_2O_3 (10$\underline{1}$2) surface. Studies of the O_2-Cr_2O_3 system over powders are complicated by the presence of numerous exposed crystal faces and by the presence of hydroxyl groups on the surface [23]. These factors make the coordination and oxidation numbers of surface cations difficult to determine and the issue often becomes unclear in the literature.

Two groups have examined oxygen adsorption over geometrically-well-defined Cr_2O_3 (0001) thin films epitaxially grown on Cr (110) single crystal surfaces. Foord and Lambert [38] gave no description of the coordination numbers associated with surface

cations, but report molecular (α) and dissociative (β) oxygen adsorption with heats of adsorption of 110 kJ mol^{-1} and 210 kJ mol^{-1}, respectively. They also report that the adsorption of oxygen at the Cr_2O_3 (0001) surface does not does not cause any pronounced changes in the Cr 2p levels in XPS, indicating that the oxidation state of surface chromium cations is not greatly affected by oxygen uptake. Interestingly, it was also observed that pre-adsorption of chlorine to the surface effectively blocks β-adsorption, while α-adsorption remains unaffected. Freund and coworkers [63, 64, 65, 66] describe both polar and non-polar terminations of the Cr_2O_3 (0001) thin film surface. Following O_2 adsorption, they report the removal of molecularly adsorbed oxygen at temperatures between 110 K and 320 K, and the removal of atomic (dissociatively adsorbed) oxygen at temperatures >800 K [63].

It is interesting to note that some of the groups that have studied oxygen adsorption over Cr_2O_3 have observed a molecular oxygen surface species [24, 27, 40] while others did not [26, 25, 35, 39]. Molecularly bound oxygen has a heat of adsorption of around 100 to 135 kJ mol^{-1}, while dissociatively adsorbed oxygen has a heat of adsorption of around 200 kJ mol^{-1} [39, 40]. Davydov [35, 36] has suggested that differences in sample preparation and pretreatment are the cause for differences in adsorption behavior, and was able to selectively prepare samples that would adsorb oxygen either molecularly or dissociatively. He proposed that molecular adsorption at Cr^{3+} sites results in the formation of a charge transfer complex $\{Cr^{4+}\text{-}O_2^-\}$, and that dissociative oxygen adsorption occurs only at Cr^{2+} sites. Davydovs' work, however, does not address the possible effects of various cation coordinations upon oxygen adsorption. In fact, specific information concerning the valence electronic configuration and the coordinate environment of surface cations is sparse throughout the literature on Cr_2O_3 chemistry.

Several groups have reported that oxygen exchange between an adsorbate and the surface O^{2-} anions may occur. Winter [40] used Cr_2O_3 pretreated with ^{18}O to demonstrate that lattice oxygen and the compounds CO and CO_2 are capable of oxygen exchange. Foord and coworkers [38] reported that only dissociatively adsorbed (β state) oxygen was capable of exchange with lattice oxygen.

Many of the references cited herein mention another type of oxygen adsorption often referred to as "irreversible uptake" [2, 26, 24, 38, 40]. The nature of this type of adsorbed oxygen is ill defined and is directly related to the problem of assigning oxidation and coordination numbers to surface cations. Irreversible oxygen adsorption occurs over Cr_2O_3 surfaces that are typically described as clean and stoichiometric, though with some unknown quantity of defects. Irreversible adsorption is most often attributed to adsorption at oxygen vacancy sites, and is stable up to 1200 K [38]. Confusion arises when one tries to distinguish between "irreversibly" adsorbed oxygen, "excess" oxygen, and other proposed forms of dissociatively adsorbed oxygen [26, 25, 34]. The variety of sample preparation techniques, oxygen exposure conditions, and a lack of surface structure information in the literature make the matter even less clear. Therefore, in virtually every study of oxygen adsorption over Cr_2O_3, whether the initial condition of the surface is oxygen-deficient, stoichiometric, or oxygen-rich is not known.

2.2 Experimental

Experiments were conducted in two different UHV systems. One system is a turbo-pumped, dual-chamber vacuum system equipped with a Leybold EA-11 hemispherical analyzer and a dual anode Mg/Al x-ray source for x-ray photoelectron spectroscopy. The second system is an ion-pumped, Physical Electronics chamber, equipped with a Model 15-155 single-pass CMA for Auger electron spectroscopy. Both systems include an Inficon Quadrex 200 mass spectrometer for thermal desorption spectroscopy and a set of Vacuum Generators 3-grid reverse view LEED optics. The base operation pressure in both systems is approximately 1×10^{-10} Torr. XPS experiments were run at pass energies of 60 eV, resulting in electronic energy resolutions (ΔE) of 0.9 eV. All XPS atomic ratios have been corrected with Leybold atomic sensitivity factors.

Matheson research grade oxygen (99.997%) was used as received. Gas doses were done by backfilling the vacuum chamber through a variable leak valve. All doses have been corrected for ion gauge sensitivity [41]. Oxygen exposures were conducted at 163 K, unless stated otherwise.

2.3 Results

2.3.1 Ion Bombardment and Annealing Experiments

The sample was bombarded with 2 keV Ar^+ ions for 30 min, and then annealed to successively higher temperatures. Thermal treatments ranged from 300 K to 1100 K in 100 K increments with heating times of two minutes at each annealing temperature. XPS spectra were collected and LEED observations were made following each annealing step after the sample was cooled to room temperature. LEED experiments at room temperature were conducted using beam energies of 150 eV or higher because charging problems were encountered at lower beam energies. XPS spectra could be collected at room temperature with an adjustment for steady state charging.

2.3.1.1 LEED

Following 30 min of Ar^+ ion bombardment at room temperature, no LEED pattern was visible for any beam energy, only a diffuse background was seen. The first faint LEED beams were observed after annealing to around 700 K. After the 800 K annealing step, the rectangular periodicity of the surface could be recognized, although the spots were broad. Annealing at 900 K for two minutes produced a sharp, rectangular (1×1) LEED pattern. This (1×1) pattern remains unchanged by additional treatments up to 1100 K.

The increased conductivity of Cr_2O_3 at elevated temperatures allowed LEED observations to be made at 725 K and beam energies of 50 eV or less. A typical (1×1) LEED pattern at a sample temperature of 725 K is shown in Figure 3. This pattern was obtained following 30 min of ion bombardment and 2 min of annealing at 900 K, and is typical of LEED patterns obtained from this surface.

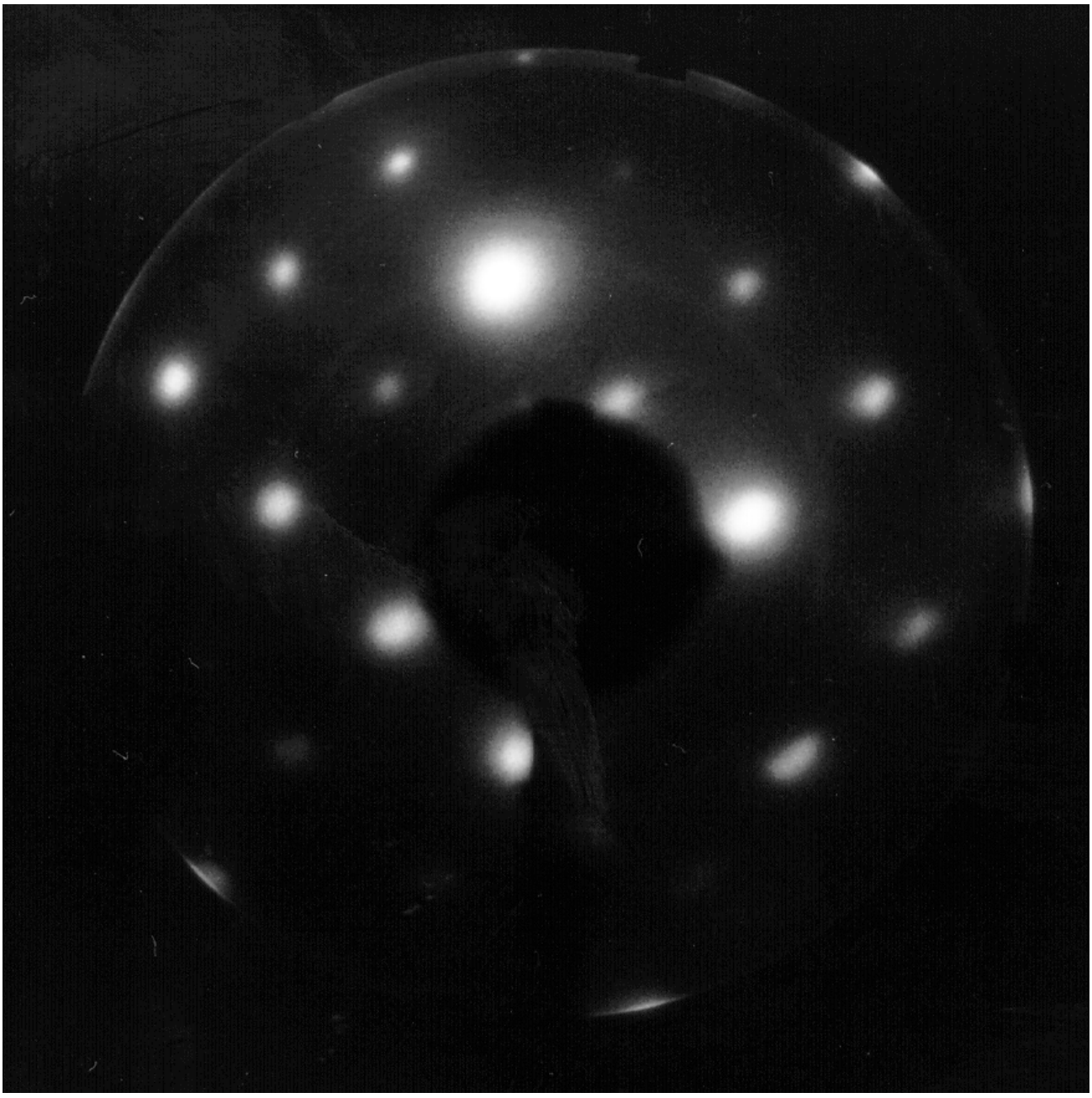

Figure 3. A LEED photograph of the (1×1) Cr_2O_3 (10$\underline{1}$2) surface taken at a sample temperature of 775 K and a beam energy of 62 eV.

2.3.1.2 XPS

It was found that XPS spectra could be collected from the insulating Cr_2O_3 (10$\underline{1}$2) surface at room temperature because of uniform steady state charging. To reference the binding energy scale, short XPS runs were made at a sample temperature of 900 K where the conductivity of the material is sufficient to prevent charging. At 900 K, the Cr $2p_{3/2}$ binding energy falls at 576.9±0.2 eV for an ion-bombarded and 900 K-annealed (ordered) surface. This value is within the range typically attributed to Cr^{3+} in Cr_2O_3 [38, 42, 43]. Figure 4 (a) shows Cr 2p and O 1s XPS data taken at room temperature for an ordered surface. The binding energy scales have been shifted to align the Cr $2p_{3/2}$ peak to 576.9 eV to compensate for steady state charging. The 530.8 eV binding energy for O 1s falls within the range expected for oxide lattice oxygen [43], and is typical for O 1s in Cr_2O_3 [42]. The 9.8 eV splitting between the Cr $2p_{1/2}$ and Cr $2p_{3/2}$ features is typical of Cr_2O_3 [42, 43].

In the ion bombardment and annealing study, XPS was used to determine the O/Cr ratio following each annealing step. As shown in Figure 5, the XPS data indicate no significant change in the O/Cr ratio as the surface is progressively annealed to higher temperatures to order the surface. The average O/Cr ratio determined using XPS is 1.52 ± 0.05. The (XPS) O/Cr ratios and binding energies suggest nearly stoichiometric surface compositions for ion bombarded and annealed surfaces.

2.3.2 AES of the Ordered Cr_2O_3 (10$\underline{1}$2) Surface

AES measurements are problematic due to the insulating nature of the sample [44-47]. However, it was possible to collect room-temperature AES spectra from this bulk insulator in cases where the primary and secondary emission are nearly balanced and differential charging is minimal. To compensate for the low signal-to noise ratio in AES at room temperature, sampling times of up to two hours were used. It was also found that charging problems in AES are eliminated at sample temperatures of 875 K and above. Sufficient thermal promotion of charge carriers occurs at this temperature to make the sample conductive [48], leading to an improved signal-to-noise ratio. An additional benefit of using the higher temperature is that AES spectra taken at 875 K can

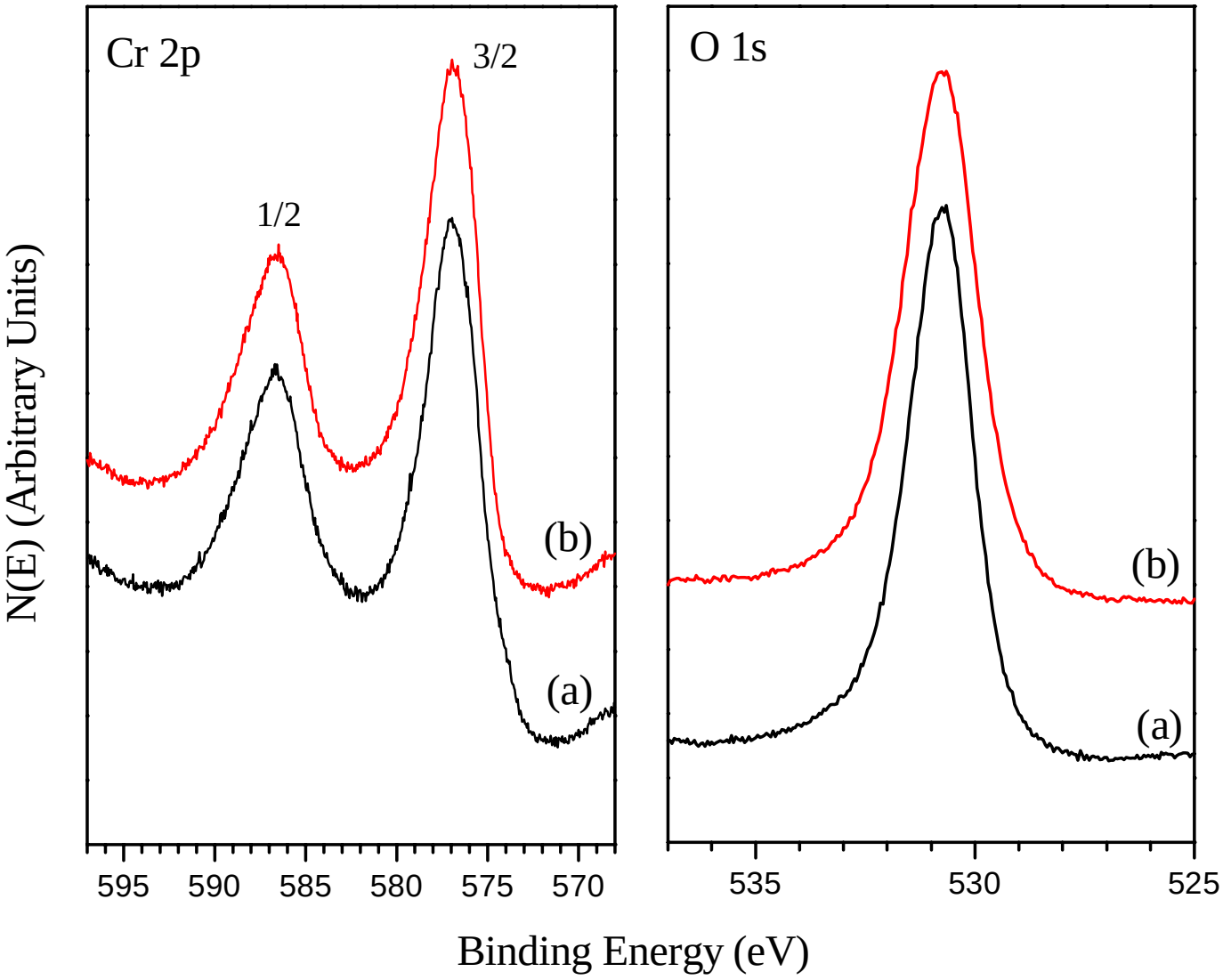

Figure 4. The Cr 2p and O 1s XPS data taken at room temperature for (a) the ion-bombarded and annealed (nearly stoichiometric) surface and (b) the oxygen-saturated surface.

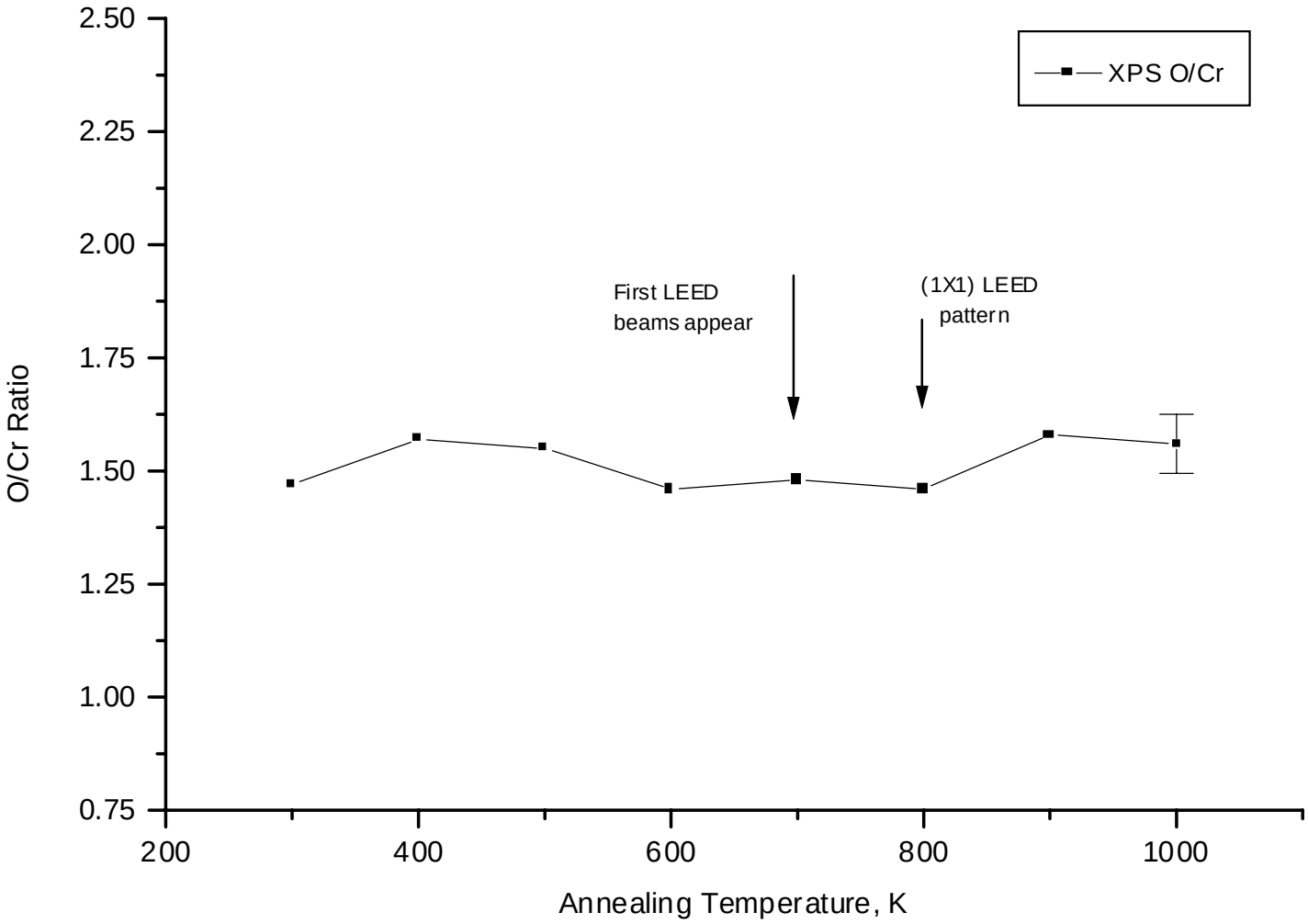

Figure 5. The O/Cr ratio versus annealing temperature measured using XPS data collected at room temperature.

be collected in a single 30 s scan. However, significant differences occur between spectra collected at room temperature and 875 K.

Figure 6 shows AES spectra of identically prepared ion bombarded and 900 K-annealed (1×1) surfaces taken at 300 K and 875 K. Differences in peak-to-peak heights and peak positions are apparent between the 300 K and 875 K spectra. For spectra collected at 875 K, the oxygen KLL line (which occurs at 520 eV at 300 K) is shifted upwards in kinetic energy by about 5 eV. As shown in Figure 6, the chromium $L_3M_{2,3}M_{4,5}$ line at 525 eV in the 875 K spectrum is decreased in kinetic energy by approximately 2 eV, relative to the 300 K spectrum, while the chromium $L_{2,3}M_{2,3}M_{2,3}$ at 499 eV shifts to downward to 490 eV. The Cr $L_3M_{4,5}M_{4,5}$ peak is almost completely obscured by noise in the 300 K spectrum, but is easily seen in the AES spectrum collected at 875 K.

The peak-to-peak height of the oxygen KLL line in Figure 6 is dramatically reduced relative to the two chromium peaks for spectra collected at 875 K. The smaller size of the oxygen signal suggests a decrease in the amount of oxygen at the surface between 300 K and 875 K, but the smaller oxygen peak-to-peak height is actually the result of a change in the shape of the signal envelope involved in the overlapping of the O KLL and Cr $L_3M_{2,3}M_{4,5}$ signals [49]. XPS spectra collected at 875 K definitively show that these differences are only artifacts of the AES measurement conditions and not evidence of a temperature-induced change in the O/Cr ratio at the surface. Additionally, the (1×1) LEED pattern at 875 K does not indicate a surface reconstruction at this temperature.

The Cr $L_3M_{2,3}M_{4,5}$ peak is the largest chromium Auger signal and is normally chosen as the (primary) signal upon which to base AES measurements of chromium concentration. However, the overlap between this primary chromium peak and the O KLL peak in spectra collected at 875 K makes using the Cr $L_{2,3}M_{2,3}M_{2,3}$ peak at 490 eV a more reasonable choice for tracking the chromium concentration. To use the Cr $L_{2,3}M_{2,3}M_{2,3}$ peak for quantification purposes, the Cr $L_3M_{2,3}M_{4,5}$/Cr $L_{2,3}M_{2,3}M_{2,3}$ peak ratio from a standard chromium metal spectrum (1.40) [50, 110] can be applied to the usual sensitivity factor for the Cr $L_{2,3}M_{2,3}M_{4,5}$ peak to estimate the sensitivity factor for the Cr $L_3M_{2,3}M_{2,3}$ peak. This scaling contains the inherent assumption that the relative

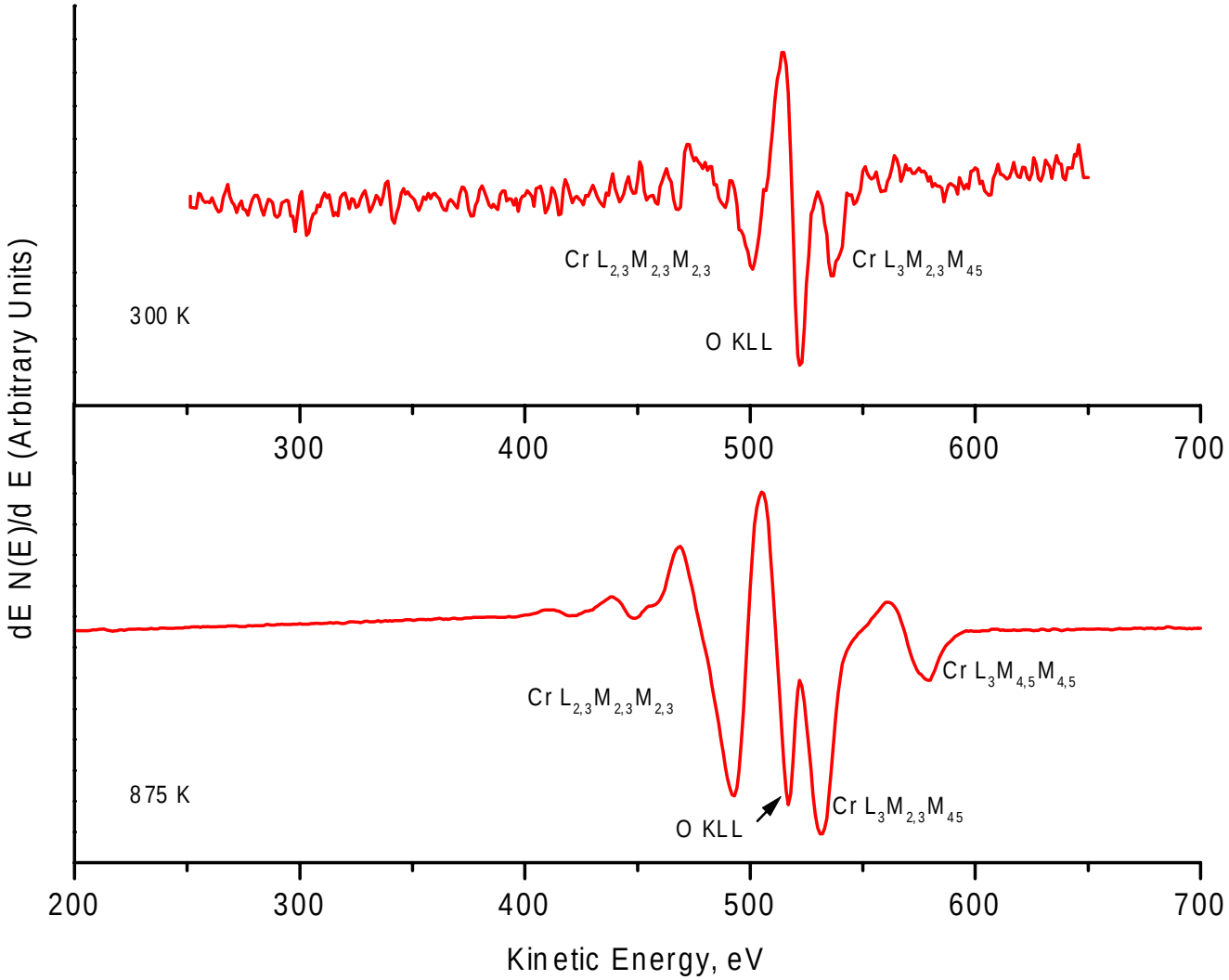

Figure 6. Shown above are AES spectra of identically prepared, ordered Cr_2O_3 (10$\underline{1}$2) surfaces. The top spectrum was taken at 300 K and the bottom spectrum was taken at 875 K.

peak-to-peak heights of the two chromium AES features are the same in both chromium metal and in Cr_2O_3. Given the overlap in the chromium and oxygen AES signals, the relative peak-to-peak heights of the chromium features in Cr_2O_3 cannot be established. Other authors have used similar methods of "scaling" the Cr_2O_3 Auger peaks [47, 51].

Because the oxygen peak-to-peak intensity in the AES derivative spectra is reduced by the O KLL and Cr $L_3M_{2,3}M_{4,5}$ signal overlap, AES O/Cr ratios measured at 875 K do not yield the true value of the O/Cr ratio at the surface. A (1×1) nearly stoichiometric surface yields an O/Cr ratio of 0.67±0.03 if the spectrum is collected at 875 K, rather than the 1.52 value obtained with XPS. The effect of temperature upon the apparent O/Cr ratio is, however, consistent between spectra. While the absolute ratio is not correct, variations in the (875 K) AES O/Cr ratio are an accurate indicator of changes in surface composition, as demonstrated below.

2.3.3 Oxygen Uptake

Thermal desorption spectra, AES, and XPS experiments were conducted on an ion-bombarded and 900 K-annealed, (nearly stoichiometric) surface was subjected to repeated 0.25 L (1 L=10^{-6} Torr s^{-1}) doses of molecular oxygen. Oxygen exposures were conducted at 163 K, and AES spectra were collected at 875 K following each TDS run. Figure 7 shows the variations in the integrated O_2 desorption signal (black) as a function of total dose. No oxygen desorbs following the first two 0.25 L exposures, suggesting that the initial oxygen doses are irreversibly adsorbed under TDS conditions (up to 650 K). For successive exposures totaling more than 0.5 L, an oxygen desorption feature is observed at 220 K in TDS. In subsequent TDS runs, the amount of O_2 desorption first increases, and then levels out to a nearly constant value. As demonstrated below with AES, the integrated desorption signal levels out once the surface becomes saturated with irreversibly adsorbed oxygen. The 220 K desorption temperature is unchanged with coverage, a characteristic of first-order desorption kinetics. Because of the low desorption temperature and first-order desorption kinetics, the desorbing oxygen is assigned as originating from a molecular oxygen (O_2) surface species. An activation energy for desorption of 57 kJ/mol is estimated for this species using the Redhead equation and assuming a normal, first-order pre-exponential factor of 10^{13} s^{-1} [52].

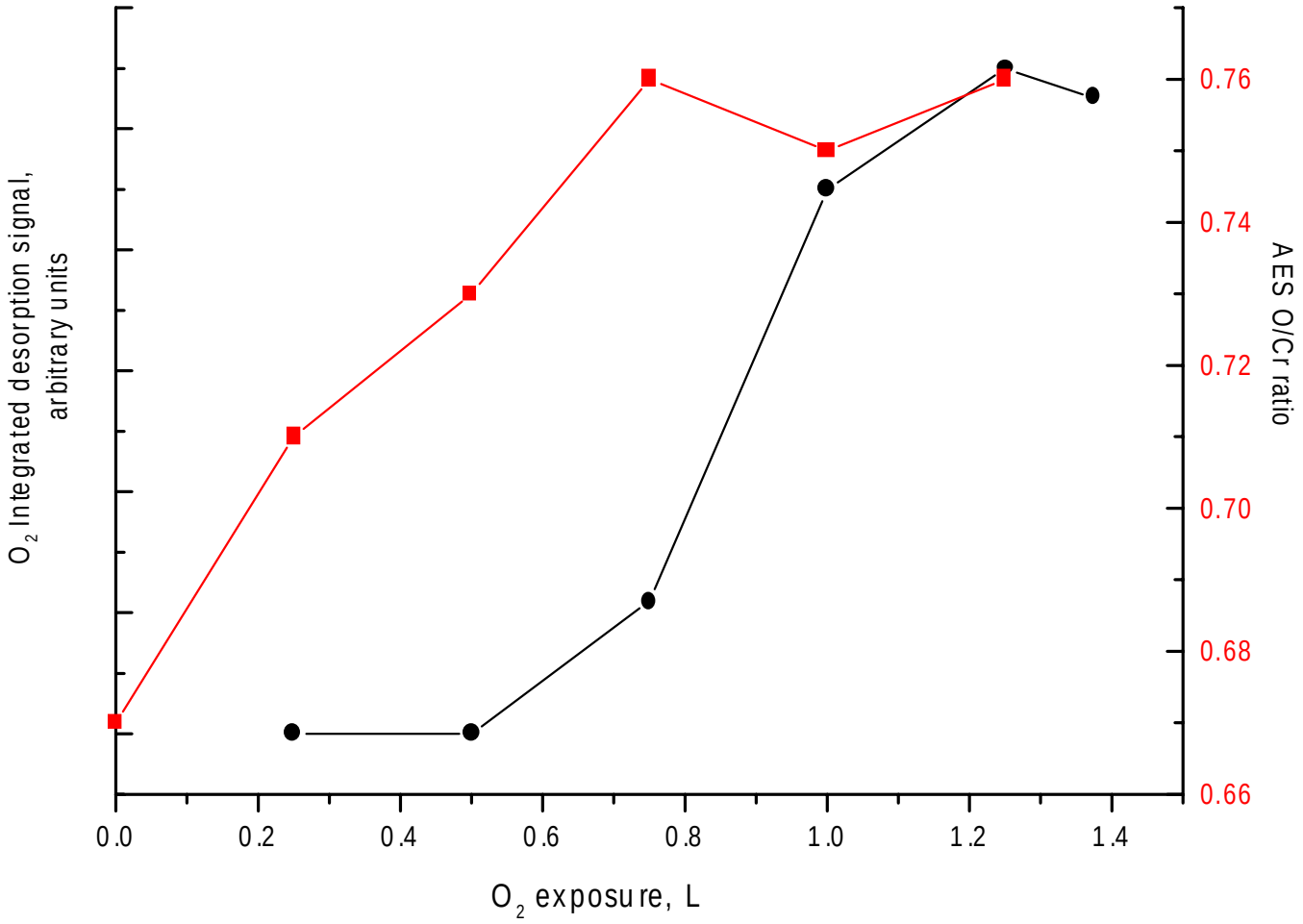

Figure 7. The AES O/Cr ratio (red), measured at 800 K, is compared with TDS measurements of the oxygen desorption signal (black). Initial 0.25 L doses of oxygen yield no desorption signal, indicating that these are irreversably adsorbed. AES measurements of the O/Cr ratio confirm oxygen uptake by the surface during the initial doses. Both curves level off after the surface has become oxygen "saturated".

The amount of surface O_2 associated with the 220 K desorption feature in TDS is small. Oxygen TDS experiments (not shown) on an oxygen-saturated surface demonstrated that the 200 K desorption feature saturates for the lowest dose investigated (0.03 L). Assuming a unity sticking coefficient for the molecular O_2 species on an oxygen-saturated surface, an upper-limit estimate of adsorption yields 1.08×10^{13} O_2 molecules per cm^2. Based on the unit cell parameters for α-Cr_2O_3, an ideal, stoichiometric (10$\underline{1}$2) surface exposes 4.86×10^{14} five-coordinate Cr^{3+} cations per cm^2. The coverage of reversibly-adsorbed molecular O_2, therefore, corresponds to 2% or less of the available chromium sites on the ideal, stoichiometric Cr_2O_3 (10$\underline{1}$2) surface.

Figure 5 (b) shows the Cr 2p and O 1s XPS data collected from a surface that was oxygenated during consecutive TDS runs, as described above. The adsorption of oxygen on the ordered, nearly stoichiometric surface results in no broadening of the Cr 2p peaks, and no new features attributable to an oxidation state greater than Cr^{3+} are observed. The only differences of note are a slight broadening (0.2 eV) and an increase in the intensity of the O 1s feature following oxygen adsorption. For the TDS treatments described above, the XPS O/Cr ratio increases from 1.52 for the ordered, nearly stoichiometric surface to 1.74 following 1.4 L of total oxygen exposure.

The amount of "irreversible" oxygen uptake during TDS experiments can be estimated from XPS data using a simple model based on the exponential decay of signal with sampling depth [53, 54]. Estimates of the expected O/Cr for an ideal, unrelaxed, stoichiometric Cr_2O_3 (10$\underline{1}$2) surface (as shown in Figure 2) yields a value of 1.52 compared to a measured value of 1.52±0.05 for an ordered, nearly stoichiometric surface. If “saturation” coverage of one oxygen atom per five-coordinate Cr^{3+} cation is assumed, an estimated O/Cr ration of 1.71 is obtained from the model. The estimated value compares to a measured value of 1.74 for an oxygen saturated Cr_2O_3 (10$\underline{1}$2) surface. The similar measured and estimated O/Cr ratios suggests an oxygen uptake yielding essentially a 1:1 ratio of oxygen adatoms to surface chromium cations on the oxygen-saturated surface.

AES also confirms the irreversible uptake of oxygen by the surface. Shown in Figure 7 (red) is the increase in the AES O/Cr ratio as the surface changes from a nearly-stoichiometric, (1×1) surface to an oxygen saturated surface that adsorbs only molecular O_2. The nearly stoichiometric surface has an O/Cr ratio of 1.52 as measured by XPS and 0.67 as measured by AES (875 K). Following oxygen saturation of the surface, the O/Cr ratio measured using XPS is 1.74 and AES measurements yield 0.76, an increase in the O/Cr ratio of 13–14% relative to the nearly stoichiometric surface for each technique. These data indicate that while AES at 875 K is a poor technique for measuring the surface O/Cr directly it can be used to track *changes* in composition accurately.

Thermal desorption experiments above 650 K were not possible with the experimental setup used, but the thermal stability of the "irreversibly" adsorbed oxygen deposited during TDS was investigated at higher temperatures. An oxygen-saturated surface was annealed at 1100 K for 2 min and then cooled. AES O/Cr ratios collected from an oxygen-saturated surface before and after annealing to 1100 K were comparable, indicating no significant loss of surface oxygen for sample temperatures of up to 1100 K. Following the thermal treatment, O_2 was also dosed onto the sample at 163 K and the resulting TDS spectra were identical to those collected from the oxygen-saturated surface. The integrated desorption areas before and after annealing were similar, indicating that the composition of the oxygen-saturated surface was unchanged by the thermal treatment.

LEED was used to investigate the ordered (nearly stoichiometric), partially-oxygenated, and fully-oxygenated surfaces. LEED observations were made at 300 K and 725 K. Only a (1×1) LEED periodicity was observed following any degree of oxygen exposure at 163 K. However, the LEED beams appeared somewhat sharper following the initial oxygen exposure.

2.4 Discussion

The (1×1) rectangular LEED pattern shown in Figure 3 for an ion-bombarded and annealed surface is consistent with a simple termination of the bulk structure of Cr_2O_3 along the (10$\underline{1}$2) plane [17, 55]. Surface energy considerations dictate that the non-polar, stoichiometric termination should be the most stable [16, 17]. However, oxide surfaces prepared by ion bombardment and annealing can exhibit non-stoichiometric terminations, particularly if one of the component ions is preferentially sputtered.

Insight into the composition of the surfaces prepared in this study can be gained by comparing XPS composition measurements to expected values of the O/Cr ratio for the different surface terminations. The O/Cr ratio is estimated using a simple exponential decay model of photoemission intensity [54]. For an ideal, non-polar, stoichiometric surface termination along Cr_2O_3 (10$\underline{1}$2), the expected XPS O/Cr ratio is 1.52, in good agreement with the value of 1.52 ± 0.05 observed experimentally for ion bombarded and annealed surfaces. If the ideal stoichiometric surface is modified by the addition of an extra terminating layer of oxygen anions (oxygen saturated), the exponential decay model [54] gives an estimated XPS O/Cr ratio of 1.71. This value agrees well with the experimentally measured O/Cr=1.74 for an oxygen saturated surface.

The observed (1×1) LEED periodicity and the similarity between the experimental and expected XPS O/Cr ratios suggests that a nearly-stoichiometric Cr_2O_3 (10$\underline{1}$2) surface can be prepared by ion bombardment and high temperature annealing. While the surface cannot be deemed defect free, the nearly-stoichiometric composition of this ordered surface suggests a simple non-polar termination that exposes predominantly five-coordinate Cr^{3+} cations as expected for an ideal termination of the bulk structure. Similarly, the repeated exposures of oxygen to a (1×1), nearly stoichiometric surface at low temperature results in an ordered uptake of oxygen approaching one oxygen atom per surface chromium cation.

2.4.1 Ion bombardment and annealing experiments

XPS spectra of the surface following ion bombardment and throughout subsequent annealing steps show no significant change in the O/Cr ratio for temperatures up to 1100 K. The O/Cr ratios measured using XPS (300 K) remain constant at 1.52 ± 0.05, a ratio similar to that expected from an ideal stoichiometric Cr_2O_3 (10$\underline{1}$2) surface. The results suggest that oxygen and chromium are removed from the surface at close to a stoichiometric rate during ion bombardment, in agreement with some previous work [21, 22]. It should be noted that no evidence for surface oxidation during ion bombardment, as seen by Henrich [19], was observed to within the error of our measurements (±0.05). However, XPS spectra were collected in normal emission mode, which is the least surface sensitive geometry. Therefore, small changes in the surface O/Cr ratio may have gone undetected.

2.4.2 Surface uptake of oxygen

The lack of an oxygen desorption signal in TDS following initial oxygen doses and the accompanying increase in the surface O/Cr ratio noted in both XPS and AES demonstrate that a nearly stoichiometric Cr_2O_3 (10$\underline{1}$2) surface strongly adsorbs oxygen at 163 K. Additionally, the adsorbed oxygen is stable up to at least 1100 K, consistent with reports of strongly bound oxygen over Cr_2O_3 powders and films [25, 36, 38]. Because the desorption temperature for molecularly-adsorbed oxygen is expected to be low [56, 63], the "irreversibly"-adsorbed species is attributed to the dissociative adsorption of oxygen.

Retention of the (1×1) LEED pattern following oxygen exposure demonstrates that the oxygen adlayer is commensurate with the stoichiometric surface periodicity, and XPS yields an estimate of nearly one oxygen atom per surface Cr^{3+} cation at saturation. The periodicity and composition of the oxygen saturated surface suggests that the dissociative adsorption of oxygen completes the coordination octahedra of the surface cations, effectively capping the single vacant coordination site of the cations at the stoichiometric surface to give six-coordinate surface chromium atoms.

Based on IR studies in the literature, the state of dissociatively adsorbed oxygen most commonly proposed in on Cr_2O_3 powders is a terminal chromyl species (*i.e.*, Cr=O)

[26, 25] having a bond order of nearly two [26, 36]. In the original study by Zecchina and coworkers [26], the predominant crystal face on microcrystalline powders was misidentified as the (0001) surface. However, a later diffraction study from the same group correctly identified (10$\underline{1}$2) as the predominant exposed crystal face on microcrystalline Cr_2O_3 powders [27]. The original misidentification led to confusion in the literature concerning the nature of available surface cations over Cr_2O_3 microcrystalline powders, and the surface was assumed to contain both four- and five-coordinate Cr^{3+} prior to oxygen adsorption [26]. Davydov and coworkers [35, 36, 37] suggested that Cr=O formation occurs at initially four-coordinate cations most likely in a 2+ oxidation state, and concluded that five-coordinate chromium cations are inert toward dissociative oxygen adsorption. It is clear from the current work, however, that five-coordinate Cr^{3+} cations on the (10$\underline{1}$2) surface actively dissociate oxygen.

For the ion-bombarded and 900 K-annealed (1×1) surface in this study, LEED and XPS indicate the presence of the expected non-polar (10$\underline{1}$2) termination of the Cr_2O_3 single crystal, suggesting that five-coordinate Cr^{3+} is the predominantly exposed surface cation. In agreement with the literature on powders, the form of dissociated oxygen on the (10$\underline{1}$2) surface is attributed to terminal chromyl species (Cr=O). The large (≈4.5Å) separation between nearest neighbor cations on the ideal (10$\underline{1}$2) surface suggests the occurrence of bridging oxide ions or peroxide species is unlikely. Following dissociative adsorption of oxygen, surface chromium cations are capped by the terminal chromyl oxygen to give six-coordinate (*i.e.* fully-coordinated) surface cations. Additionally, LEED observations show that the surface periodicity is unchanged by oxygen uptake, indicating that the octahedral coordination environment of the cations is retained.

Formation of terminal Cr=O may be formally described as a two electron oxidation of chromium Cr^{3+} cations to Cr^{5+} [35]. Unfortunately, the XPS results offer little insight into this oxidation process. Similar to the findings of Foord and Lambert [38] for Cr_2O_3 (0001) films, XPS following oxygen adsorption on Cr_2O_3 (10$\underline{1}$2) gives no indication of a change in the oxidation state of surface chromium cations. Employing the same exponential decay model used to estimate the surface compositions [54], the fraction of the Cr 2p XPS signal originating from surface chromium cations is expected to be about 16%. If a chemical shift involving 16% of the Cr 2p signal occurred upon

oxidation, it should be readily observable as a broadening or a shoulder in the Cr 2p XPS signal. Complicating the interpretation of the XPS data is the lack of standard spectra for Cr^{5+} [43], likely due to the restricted chemistry exhibited for Cr^{4+} and Cr^{5+} compounds [57]. No clear indication is available from the literature as to the XPS binding energy of Cr^{5+}. One study of supported chromia catalysts suggests that the binding energy of Cr^{5+} falls *between* that of Cr^{3+} and Cr^{4+} [58], although these assignments are based on peak fits rather than standard spectra. Even the binding energy of Cr^{4+} oxides is unclear. Some references suggest the binding energy is less than that of Cr^{3+} in Cr_2O_3 [43, 59], while others suggest that it is greater [58].

In addition to the "irreversible" dissociative adsorption of oxygen, the observation of a low temperature (220 K) desorption feature in TDS indicates that reversible molecular adsorption of O_2 also occurs. Since this desorption feature grows in intensity as the surface concentration of dissociatively adsorbed oxygen increases, it seems clear that molecular O_2 adsorption occurs on oxide-terminated regions of the surface formed by the initial dissociative adsorption of oxygen. This interpretation is in agreement with the findings of Davydov and coworkers [36, 37] who observed that dissociative and molecular adsorption of oxygen occurs over reduced and oxidized Cr_2O_3 samples, respectively.

The adsorption of molecular oxygen at Cr^{3+} sites to form Cr^{4+}-O_2^- has been proposed previously in the literature on Cr_2O_3 powders [23, 36]. While the nearly stoichiometric Cr_2O_3 (10$\underline{1}$2) surface exposes many Cr^{3+} sites, the XPS results suggest that nearly all of the surface cations are capped by terminal chromyl oxygen species during the initial stages of oxygen adsorption. The low uptake of molecular oxygen (2% coverage or less of surface cations) is consistent with this idea. Because of the low coverage of molecular oxygen, the corresponding adsorption sites are attributed to cations present at a low concentration as defects in the oxygen-terminated surface. The current data shed no light on the nature of these defect sites. They could originate from defective sites on the nearly stoichiometric surface that are not amenable to dissociative oxygen adsorption, or they could simply be five-coordinate cations with no vacant neighbors capable of providing a site pair for O_2 dissociation.

2.5 Conclusions

It has been demonstrated that both (1×1) nearly stoichiometric and oxygenated Cr_2O_3 (10$\underline{1}$2) surfaces are stable in UHV at temperatures of up to 1100 K. LEED and XPS data suggest that the ion-bombarded and 900 K-annealed surface periodicity and stoichiometry are reasonably explained as a nearly stoichiometric, non-polar (1×1) termination of the surface. The nearly stoichiometric surface interacts strongly with oxygen. Molecular oxygen adsorbs dissociatively and "irreversibly" (up to 1100 K) with a (1×1) periodicity, and in an amount corresponding to nearly one oxygen atom per surface chromium cation. The oxygen adatoms are attributed to terminal (*i.e.*, Cr=O) chromyl species that complete the coordination shell of five-coordinate Cr^{3+} cations at the nearly stoichiometric surface. The adsorption of small quantities of molecular oxygen is observed on the oxide-terminated surface, and the corresponding adsorption sites are assigned to cation defect sites in the terminating oxide layer.

Chapter 3
Reaction of 1-chloro-1-flouroethene over the Cr_2O_3 (10$\underline{1}$2) Surface

3.1 Introduction

Much of the literature concerning halocarbon chemistry over Cr_2O_3 has been devoted to compounds that are intermediates or byproducts formed during the manufacture of alternative refrigerant compounds [4, 91, 102, 105]. Unsaturated halocarbons are used as feedstocks (see Figure 1) for the manufacture of industrially important HCFCs, and are often cited as both intermediates and non-selective products [4, 99].

Vecchio and coworkers [60] studied the fluorination (replacement of chlorine or hydrogen by fluorine) of many halocarbons over aluminum fluoride (AlF_3) catalyst and observed many of the same reactions that were later reported over Cr_2O_3 and other fluorination catalysts [4, 105, 106]. They observed that fluorination is the dominant reaction in the presence of HF, but that HF and HCl abstraction from halo-ethanes to form halo-ethenes occurs in the absence of HF. A build-up of HX (X=Cl or F) on the surface caused the subsequent re-addition of HF and HCl to the halo-ethenes. The re-addition of HX combined with the exchange of halogen between the HCFC molecules and the surface resulted in a broad mix of saturated and unsaturated products. In the words of the authors [60], "In the absence of added hydrogen halide, these (reactions) can lead to a given fluoroethane being converted into most of its fellows".

Surface reactions over Cr_2O_3 powders are similar to those found over AlF_3 [61]. Kavanagh and coworkers [62] used deuterium labeled HF (DF) to study the addition of HF to trichloroethene (TCE) and subsequent halogen exchange reactions over microcrystalline Cr_2O_3 catalyst that was pretreated with HF. They reported that HX addition/elimination reactions and direct halogen exchange with the surface may each occur for HCFC's over Cr_2O_3. In deuterium labeling experiments using DF and TCE, the label indicated that that HX addition to TCE follows the Markovnikov rule. The

incorporation of only a single deuterium label in product molecules that contained multiple fluorine atoms indicated that halo-alkanes must also undergo F-for-Cl exchange with a halogen species on the catalyst surface. Multiple HF elimination/ DF addition steps would have introduced more deuterium labels into the product. The addition of HF across the C=C double bond was postulated as a first step in the reaction of HF and TCE. Subsequent fluorination is though to occur via halogen exchange with surface fluorine. Hydrofluorination of TCE at 523 K was reported to yield about 90% CF_3CH_2Cl (HCFC-133a). Kavanagh and coworkers [62] report the cation oxidation state as Cr^{3+}, but no specific information concerning the catalyst surface was offered.

Kemnitz and coworkers [101, 106] used deuterium labeled HCl (DCl) and HF (DF) to study CHF_2CHF_2 isomerization to CF_3CH_2F (HFC-134 $\rightarrow$ HFC-134a). They reported that if microcrystalline Cr_2O_3 was pretreated with HF, then isomerization proceeds via HF elimination to form CF_2=CHF followed by the re-addition of HF, in accordance with the Markovnikov rule, to form CF_3CH_2F. Interestingly, if the catalyst was pretreated using DCl then a complex set of reactions ensued that included HX elimination, followed by both Markovnikov and anti-Markovnikov HX addition. The presence of chlorine on the Cr_2O_3 surface promoted the formation of a broad range of saturated and unsaturated products. This result echoes the earlier work of Vecchio and coworkers [60] who made the similar observations over AlF_3.

Brunet *et al.* [105] have studied the reaction of CF_3CH_2Cl (HCFC-133a) over Cr_2O_3 powder and reported that HF elimination occurs both in the presence and absence of HF. Over Cr_2O_3 samples that were not pre-fluorinated and in the absence of added HF, the formation of CF_2=CHCl (HCFC-1122a) via HF elimination was reported as the primary reaction. The overall reaction was reported as

$$CF_3CH_2Cl \rightleftharpoons CF_2{=}CHCl + HF$$

At equilibrium, approximately equal amounts of HCFC-1122a and HCFC-133a were found in the reaction mix. Brunet *et al.* reported that no surface chlorine was observed with XPS on the catalyst following HCFC-133a reaction in the absence of HF. Direct exposure of the catalyst to HF at 280 °C for 2 hours resulted in a maximum (XPS) F/Cr ratio of 0.36.

Freund and coworkers [63-66] have studied ethene adsorption in UHV over stoichiometric and oxygen-exposed Cr_2O_3 (0001) thin films that were epitaxially grown on Cr (110). Over the stoichiometric surface they reported that ethene forms a π-complex at surface cation sites that has a desorption temperature of 220 K. This corresponds to a first-order activation energy for desorption of around 57 kJ/mol, using the Redhead method [52]. Surfaces that were pre-exposed to oxygen adsorbed ethene only at defect sites, strongly attenuating the amount of uptake for an oxygen-saturated surface. Scarano *et al.* [67] reported similar findings over Cr_2O_3 microcrystalline powders that contained predominantly (10$\underline{1}$2) faces. Both groups [63, 64, 67] have suggested that the ethene molecule is arranged with its molecular axis parallel to the Cr_2O_3 surface. Both groups also suggest that surface-adsorbate bonds consist of a small amount of charge transfer from the molecule to the surface with minimal backbonding by the Cr^{3+} cations.

The work described herein is most closely related to the work performed by Freund and coworkers [63-66]. Studies of unsaturated HCFC's are lacking in the surface science literature. The TDS of ethene over Cr_2O_3 (0001) films by Freund and coworkers provides an interesting comparison to the $CFCl=CH_2$ TDS on the Cr_2O_3 (10$\underline{1}$2) surface, as discussed below. Despite the common occurrence of halo-ethenes as intermediates and non-selective products during the manufacture of HFC-134a over Cr_2O_3-based catalysts, little is known about their reactivity over Cr_2O_3. This work is the first study of an unsaturated halocarbon over single crystal Cr_2O_3. In contrast to many studies of halocarbons over Cr_2O_3 powders that may be found in the literature, HF was not used as a reactant or pre-treatment gas for any of the experiments described herein [61, 62, 99, 105].

3.2 Experimental

PCR Inc. 1-chloro-1-fluoroethene ($CFCl=CH_2$) (97 %), Matheson acetylene ($HC\equiv CH$) (99.6 %), Matheson oxygen (99.997 %), and Matheson deuterium (99.997 %) were used as received. The 1-chloro-1-fluoroethene was analyzed by mass spectrometry for acetylene (m/z=26) contamination and none was found. Gas dosing was

accomplished by backfilling the chamber through a variable leak valve. All dose sizes have been corrected for ion gauge sensitivity [41], and desorption quantities have been corrected for mass spectrometer sensitivity [68, 69].

The reaction of $CFCl=CH_2$ (HCFC-1131a) over nearly stoichiometric and oxide-terminated (1×1) Cr_2O_3 (10$\underline{1}$2) surfaces was investigated using thermal desorption spectroscopy (TDS), Auger electron spectroscopy (AES) and low-energy electron diffraction (LEED). A nearly stoichiometric, (1×1) surface was prepared by ion-bombardment followed by annealing to 900 K. The oxygen-saturated surface was prepared by repeated 0.2 L oxygen exposures at 163 K, following preparation of the nearly stoichiometric surface (Chapter 2). Oxygen saturation of the surface was confirmed using TDS and AES, which both indicate a concentration of adsorbed oxygen corresponding to nearly one oxygen atom per surface Cr^{3+} cation. The oxygen-saturated surface consists almost entirely of fully coordinated chromium cations that are capped by oxide ions to form a terminal layer of surface chromyl species (Cr=O).

AES measurements were conducted at 800 K to avoid sample charging. Because of overlap between the primary oxygen and chromium Auger peaks, the surface chromium concentration was followed by measuring the Cr $L_{2,3}M_{2,3}M_{2,3}$ (490 eV) peak-to-peak height (section 2.3.2). The amount of chlorine on the surface was determined using the Cl KLL signal (190 eV). All doses for $CFCl=CH_2$ and acetylene TDS experiments were conducted at 163 K.

3.3 Results

$CFCl=CH_2$ (HCFC-1131a) reacted readily with an ordered, nearly stoichiometric Cr_2O_3 (10$\underline{1}$2) surface. Following a product search that included all mass numbers (m/z) from 2 - 200, acetylene (HC≡CH) was determined to be the single gas-phase product formed. Specifically, no fluoroacetylene, chloroacetylene, HCl or HF reaction products were observed during TDS. The $HC{\equiv}CH_{(g)}$ product identification was made by comparison of mass spectrometer cracking patterns for acetylene with thermal desorption peak intensities. The relative intensities of four m/z signals were used to positively identify acetylene (27, 26, 25, 13). The acetylene cracking pattern is in good agreement

with published data for acetylene [70]. The primary mass peak for acetylene m/z=26, and this mass number was monitored to follow acetylene desorption. AES was used to demonstrate that halogen removed from the reactant molecule remains on the sample surface following reaction.

3.3.1 $CFCl=CH_2$ Thermal Desorption from a Nearly Stoichiometric Surface

The top and bottom panels of Figure 8 show desorption traces of reactant and product from $CFCl=CH_2$ TDS experiments initiated on a nearly stoichiometric Cr_2O_3 (10$\underline{1}$2) surface. Both reactant and product desorption features undergo peak temperature shifts and significant intensity changes. Therefore, a dose size of 0.03 L is shown for $CFCl=CH_2$ and 0.06 L is shown for HC≡CH, to best illustrate the changes observed for each molecule.

3.3.1.1 $CFCl=CH_2$ Desorption

The top panel of Figure 8 follows desorption of the dosed molecule, $CFCl=CH_2$ (m/z=80), during a TDS series of consecutive 0.03 L doses initiated over a nearly stoichiometric, (1×1) Cr_2O_3 (10$\underline{1}$2) surface. The peak desorption temperature is 180 K following the first dose and shifts upwards to 200 K by 0.10 L of total exposure. In subsequent doses the intensity of the 200 K feature increases and the 180 K feature reappears. As the total dose reaches 0.16 L, the intensity of the 200 K feature decreases, leaving the 180 K feature as the primary contribution to the desorption spectrum. The initial upward shift in peak desorption temperature of around 20 K suggests that the surface-adsorbate interaction is initially strengthened by $CFCl=CH_2$ exposure (initial surface halogenation), but this effect is reversed for total exposures beyond about 0.16 L.

In TDS experiments conducted using larger dose sizes the upward shift in peak desorption temperature is missed because the majority of $CFCl=CH_2$ detected arises from the 180 K feature. For dose sizes of 0.13 L or more, the feature at 200 K only appears as a small, high-temperature shoulder.

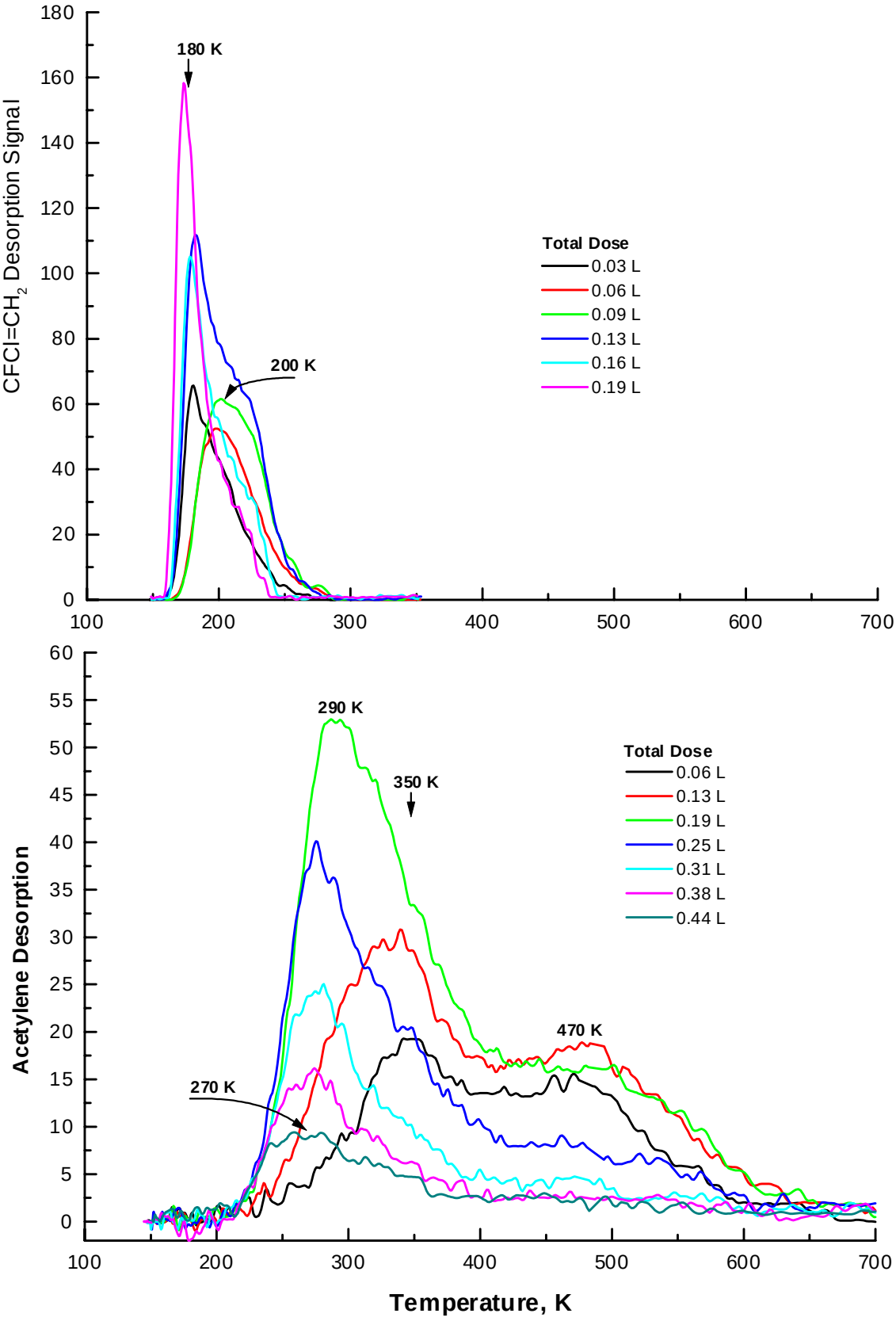

Figure 8. Desorption traces of the $CFCl=CH_2$ reactant (top) and the acetylene product (bottom) for a series of 0.03 L and 0.06 L doses, respectively. The legend indicates the total exposure for each trace in the TDS series.

3.3.1.2 Product HC≡CH Desorption

Acetylene product desorption occurs in two temperature regions, as seen in the bottom panel of Figure 8. Peak desorption temperatures of 350 K and 470 K are observed for acetylene on the initial TDS run (0.06 L). In the second and third TDS runs, the low temperature (350 K) peak grows in intensity and shifts to 280 K, and the high temperature (470 K) feature remains relatively unchanged for total $CFCl=CH_2$ exposures below 0.19 L.

Following 0.19 L of total $CFCl=CH_2$ exposure, the low-temperature acetylene peak continues to shift to lower temperatures, but gradually decreases in intensity with successive TDS runs. The high-temperature acetylene peak rapidly loses intensity for total exposures of 0.25 L and greater. The 470 K desorption temperature for the high-temperature HC≡CH feature does not appear to change significantly as desorption intensity declines. AES experiments following various $CFCl=CH_2$ exposures demonstrate that the initial increase in activity and the eventual deactivation of the surface are linked to the degree of halogenation of surface cation sites (section 3.3.3).

3.3.1.3 Chemisorbed Acetylene

TDS was also used to investigate the desorption kinetics of chemisorbed acetylene dosed directly onto the surface. Figure 9 shows acetylene desorption following a 0.03 L dose of HC≡CH at 163 K on a nearly stoichiometric surface. Also shown for comparison is a TDS trace for product acetylene formed from a 0.06 L dose of $CFCl=CH_2$. Small doses of acetylene yield a single desorption feature near 325 K. No reaction of acetylene with the surface was observed. Specifically, water, CO, and CO_2 were not observed as desorption products and AES shows no surface carbon following acetylene TDS.

The desorption temperature of dosed acetylene coincides with the low temperature (350 K – 270 K) feature from the acetylene product. Similarities between the desorption temperatures and peak shapes of the acetylene product and dosed acetylene indicate that the low-temperature HC≡CH peak is desorption limited. No acetylene desorption is observed at 470 K during acetylene TDS, demonstrating that the high temperature product feature is reaction-limited.

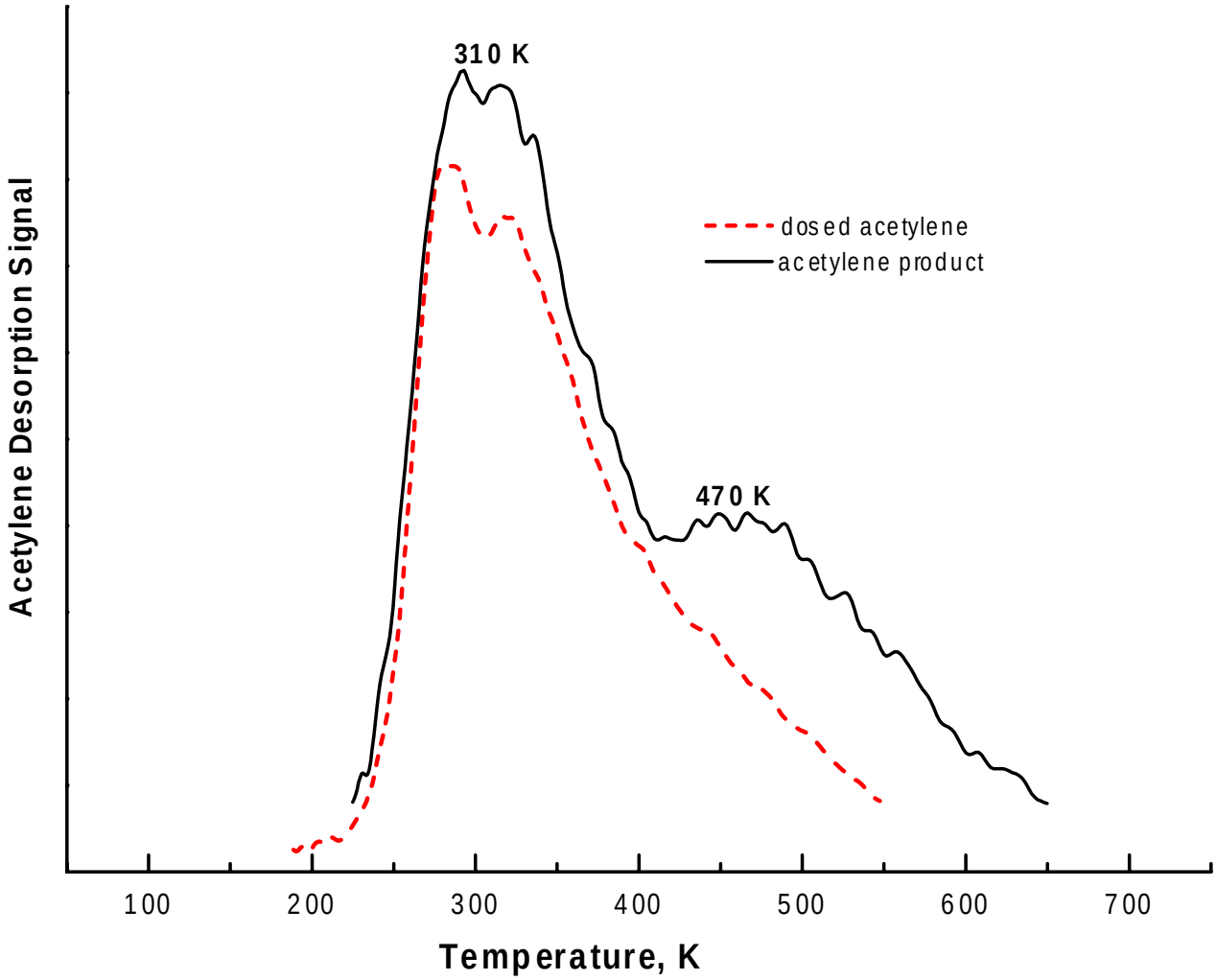

Figure 9. Comparison of TDS traces of 0.06 L of acetylene (HC≡CH) product with the spectra obtained from dosing pure acetylene on to the Cr_2O_3 (10$\underline{1}$2) surface. The 470 K feature is absent from the pure acetylene trace.

3.3.2 Post-reaction AES Analysis

Figure 10 shows the increase in the surface (AES) Cl/Cr ratio for a TDS series of consecutive 0.13 L doses of $CFCl=CH_2$ begun over a nearly stoichiometric surface. The F/Cr is not shown because fluorine underwent rapid electron stimulated loss from the surface and could not be quantified using AES. The Cl/Cr ratio increased linearly following each $CFCl=CH_2$ dose until reaching a total exposure of around 0.5 L. Between 0.5 L and 1.0 L of total exposure, the Cl/Cr ratio levels off at a maximum value of around 0.16. The surface O/Cr ratio was measured for the nearly stoichiometric surface and after $CF=CH_2$ TDS experiments. The O/Cr ratio did not change due to the deposition of surface halogen. No evidence was seen for the replacement of lattice oxygen by halogen on the nearly stoichiometric Cr_2O_3 (10$\underline{1}$2) surface.

Figure 10 also shows the relative quantities of $CFCl=CH_2$ and $HC\equiv CH$ desorbed from the surface during a TDS series of consecutive 0.13 L doses of $CFCl=CH_2$. The amounts of both reactant and product desorbed from the surface increased initially and then steadily decreased. Acetylene production and chlorine deposition both ceased at around 1.0 L of total exposure. Surfaces that have a Cl/Cr ratio of 0.16 following $CFCl=CH_2$ TDS experiments no longer produce acetylene product and are said to be deactivated.

The total of both desorbing species (blue) is also shown in Figure 10. Changes in the total are indicative of changes in the sticking coefficient of $CFCl=CH_2$ to the sample surface. Initially, the total increases, but, beyond around 0.25 L of total exposure the total of desorbing species declines, indicating a decrease in the $CFCl=CH_2$ sticking coefficient as the surface chemistry shuts down. The maximum value of the sticking coefficient occurs at a surface Cl/Cr ratio of 0.055.

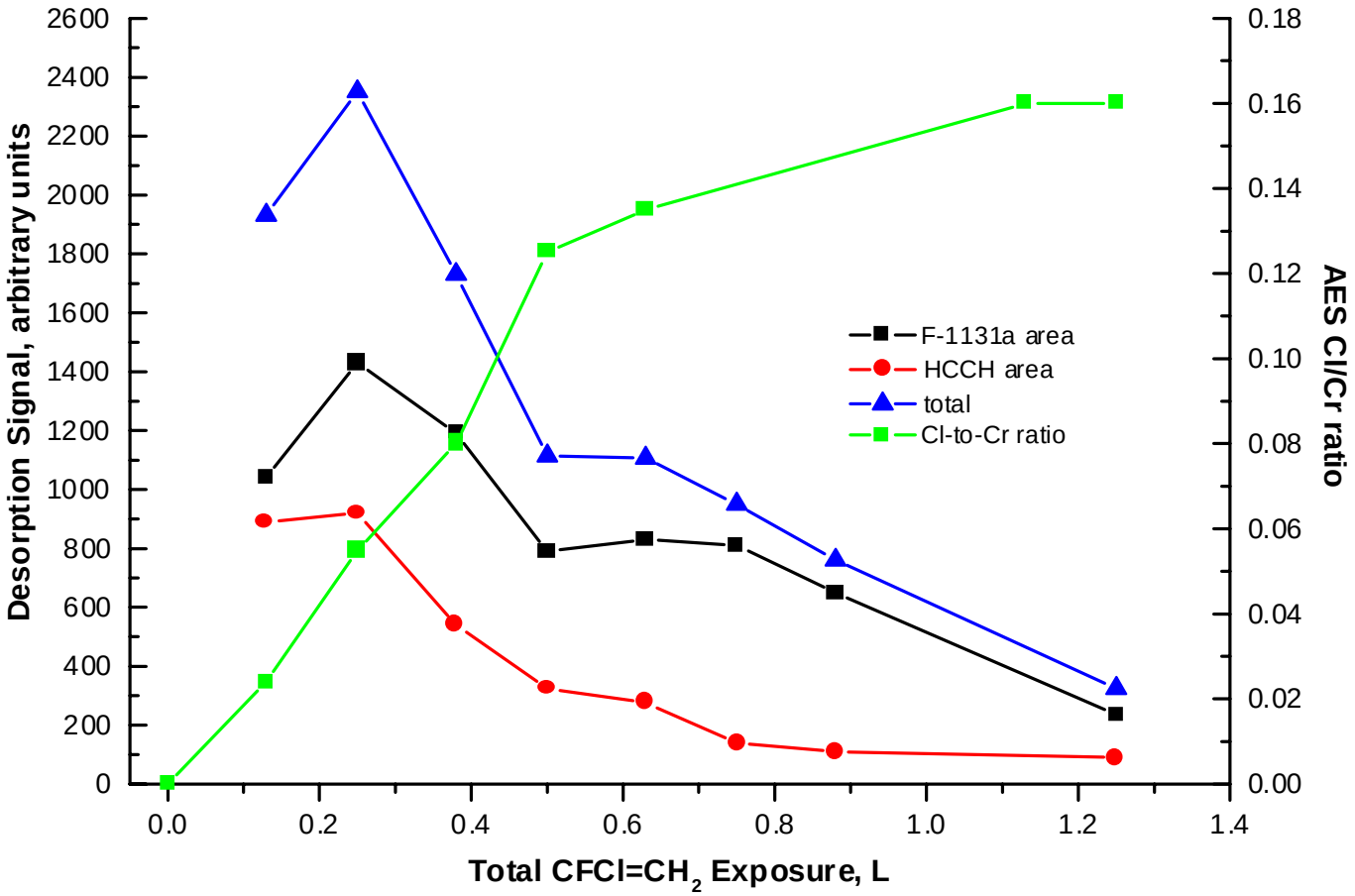

Figure 10. The relative quantities of desorbed $ClFC{=}CH_2$ (reactant) and $HC{\equiv}CH$ (product) from a TDS series of consecutive 0.13 L does of $CFCl{=}CH_2$ are shown along with the increasing surface Cl/Cr ratio as measured using AES.

Consecutive TDS runs using various $CFCl=CH_2$ dose sizes (0.03 L – 1.0L) were carried out until acetylene production ceased, and yielded a final AES Cl/Cr ratio of 0.16, regardless of the dose size and total exposure. As demonstrated in Chapter 4, a Cl/Cr ratio of 0.32 represents approximately one adsorbed chlorine per surface cation. A Cl/Cr ratio of 0.16 implies that approximately half of the surface cations are capped by adsorbed chlorine. Figure 11 shows an AES spectrum of a halogenated sample surface having a Cl/Cr ratio of 0.16. A Cl/Cr of 0.16 corresponds to a surface that has been deactivated by $CFCl=CH_2$ exposure under TDS conditions.

The reaction stoichiometry for forming $HC\equiv CH$ from $CFCl=CH_2$ decomposition requires that chlorine and fluorine be removed from the reactant in equal proportions. Therefore, assuming that all of the removed halogen remains on the surface, a surface that has been halogenated by $CFCl=CH_2$ decomposition to form $HC\equiv CH$ is expected to contain equal concentrations of chlorine $Cl_{(s)}$ and fluorine $Fl_{(s)}$, regardless of the degree of surface halogenation. As indicated above, a surface having a $Cl_{(s)}$:Cr^{3+} of 1:1 has an (AES) Cl/Cr ratio of 0.32. The Cl/Cr=0.16 measured for surfaces deactivated by $CFCl=CH_2$ TDS suggests that half of the cation sites are covered by chlorine and half by fluorine. Deactivation of the surface is attributed to site blocking by $F_{(s)}$ and $Cl_{(s)}$, but only chlorine may be seen using electron-stimulated AES. Therefore, nearly 100% of the cations at the deactivated surface are expected to be coordinated to a halogen adatom.

The TDS data shown in Figure 10 demonstrate an increase in $CFCl=CH_2$ uptake and a coincident increase in $HC\equiv CH$ product for low total exposures. The increase and subsequent decrease in the desorption total demonstrates that the $CFCl=CH_2$ sticking coefficient is a function of the degree of surface halogenation. The 20 K increase in the $CFCl=CH_2$ desorption temperature suggests that the strength of the $CFCl=CH_2$-surface interaction is also a function of surface halogen coverage. For halogen coverages of up to approximately one-third of surface cations (Cl/Cr=0.055), the $CFCl=CH_2$ sticking coefficient increases. For higher levels of surface halogen content, the sticking coefficient declines, dropping to approximately 20% of its maximum value by 1.0 L of total $CFCl=CH_2$ exposure for a series of 0.13 L doses. The observed increase in acetylene product made for low total exposures is attributed to an increase in the $CFCl=CH_2$ sticking coefficient.

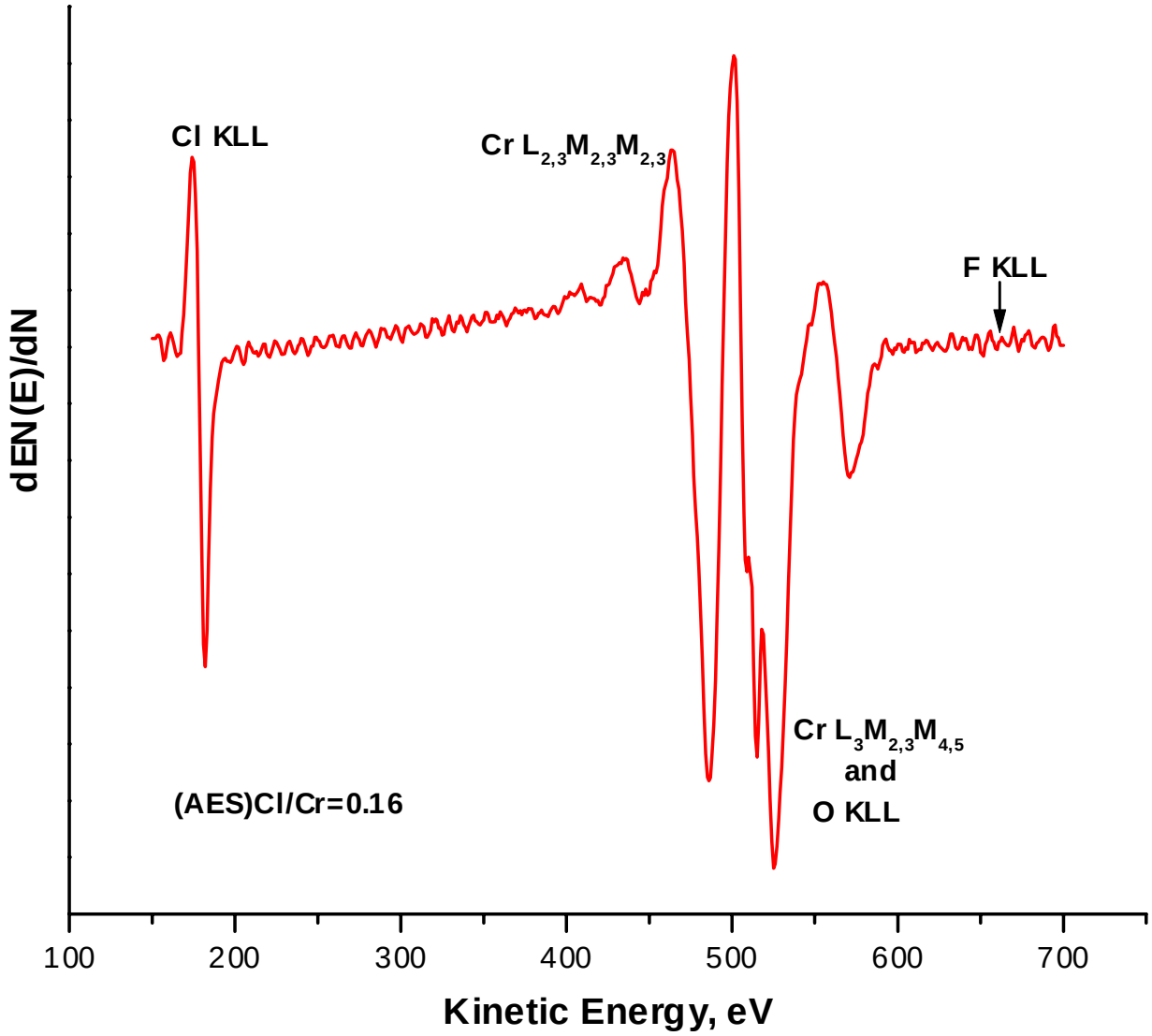

Figure 11. AES spectrum of a Cr_2O_3 (10$\underline{1}$2) surface that has been deactivated by exposure to $CFCl=CH_2$ under TDS conditions (163 K exposures) and has an (AES) Cl/Cr of 0.16. The expected location of the fluorine (F KLL) AES signal is also indicated.

3.3.3 $CFCl=CH_2$ Thermal Desorption from an Oxygenated Surface

$CFCl=CH_2$ TDS over surfaces that were pre-exposed to oxygen showed that the surface reaction is completely inhibited over an oxide-terminated surface. TDS experiments using successive 0.03 L doses of $CFCl=CH_2$ over the oxygen-saturated surface yielded no $HC\equiv CH$ or any other gas-phase product. Specifically, no H_2, H_2O, CO, CO_2, nor any carbon, fluorine, or chlorine containing compounds (other than $CFCl=CH_2$) were observed during TDS experiments. Additionally, AES of the oxygenated surface following $CFCl=CH_2$ exposures (163 K) showed no indication of chlorine or carbon deposition. The TDS and AES data clearly demonstrate $CFCl=CH_2$ decomposition does not occur over an oxygen-saturated surface.

3.4 Discussion

The 1,1-dihalo-elimination (decomposition) reaction of $CFCl=CH_2$ to acetylene over Cr_2O_3 (10$\underline{1}$2) was found to occur readily over a nearly stoichiometric, (1×1) surface. The overall reaction may be represented as:

$$CFCl=CH_2 \rightarrow HC\equiv CH_{(g)} + Cl_{(s)} + F_{(s)}$$

The deposition of halogen ($Cl_{(s)}$ and $F_{(s)}$) on the surface is coincident with changes in surface reactivity and the eventual deactivation of the surface towards $CFCl=CH_2$ decomposition. The occurrence of a 1-chloro, 1-fluoro elimination reaction is somewhat unexpected because of its lack of precedent in the catalysis literature. This is the first documentation of a dihalo-elimination reaction for gas phase halo-ethenes over Cr_2O_3 under any conditions.

3.4.1 Low Temperature (350 K) Acetylene Product

The occurrence of two features for the acetylene product in $CFCl=CH_2$ thermal desorption indicates that two energetically different desorption processes occur. Comparison of dosed acetylene and product acetylene desorption traces demonstrate that the low temperature peak is desorption limited and the high temperature peak is reaction-limited. This suggests that the 350 K portion of the product acetylene signal is the result of $CFCl=CH_2$ that reacts to form acetylene at a lower temperature, and then remains

adsorbed to the surface until the acetylene desorption temperature is reached. Acetylene formation may occur upon adsorption at 163 K, or at any intermediate temperature during a TDS run, up to 350 K. The rate limiting step for HC≡CH desorption via the low temperature reaction channel is assigned as the desorption of a molecular surface species. Assuming a first-order process and a normal first-order pre-exponential of 10^{13} s^{-1}, an activation energy for desorption of 90 kJ/mol is calculated for the desorption-limited acetylene peak [52].

During $CFCl=CH_2$ TDS, the peak desorption temperature for the low temperature HC≡CH product peak undergoes a significant shift to lower temperature (see Figure 8). The majority of this temperature shift occurs for total $CFCl=CH_2$ exposures of 0.40 L and less. The surface Cl/Cr ratio also changes rapidly throughout this range of $CFCl=CH_2$ exposure. The increase in surface halogen content corresponds to approximately 30 % coverage of surface Cr^{3+} cations following 0.40 L of total exposure. Therefore, the shift in the low temperature acetylene feature from 350 K to 270 K is attributed to a decrease in the activation energy for molecular acetylene desorption caused by the modification of the surface by $F_{(s)}$ and $Cl_{(s)}$.

The additional HC≡CH produced during initial $CFCl=CH_2$ TDS runs is adsorbed almost entirely into the low temperature state. Figure 10 shows that the maximum amount of acetylene is produced over a surface having a total $CFCl=CH_2$ exposure of around 0.25 L and a Cl/Cr ratio of 0.055. This level of surface chlorination corresponds to approximately one-third of surface cations being covered by a 1:1 mixture of $F_{(s)}$ and $Cl_{(s)}$. Comparison of the total integrated desorption areas for reactant and product shows that the increase in desorption quantities are attributable to an increase in the sticking coefficient for $CFCl=CH_2$ on the Cr_2O_3 (10$\underline{1}$2) surface. The increase in product HC≡CH demonstrates that the surface has become "activated" toward $CFCl=CH_2$ decomposition due to an increase in the $CFCl=CH_2$ sticking coefficient. The observation that all of the additional HC≡CH made is adsorbed into the low temperature surface state indicates that the activation energy (E_a) for the surface reaction is also decreased over a partially halogenated surface. The total of desorbing species shows a sharp decline as more than one-third of surface cations becomes halogenated. The eventual decline in $CFCl=CH_2$

and HC≡CH desorption as the degree of surface halogenation increases is attributed to cation site blocking by adsorbed halogen.

No literature studies exist for acetylene or $CFCl=CH_2$ adsorption over Cr_2O_3 single-crystals in UHV, but both molecular and dissociative HC≡CH adsorption have been reported over single-crystal metal and metal oxide surfaces [13, 71]. Vohs and Barteau [72] reported that HC≡CH is adsorbed over ZnO (000$\underline{1}$) in both molecular and dissociated states. The molecularly bound state is reported to desorb at around 200 K. Dissociative HC≡CH adsorption results in the formation of a surface acetylide (HC≡C-) that is stable until decomposition to CO, CO_2, and water occurs at 780 K. The thermal stability of this acetylide is much higher than observed for the 270 K – 350 K desorption-limited acetylene feature. The lower thermal stability, the absence of surface carbon in AES experiments, and the lack of CO, CO_2, and water in thermal desorption indicate that the adsorbed species is not an acetylide and suggests a simple molecular acetylene adsorbate.

3.4.2 High Temperature (470 K) Acetylene Product

The absence of a 470 K feature in the TDS spectra of dosed acetylene demonstrates that desorption via this high temperature channel is reaction-limited. As the intensity of the 470 K feature declines during surface deactivation, no significant change in peak desorption temperature is observed. The constant peak temperature suggests first-order desorption kinetics. The first-order activation energy for desorption from this state is about 125 kJ/mole using the Redhead method, and assuming a normal first-order pre-exponential of 10^{13} s^{-1} [52].

The surface intermediate associated with the reaction-limited production of acetylene cannot be definitively identified with only TDS and AES data. However, the properties of $CFCl=CH_2$ along with precedents from the organometalic literature [73, 74, 76, 78, 79] can provide some insight into possible reaction pathways, surface intermediates, and rate limiting steps. Table 4.1 shows the bond dissociation energies for $CFCl=CH_2$, predicted from CBS-Q calculations with Gaussian 94 [75]. The weakest bond in $CFCl=CH_2$ is the C-Cl bond, regardless of whether homolytic or heterolytic bond cleavage is considered. Also, it has been demonstrated using AES that the decomposition

Table 3.1 Predicted Bond Dissociation energies for $CFCl=CH_2$.

Products	**Bond Dissociation Energies***
$CH_2=CF + Cl$	403 kJ/mol
$CH_2=CCl + F$	507 kJ/mol
$CFCl=CH + H$	480 kJ/mol
$CH_2=CF^+ + Cl^-$	900 kJ/mol
$CH_2=CCl^+ + F^-$	965 kJ/mol

*CBS-Q energies from Gaussian 94 [75]

of $CFCl=CH_2$ deposits chlorine on the sample. Given these facts, it is reasonable to assume that the initial reaction step is the dissociative adsorption of $CFCl=CH_2$ at a Cr^{3+} cation via carbon-chlorine bond cleavage. Homolytic bond cleavage is expected based upon analogy to the work of Gellman and coworkers [114, 115]. They report homolytic carbon-chlorine bond cleavage for the adsorption of several halo-ethanes over Pd (111). Cleavage of the C-Cl bond upon dissociative adsorption is expected to result in the formation of a surface fluorovinyl species ($-CF=CH_2$) and adsorbed chlorine, each attached at a cation site.

Following dissociative adsorption of $CFCl=CH_2$, the reaction is postulated to proceed via α-fluorine elimination to a vinylidene surface intermediate and adsorbed fluorine. The Group (VI) transition metals chromium, molybdenum, and tungsten are known to form vinylidene complexes [76], and α-elimination of halogen from 1-halo-olefins is a well-known method of preparing these organometalic complexes [77, 78]. The final reaction step requires the rearrangement of vinylidene to acetylene via a 2,1–hydrogen shift.

The acetylene product in both the desorption-limited and reaction-limited states is assumed to be made via the same overall surface mechanism, though the rate-limiting steps are different. For the low temperature reaction channel, the desorption of molecular

acetylene is the rate-limiting step, and hydrogen rearrangement was assigned above as occurring on the surface. In the high temperature channel, whether the surface vinylidene desorbs as a carbene ($H_2C{=}C$**:**) and rearranges to HC≡CH in the gas phase, or a 2,1-hydrogen shift occurs on the surface is uncertain. Carbenes have been postulated as surface intermediates in the hydrogen-for-halogen exchange reactions of some halo-alkanes catalyzed by palladium supported on carbon [79]. The proposed overall mechanism for $CFCl{=}CH_2$ decomposition on the nearly stoichiometric Cr_2O_3 (10$\underline{1}$2) surface is represented below.

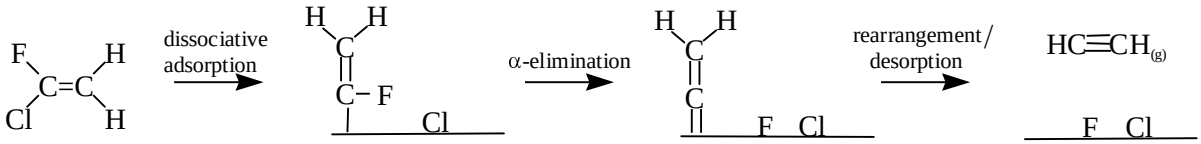

Likely surface intermediates for the above mechanism are shown below. The mechanism proceeds through an adsorbed fluorovinyl species (**a**) to form a vinylidene surface intermediate (**b**) via α-fluorine elimination. The exact coordination of the surface vinylidene can not be determined from this study, although the vinylidene complex shown below is considered most likely based upon the known ability of chromium to form vinylidene complexes and by analogy to the organometalic literature [76, 78].

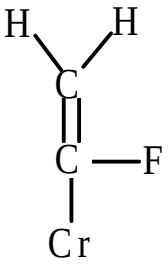

(a)

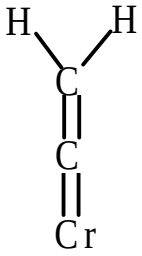

(b)

The rate-limiting step for the 470 K reaction channel must be a step prior to the formation of molecular acetylene, which would desorb at 350 K. In the mechanism proposed above, both α-fluorine elimination and hydrogen rearrangement are possible rate-limiting steps for the high temperature channel. If fluorine elimination from the α-carbon of the adsorbed fluoro-vinyl (**a**) is rate limiting, then the process will have first-order desorption kinetics, as observed in the 470 K acetylene desorption peak. The rearrangement/desorption to form HC≡CH may occur by three possible pathways to form gas-phase acetylene, and each pathway contains possible first-order and rate-limiting steps, as shown below.

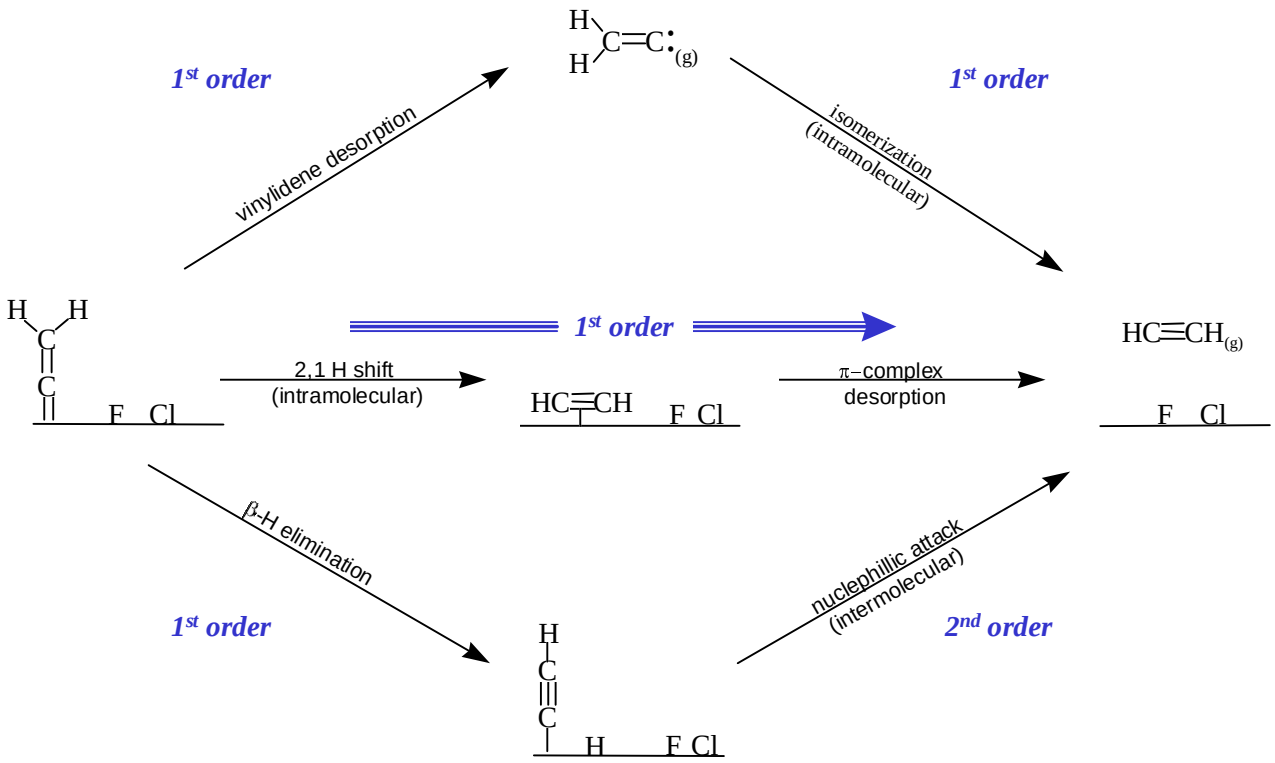

If the surface reaction proceeds through a vinylidene as proposed, then a hydrogen rearrangement must occur to form the acetylene molecule (HC≡CH). Gas phase isomerization and surface rearrangement steps may be envisioned to achieve the hydrogen shift. While the observation of a first-order, desorption-limited acetylene peak at 350 K implies that hydrogen rearrangement can occur on the surface, the possibility of gas-phase rearrangement at 470 K cannot be disregarded. First-order desorption kinetics are expected for vinylidene desorption. Vinylidene desorption followed by gas-phase isomerization to acetylene is represented in the top pathway shown above.

Assuming the rearrangement of vinylidene does occur on the surface at 470 K, then two possibilities must be considered.

1. β-hydride elimination (acetylide formation) followed by hydrogen addition to the α-carbon to form HC≡CH.
2. An intramolecular 2,1-hydrogen shift to form HC≡CH, which immediately desorbs

Surface rearrangements (1) and (2) are represented in the above drawing by the lower and middle pathways, respectively. Each possible pathway is considered below.

An intermolecular rearrangement to acetylene via surface acetylide (1) is shown by the lower pathway in the above drawing. TDS data indicate that the rate-limiting step is first order. Therefore, β-hydride elimination must be rate limiting if the isomerization is intermolecular. Vohs and Barteau [72] report the formation of an acetylide species following acetylene adsorption at 160 K on ZnO (0001). However, the acetylide decomposes at 780 K to CO, CO_2, and H_2O. In unpublished work from this group [86], TDS experiments using $CFCl=CH_2$ co-adsorbed with D_2 were performed in an attempt to identify a possible recombination step. The presence of DC≡CH would demonstrate that the reaction mechanism proceeds through an acetylide intermediate, recombining with surface hydrogen prior to desorption. No DC≡CH was detected in either the low temperature or high temperature states, suggesting that a recombination step is not involved. However, the results are not completely conclusive because D_2 desorbed at 285 K, well below the 470 K reaction temperature. Because no decomposition products (CO, CO_2, H_2, or surface carbon) are observed and because no DC≡CH was observed, acetylide formation (*i.e.* intermolecular rearrangement) is considered less likely than intramolecular rearrangement.

The reverse of the intramolecular hydrogen shift (2) proposed above has been observed on the metals palladium, and platinum by adsorption of acetylene gas followed by a 1,2-hydrogen shift to form surface vinylidene [80, 81, 82]. While vinylidene species have been identified on metal surfaces, they are consistently reported to decompose rather than desorb [83, 84, 85, 80]. Ormerod *et al.* [80] reported that vinylidene formed following acetylene adsorption on Pd (111) decomposes at 480 K, virtually identical to the 470 K peak desorption temperature observed for the high temperature acetylene feature. If the surface reaction proceeds via an intramolecular rearrangement, as shown in the middle pathway, then the rate-limiting step must be either molecular rearrangement or α-fluorine elimination. A literature precedent for a rate-limiting step in this instance could not be found.

Based upon the preceding discussion, an intramolecular 2,1-hydrogen shift from surface vinylidene to adsorbed acetylene is considered the most likely pathway for hydrogen rearrangement. A limited capacity for backbonding by Cr^{3+} cations on the nearly stoichiometric Cr_2O_3 (10$\underline{1}$2) surface has been indicated by previous TDS experiments using CO [86]. The low activation energy for desorption (50 kJ/mol) for the well-known electron acceptor CO, indicate that the surface-adsorbate interaction is predominantly sigma and that backbonding is minimal from the nearly stoichiometric surface. The literature [27, 71] clearly demonstrates that electron density donated to an adsorbed vinylidene through backbonding with metal centers tends to weaken the C=C bond, as evidenced by an increase in the C=C bond distance. It is suggested that the lack of backbonding from Cr_2O_3 (10$\underline{1}$2) may favor the rearrangement/desorption of an adsorbed vinylidene over the complete decomposition of the species, as observed on metal surfaces.

3.4.3 $CFCl=CH_2$ Desorption

The low peak desorption temperature (180 K – 200 K) for $CFCl=CH_2$ suggests that this desorption feature is associated with a molecular surface species. Freund and coworkers [63, 64] have studied the adsorption of ethene in UHV on Cr_2O_3 (0001) films. Following doses of 0.1 L they reported an ethene peak desorption temperature of 220 K. Freund and coworkers used RAIRS, EELS and XPS to argue that molecular ethene is

bound via a π-complex to the Cr_2O_3 (0001) surface at five-coordinate Cr^{3+} sites. Based upon the similar desorption temperatures, it is suggested that $CFCl=CH_2$ also forms a molecular surface species at cation sites on Cr_2O_3 (10$\underline{1}$2). The first-order activation energy for desorption for this complex is approximately 46 kJ/mol, as calculated by the Redhead method [52] assuming a normal first-order pre-exponential of $10^{13}s^{-1}$.

Following initial doses of 0.03 L over a nearly stoichiometric surface, molecular $CFCl=CH_2$ desorbed at around 180 K. Following a total exposure of 0.10 L, the $CFCl=CH_2$ peak desorption temperature shifts to 200 K while the amounts of both reactant and acetylene product are observed to increase. It seems apparent that the increase in $CFCl=CH_2$ desorbed is the result of an increased sticking coefficient. The 20 K upwards shift in $CFCl=CH_2$ peak desorption temperature indicates an increase in the heat of adsorption (ΔH_{ads}). Both of these effects are attributed to the deposition of a favorable amount of halogen (approximately one-third cation coverage) on the sample surface.

Interestingly, Freund and coworkers [63-66] found that for sub-monolayer coverage of sodium, the strength of the chromium-ethene interaction was "slightly" increased. They suggested that charge redistribution at the surface is caused by the presence of sodium, and alters the ethene bonding mode from the π-complex suggested over a stoichiometric surface to a di-σ complex at a single surface cation [63]. The stronger surface-adsorbate interaction in the presence of sodium was attributed to a through surface effect because it was found that sodium coverage of a monolayer or more would block all ethene adsorption, except at surface defect sites.

Several comparisons may be drawn between the work of Freund and coworkers [63, 64] and the effect of surface halogen upon $CFCl=CH_2$ desorption from Cr_2O_3 (10$\underline{1}$2). The molecularly adsorbed states of ethene and $CFCl=CH_2$ at five-coordinate Cr^{3+} sites are proposed to be similar π-complexes having approximately the same molecular orientation and surface bond strength. In addition, when approximately one-third of surface Cr^{3+} cation sites are capped by adsorbed halogen, a slight stabilization of $CFCl=CH_2$ at neighboring Cr^{3+} cation sites occurs. TDS experiments demonstrate this stabilizing effect by the increase (20 K) in the $CFCl=CH_2$ peak desorption temperature, and by the observed increase in $CFCl=CH_2$ sticking coefficient. It is suggested that this

effect is due to the redistribution of charge at the Cr_2O_3 (10$\underline{1}$2) surface caused by halogen deposition, as proposed by Freund [63] for sodium adsorption on Cr_2O_3 (0001). The difference in ionic charges expected for sodium and chlorine adatoms make their similar effect upon surface-adsorbate interaction surprising. The nature of this through surface effect is not understood.

After TDS experiments reach a total $CFCl=CH_2$ exposure of 1.0 L or greater, the surface is completely deactivated and the $CFCl=CH_2$ molecular feature at 180 K no longer contains any significant contribution from the 200 K feature observed at lower total exposures. AES experiments suggest that site blocking by both chlorine and fluorine is responsible for the eventual deactivation of the surface during $CFCl=CH_2$ TDS. Site blocking was also reported by Freund and coworkers [63] as the reason for the attenuation of ethene adsorption at monolayer coverage of chlorine and sodium on Cr_2O_3 (0001). The decrease in total desorption from a halogen-saturated (deactivated) surface relative to the nearly stoichiometric surface is an indication of site blocking by chlorine adatoms.

3.4.4 Cr_2O_3 (10$\underline{1}$2) Surface Activity

The amount of product HC≡CH formed during a TDS series of consecutive $CFCl=CH_2$ doses (0.03 L – 0.13 L) increased initially and then steadily declined. For the series of 0.06 L $CFCl=CH_2$ doses shown in Figure 8 (bottom), the product HC≡CH maximum occurs at 0.19 L, and the increase is associated only with the desorption-limited acetylene peak. The maximum in acetylene production corresponded to approximately one-third coverage of surface cations by adsorbed halogen. The "activating" effect of halogen adsorption for $CFCl=CH_2$ decomposition in this case is most simply explained as a through-surface effect that increases the strength of the Cr^{3+}-$CFCl=CH_2$ interaction at neighboring cations sites and lowers E_a for $CFCl=CH_2$ decomposition to acetylene. This suggests the existence of an optimal surface ensemble consisting of bare Cr^{3+} sites in combination with neighboring halogenated cations in approximately a 2:1 ratio. Halogenation of the surface beyond the optimal halogen content blocks available cations sites and eventually causes surface deactivation.

The necessity of a surface activation period before Cr_2O_3 microcrystalline powders become active for halogen exchange has been well documented in the literature [97, 98, 102, 105]. Activation of the Cr_2O_3 catalyst in these cases has been attributed to the reduction of high-valent chromium species to Cr^{3+} followed by the formation of chromium halides at the surface via oxidation of the HCFC gas. Coulson and coworkers [98] have reported that the reduction of high-valent chromium ions to produce coordinately unsaturated Cr^{3+} cations is the initial step in the catalyst activation process. The lack of activity observed for the oxygen-saturated Cr_2O_3 (10$\underline{1}$2) surface in this work is in agreement with the suggestion of Coulson and coworkers as it demonstrates that coordinately-unsaturated Cr^{3+} centers are also a prerequisite for $CFCl=CH_2$ decomposition to acetylene. $CFCl=CH_2$ exposures under TDS conditions are not capable of reducing oxide-terminated surface cations (chromyl species) on the oxygen-saturated Cr_2O_3 (10$\underline{1}$2) surface [86].

Coulson and coworkers [98] have studied the disproportionation of CHF_2Cl over a microcrystalline Cr_2O_3 catalyst. They reported that coordinately unsaturated Cr^{3+} cations formed during the initial reduction step were active for the oxidation of CHF_3, and CHF_2Cl to CO, CO_2, HF, and H_2O. They also observed the simultaneous uptake of halogen by the surface during oxidation, and suggested that the replacement of surface lattice oxygen by halogen makes the surface active for CHF_3 and CHF_2Cl disproportionation [98]. Kemnitz and coworkers [102] have reported similar results for CF_2Cl and CHF_2Cl exposures over Cr_2O_3 microcrystalline powders. No evidence for the replacement of lattice oxygen by chlorine or fluorine was observed over the Cr_2O_3 (10$\underline{1}$2) surface under the conditions of this study.

Coulson and coworkers [98] also demonstrated that the disproportionation of CHF_2Cl was inhibited over catalysts that were pre-exposed to the Lewis base dimethyl ether. They found that the uptake of dimethyl ether is directly proportional to the activity of the catalyst for disproportionation, suggesting that an increase in Lewis acidity is coincident with the onset of catalytic activity. They also report that Lewis acidity is greatest for cation sites that had been fluorinated and remained coordinately unsaturated. An increase in site Lewis acidity resulting from surface halogenation is also indicated over Cr_2O_3 (10$\underline{1}$2) in this work by the 20 K increase in the $CFCl=CH_2$ desorption

temperature following partial halogenation of a nearly stoichiometric surface. If the Cr^{3+}-$CFCl=CH_2$ bonding interaction is predominantly a sigma donation, as described above, then the increase in $CFCl=CH_2$ desorption temperature can be attributed to an increase in Lewis acidity at neighboring unhalogenated Cr^{3+} sites. In this work, the increase in active site Lewis acidity is limited to the "through-surface" effect because once halogenated, a Cr^{3+} cation is fully coordinated, and is no longer active for $CFCl=CH_2$ decomposition to acetylene.

Kemnitz and coworkers [102] studied chlorine/fluorine exchange reactions for various two-carbon HCFC compounds over powdered Cr_2O_3. They attributed the onset of activity to the formation of an active crystalline phase at the surface, which resembles β-CrF_3 in structure. They proposed active surface sites for fluorination contain fluorinated Cr^{3+} cations that are coordinately unsaturated, and are strong Lewis acids. The halogenated Cr_2O_3 (10$\underline{1}$2) surface would not be expected to demonstrate activity based upon analogy to the work of Kemnitz and coworkers [102] because the halogenated Cr^{3+} sites are fully coordinated and inaccessible to adsorbing HCFC molecules.

While the reactions involved during the "activation" treatments are ill-defined in the literature, most work in the area concludes that Cr_2O_3 powders are only active toward HCFC fluorine-for-chlorine exchange (fluorination) reactions over fluorinated cation sites [98, 102, 106]. It seems clear that the reactivity of $CFCl=CH_2$ observed over the nearly stoichiometric Cr_2O_3 (10$\underline{1}$2) surface is due to the presence of five-coordinate Cr^{3+} cations. It is suggested that the decomposition of $CFCl=CH_2$ and similar HCFC compounds may play a role in the deposition of halogen on the Cr_2O_3 surface during the "activation" of Cr_2O_3 catalysts for halogen exchange reactions [98, 99, 102, 106].

Surface deactivation has also received much attention in literature studies of halogen exchange over Cr_2O_3 powders. Deactivation of powdered Cr_2O_3 catalysts has been attributed to carbon deposition [4], and to the formation of inactive crystalline phases at the surface that sterically isolate cations from the surface [102]. In this work, it is apparent from the AES data that deactivation of the Cr_2O_3 (10$\underline{1}$2) surface toward $CFCl=CH_2$ decomposition occurs due to site blocking because nearly 100% of surface cations are coordinated to adsorbed halogen on a deactivated Cr_2O_3 (10$\underline{1}$2) surface. No

carbon was detected on surfaces that were deactivated by $CFCl=CH_2$ exposure under any conditions.

3.5 Conclusions

The 1,1-dihalo-elimination reaction of $CFCl=CH_2$ over a nearly stoichiometric Cr_2O_3 (10$\underline{1}$2) surface has been investigated under UHV conditions. The products are acetylene gas and adsorbed chlorine and fluorine. Thermal desorption experiments revealed two acetylene desorption features. The lower energy state is desorption-limited (E_a= 92 kJ/mole) while the formation of a stable vinylidene surface intermediate is suggested by the occurrence of a higher energy (E_a= 124 kJ/mole) reaction-limited acetylene desorption peak. The deposition of halogen onto the sample surface by the $CFCl=CH_2$ decomposition reaction initially increased the $CFCl=CH_2$ sticking coefficient, and "activated" the surface towards $CFCl=CH_2$ decomposition. Halogen coverage of more than approximately 30% of surface cations decreases surface activity and ultimately leads to deactivation of the surface due to site blocking.

The Cr_2O_3 (10$\underline{1}$2) surface ceased $CFCl=CH_2$ decomposition at a Cl/Cr ratio of around 0.16, under TDS conditions. AES and TDS data suggest that chlorine and fluorine are deposited at an equal rate during TDS experiments, as reaction stoichiometry predicts. No evidence was seen for the replacement of surface lattice oxygen by halogen, and no carbon was detected on the deactivated surface. Surfaces that were pre-exposed to oxygen did not react with $CFCl=CH_2$.

Chapter 4

Reactions of 1, 1, 2-trichloro-1-fluoroethane over the Cr_2O_3 (10$\underline{1}$2) Surface

4.1 Introduction

The reactions of halo-substituted alkanes have been more studied than their unsaturated counterparts. The research is largely motivated by the vapor-phase manufacture of HFC compounds, especially environmentally conscious (low ODP) refrigerants, or by the destruction of their chlorine containing analogs (HCFCs) [4, 61, 87, 88]. The halocarbon reactions most commonly reported over Cr_2O_3 are summarized in Table 2.

Table 4.1 Halocarbon reactions reported to occur over Cr_2O_3.

HF addition to C=C double bond	Dominant reaction in the presence of HF
Halogen Exchange	Replacement of Cl by F is usually the desired reaction and is favored in the presence of HF.
Dehydrohaolgenation (HF and HCl removal)	Reaction may occur in the presence and absence of HF.
Disproportionation (dismutation)	Presence of HF not required.
Isomerization	Presence of HF not required.

Rowley, Webb, Winfield, and coworkers [89-92] have studied the interaction of halogen compounds with Cr_2O_3 microcrystalline powders using radiolabeled HF, HCl, and halocarbon compounds. They unambiguously demonstrated the uptake of halogen by Cr_2O_3 during the initial "activation" phase of reaction. They found that ^{36}Cl and ^{18}F could be deposited on both untreated and pre-halogenated Cr_2O_3 catalyst by exposure to HX or HCFC compounds at 623 K, and they inferred the presence of at least two surface species for both chlorine and fluorine [89, 90]. It was also reported that Cl and F were capable of replacing one another on the surface, and exchanging halogen between the

surface and adsorbed trichloro-trifluoroethane (HCFC-113) isomers [92]. The resulting halogen exchange sequence yielded a mix of HCFC compounds over both untreated and halogenated Cr_2O_3 catalyst.

Rowley *et al.* [89, 91] also reported that fluorination and chlorination reactions occur with the compounds trichloro-trifluoroethane and dichloro-tetrafluoroethane (isomer mix) over pre-halogenated Cr_2O_3 powder, and report that surface ^{36}Cl and ^{18}F are incorporated into these compounds via direct halogen exchange with a surface $(HF)_n$-HX oligomer species. Catalysts that were pretreated with $H^{18}F$ or $H^{36}Cl$ quickly accumulated radiolabeled chlorine and fluorine following exposures at 700 K. The trichloro-trifluoroethane and dichloro-tetrafluoroethane reactants formed fluorination and chlorination products containing radio labels from surface halogen sites [91]. Interestingly, isomerization of $CFCl_2CF_2Cl$ to CCl_3CF_3 occurred over fluorinated Cr_2O_3, but without radiolabeled halogen being introduced into the isomerized product. Because of the lack of radiolabeled $CFCl_2CF_2Cl$, Rowley and coworkers [91] postulated that the $CFCl_2CF_2Cl$ isomerization reaction is intramolecular.

The work of Webb, Winfield, and coworkers [5, 89-92] demonstrates that different Cr-X species exist at the Cr_2O_3 surface, and that at least one species is inactive toward fluorination reactions. They also suggested that different reactions such as halogen exchange, isomerization, and HX abstraction might occur at different surface sites [90, 91]. These observations are repeated throughout the scientific and patent literature concerning halocarbon reactions over Cr_2O_3, as well as other materials used for halogen exchange processes [4, 5, 60, 93].

Blanchard and coworkers have also studied the trichloro-trifluoroethane/Cr_2O_3 system. The early work from this group focused on the disproportionation and isomerization of $CFCl_2CF_2Cl$ to CCl_3CF_3 over Cr_2O_3 powder, supported Cr_2O_3, and AlF_3 [94, 95, 97]. They found that disproportionation and isomerization reactions dominate over Cr_2O_3 in the absence of HF. Bechadergue *et al.* [94, 95] reported that halo-alkanes having more chlorine contain more reactive C-X bonds. They also observed that pre-treating the surface with pyridine, a Lewis base, inhibits surface activity, indicating that Lewis acid sites (cation centers) are important to the reaction mechanism [94]. The presence of small amounts of the unsaturated impurities $CCl_2=CCl_2$ and $CFCl=CCl_2$ were

also reported in the product mix. Interestingly, the asymmetric HCFC-113a (CCl_3-CF_3) molecule was reported to decompose to form chromium carbide on the surface, leading to surface deactivation. The presence of Cr-F sites was deemed unnecessary to carry out disproportionation and isomerization reactions over Cr_2O_3 [95].

Later work from Blanchard and coworkers [61] focused a broader spectrum of halocarbon surface reactions including disproportionation, isomerization, dehalogenation, dehydrohalogenation, and halogen exchange. They reported that halogen exchange dominates in the presence of HF, but that disproportionation, isomerization, and dehydrochlorination occurs with out HF [96]. It was speculated that fluorination, in the presence of HF, was governed by the acidity of the catalyst.

Blanchard and coworkers [97, 105] also reported that the catalytic activity of powdered Cr_2O_3 catalyst for the fluorination of CF_3CH_2Cl to CF_3CH_2F is a function of the number of reversibly oxidizable chromium sites on the catalyst surface, and that the catalytically active site is a Cr-F surface species on a partially fluorinated catalyst. They also postulate that the fluorination of CF_3CH_2Cl occurs via fluorine for chlorine exchange between HF oligomers on the surface and co-adsorbed CF_3CH_2Cl molecules. No specifics concerning the catalyst surface were offered, but it was suggested that the thermal history of the sample plays an essential role in determining the number of active sites present [97]. Catalytic activity for fluorination was only reported over partially fluorinated Cr_2O_3 catalyst. XPS measurements of fluorine uptake by the catalyst following exposures to HF and CF_3CH_2Cl yielded a maximum F/Cr ratio of 0.36, regardless of the treatment gas used [105].

Other authors have postulated that the oxidation state of surface ions plays a crucial role in determining surface activity. Based on product distribution and thermal desorption data, Coulson *et al*. [98] propose that the reduction of high-valent chromium ions to Cr^{3+} is necessary to create active sites for the disproportionation of CHF_2Cl over powdered Cr_2O_3 microcrystalline catalyst. They argue that the active site is a coordinately unsaturated Cr-X center, which acts as a strong Lewis acid. Following exposures at 773 K, Coulson and coworkers [98] report atomic percentages that correspond to F/Cr ratios of 0.22 and 0.30 for CHF_3 and HF, respectively. It was also suggested that the sites responsible for disproportionation of HCFC compounds are also

responsible for fluorination reactions, an important reaction in the manufacture of HFC-134a.

Kohne and Kemnitz have studied several HCFC/Cr_2O_3 systems, with the intent of identifying the reaction pathway from trichloroethene to CF_3CH_2F (HCFC-134a) in the presence of HF. Experimental evidence and thermodynamic calculations were offered that indicated CF_3CH_2Cl is the most stable of the HCFC intermediates in this pathway [99]. They found that both direct halogen exchange as well as HX abstraction/addition reactions occur over fluorinated Cr_2O_3 catalyst in the presence of HF at 573 K. The primary products for the reaction of trichloroethene with HF were reported to be $CFCl_2CH_2Cl$, CF_2ClCH_2Cl, and CF_3CH_2Cl. Significant amounts of unsaturated halo-alkenes were also found in the product mix, even in the presence of HF. Kohne and Kemnitz [99] argue that the product mix is the result of a sequence of reactions.

1. dehydrohalogenation (HX abstraction) reactions, followed by
2. hydrohalogenation (HX addition-Markovnikov addition not required), and
3. direct halogen exchange between surface and adsorbate.

Isomerization and disproportionation reactions may be disregarded, claim Kohne and Kemnitz, with or with out HF present in the reaction mix. A significant degree of CF_3CH_2Cl fluorination to CF_3CH_2F was observed only in the presence of a large excess HF [99].

Kemnitz and Niedersen [100] have also reported on the isomerization reaction of CHF_2CHF_2 to CF_3CH_2F (HCFC-134a) over fluorinated Cr_2O_3, without HF. They propose that isomerization reactions occur in two steps, a departure from the conclusions of earlier work in the area [91]. From deuterium labeling experiments, it was concluded that if chlorine could be excluded from the reacting system, then the isomerization reaction proceeds through HF elimination and subsequent HF addition by the Markovnikov rule. The presence of HCl or any chlorine containing halocarbons produced a “complex set of side reactions” [100].

Niedersen *et al.* [101] propose that Lewis acid sites are responsible for the CHF_2CHF_2 to CF_3CH_2F isomerization activity of Cr_2O_3. They used IR and UV-vis spectroscopy of adsorbed CO and NH_3 to argue that Lewis acid sites are responsible for the isomerization. Using IR of adsorbed CO as a probe of the valence states and coordination numbers of surface chromium cations for various surface preparations, they

report that five-coordinate Cr^{3+} is predominant on a fresh Cr_2O_3 catalyst, and that fluorination creates active isomerization sites by formation of CrF_3 which increases the Lewis acidity of the cation.

Changes to Cr_2O_3 that result from "activation" and fluorination were studied by Kemnitz and coworkers [102] using XPS and x-ray excited AES to compare catalyst samples to Cr- and Al-fluoride standards. They argued that pretreatment of Cr_2O_3 by either HX or HCFCs causes the formation of α- and β-CrX_3 phases. The nature of these sites was determined to be independent of the halogen source, in agreement with the work of Rowley *et al*. [89]. Kemnitz *et al*. postulated that coordinately unsaturated (Lewis acid) Cr^{3+} ions are exposed in the β-CrF_3 structure, and suggested that the Lewis acidity of these sites is responsible for their catalytic activity. The α-CrF_3 phase, it was proposed, is inactive because the Cr^{3+} ions are sterically isolated from adsorbates on the surface. They also proposed that all surface activation (*i*.e. halogen deposition) reactions occur via HX elimination, and that over a clean surface HCFC compounds decompose to CO_2, HF, and HCl, which in turn halogenate the surface [102]. Interestingly, Kemnitz *et al*. report that the total amount of halogen uptake (Cl and F) by the surface is constant, regardless of the pretreatment gas used [89, 102]. Kemnitz *et al*. reported a X/Cr ratio of 0.43.

The literature on Cr_2O_3 contains much speculation concerning the reason for the eventual deactivation of the catalyst toward fluorination reactions. However, a clear picture of Cr_2O_3 deactivation has not emerged. Coke formation caused by the degradation of various HCFC compounds is often reported as the cause of surface deactivation [4]. Niedersen *et al.* [101] reported that surface coke may be burned off in the presence of O_2 at 673 K. The formation of halocarbon oligomers and structural changes to the surface have also been cited as mechanisms for surface deactivation [97, 102]. Changes to the oxidation state of surface cations have also been postulated as a cause for surface deactivation [97, 98].

4.2 Experimental

PCR 1,1,2-trichloro-1-fluoroethane ($CFCl_2CH_2Cl$) (97 %), PCR 1-Chloro-1-fluoroethene ($CFCl=CH_2$) (97 %), and Matheson acetylene ($HC\equiv CH$) (99.6 %) were used

as received. $CFCl_2CH_2Cl$ (HCFC-131a) is a liquid at room temperature and atmospheric pressure, therefore introduction of this compound into the UHV system was accomplished by filling a stainless steel tube with HCFC-131a liquid and attaching it to the gas distribution manifold. All dose sizes have been corrected for ion gauge sensitivity [41], and desorption quantities have been corrected for mass spectrometer sensitivity [103].

The reaction of $CFCl_2CH_2Cl$ over the nearly stoichiometric (1×1) Cr_2O_3 (10$\underline{1}$2) surface was investigated using thermal desorption spectroscopy (TDS), Auger electron spectroscopy (AES) and low energy electron diffraction (LEED). A nearly stoichiometric surface was prepared by ion-bombardment followed by annealing the sample to 900 K. Additional details concerning surface preparations may be found in Chapter 2. AES measurements were conducted at 800 K to avoid sample charging. Because of overlap between the primary oxygen and chromium Auger peaks, the Cl/Cr ratios were calculated using the Cr LMM (490 eV) peak-to-peak height as discussed in Chapter 2. All doses for TDS experiments were conducted at 163 K.

4.3 Results

A combination of thermal desorption and AES results for an ion-bombarded and annealed, (1×1), Cr_2O_3 (10$\underline{1}$2) surface reveals that $CFCl_2CH_2Cl$ decomposes into $CFCl{=}CH_{2(g)}$ (HCFC-1131a), acetylene ($HC{\equiv}CH_{(g)}$), and adsorbed halogen ($Cl_{(s)}$ and $F_{(s)}$). Gas-phase products were identified by comparison of mass spectrometer cracking patterns to thermal desorption peak intensities. The relative intensities of four m/z signals were used to identify both HCFC-1131a (80, 45, 26, 31) and acetylene (26, 25, 27, 13). Other products were excluded by a search that included mass numbers ranging from 2 to 200. Specifically no CO, CO_2, HCl, HF, Cl_2, F_2, chloroacetylene, fluoroacetylene, or chromium halide gas-phase reaction products were observed during TDS. No surface carbon was detected with AES following $CFCl_2CH_2Cl$ decomposition, only surface halogen was observed. The combination of TDS and AES data is used to demonstrate that the deposition of halogen leads to eventual surface deactivation.

4.3.1 $CFCl_2CH_2Cl$ Thermal Desorption

Figure 12 shows representative desorption traces for the reactant and gas-phase products following the second dose in a TDS series of consecutive 0.03 L doses of $CFCl_2CH_2Cl$. Nearly 100% of the $CFCl_2CH_2Cl$ reactant is converted to products during initial TDS runs as evidenced by the small desorption peak for the reactant molecule (black). The principal product is the halo-ethene $CFCl=CH_2$ (green), formed by a dihalo elimination reaction from $CFCl_2CH_2Cl$. The $CFCl=CH_2$ product desorption temperature is close to the desorption temperature for the $CFCl_2CH_2Cl$ reactant, suggesting a rate-limiting surface reaction involving a common surface intermediate for these two desorbing species. Acetylene (red) is also formed when $CFCl=CH_2$ total exposure is low and yields two desorption features, one at around 335 K and another around 480 K. Acetylene desorption from $CFCl_2CH_2Cl$ decomposition yields an acetylene TDS spectrum that is very similar to the spectrum obtained from dosing $CFCl=CH_2$ directly onto the sample surface (Chapter 3).

Initially, the nearly stoichiometric Cr_2O_3 (10$\underline{1}$2) surface is very reactive toward $CFClCH_2Cl$, converting nearly 100% of the reactant to products. Figure 13 shows the relative amounts of reactant and products desorbed from the surface during a series of consecutive 0.03 L doses of $CFCl_2CH_2Cl$ initiated on a nearly stoichiometric surface. Desorption quantities were calculated by integrating the area under the TDS desorption curves. The amount of $CFCl_2CH_2Cl$ desorbed from the surface is small following the first two doses, but increases significantly following 0.10 L of total exposure. The high reactivity of CF_2ClCH_2Cl over Cr_2O_3 (10$\underline{1}$2) is evidenced by the small desorption signal intensity of the reactant molecule during initial TDS runs. The ratio of CF_2ClCH_2Cl-to-$CFCl=CH_2$-to-$HC\equiv CH$ in the desorbing gases from an initial 0.03 L TDS run is 1:512:40.

As shown in Figure 13, the quantity of $CFCl=CH_2$ and acetylene desorbed remains relatively constant for the first three 0.03 L doses of $CFClCH_2Cl$, and then the amount of each rapidly declines. Acetylene production ceases at around 0.13 L of

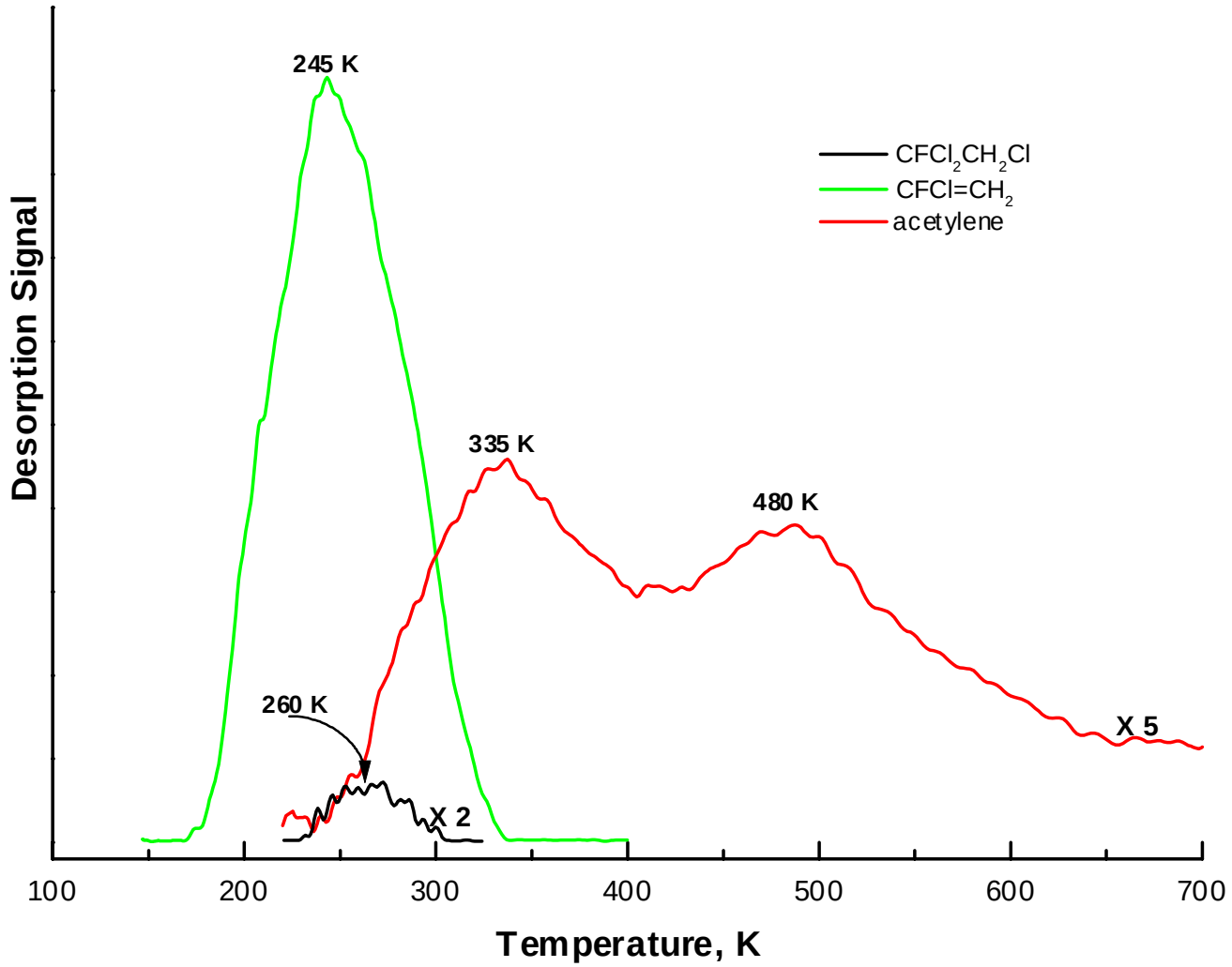

Figure 12. Desorption features observed following the second 0.03 L dose of $CFCl_2CH_2Cl$ in a TDS series. A desorption trace of the reactant ($CFCl_2CH_2Cl$) is shown in black, the reaction products $CFCl{=}CH_2$ (green), and $HC{\equiv}CH$ (red) are also shown.

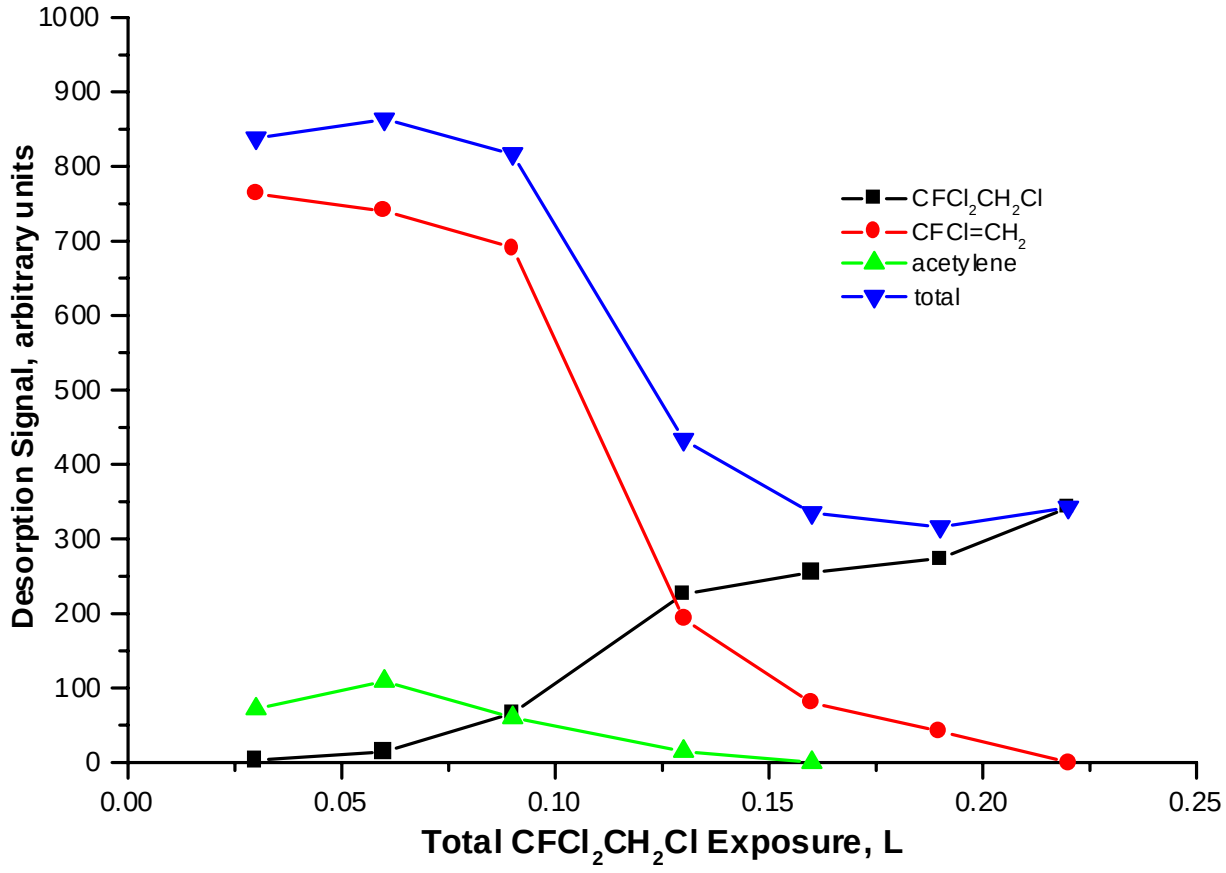

Figure 13. The relative quantities desorbed for each $CFCl_2CH_2Cl$ decomposition product, as well as the signal of the reactant molecule and total for all is shown above. The TDS experiment consisted of sequential 0.03 L doses over a sputter-annealed (1×1) Cr_2O_3 (10$\underline{1}$2) surface.

total exposure and $CFCl=CH_2$ production continues until a total $CFCl_2CH_2Cl$ exposure of around 0.22 L is reached. The decline in product quantities indicates that the surface becomes deactivated toward $CFCl_2CH_2Cl$ decomposition by a total exposure of 0.25 L. The sum of all desorbing species (blue) decreases by approximately 50% as the surface becomes deactivated, indicating a decrease in the $CFCl_2CH_2Cl$ sticking coefficient as the surface chemistry shuts down. AES data presented elsewhere demonstrate that as the amount of products detected in TDS declines, the surface Cl/Cr ratio steadily increases. This suggests that deposition of halogen onto the sample surface is responsible for surface deactivation. As quantified below, a deactivated surface contains surface halogen in a nearly one-to-one ratio with surface cations.

Figure 14 (top) and the inset show the desorption spectra of the dosed molecule, CF_2ClCH_2Cl, for the same series of consecutive 0.03 L doses shown in Figure 13. Two features are apparent in the desorption spectra of the reactant molecule: a high-temperature feature at 265 K and a lower temperature feature around 190 K – 215 K. The high-temperature contribution occurs at low total exposures and initially has a peak desorption temperature of 245 K. The high-temperature feature increases in intensity, and shifts to 265 K following the first three 0.03 L doses. Following the fourth dose, a low-temperature contribution to the $CFCl_2CH_2Cl$ desorption feature is observed around 215 K, while the high-temperature peak remains relatively unchanged, as compared to the third TDS run. In subsequent TDS runs, the high-temperature feature rapidly dies out while the low-temperature feature increases in intensity and shifts downward to around 190 K. Differences in the peak desorption temperatures and the shapes of the two CF_2ClCH_2Cl desorption features suggest that two separate desorption processes occur for the reactant molecule.

The bottom panel of Figure 14 shows desorption traces for the product $CFCl=CH_2$ formed during the same series of 0.03 L doses. The $CFCl=CH_2$ peak desorption temperature initially occurs around 240 K and shifts to 265 K prior to surface deactivation. A decrease in the signal intensity for $CFCl=CH_2$ is observed around 0.13 L as the 1,2-dihalo-elimination reaction of $CFCl_2CH_2Cl$ to $CFCl=CH_2$ shuts down. The

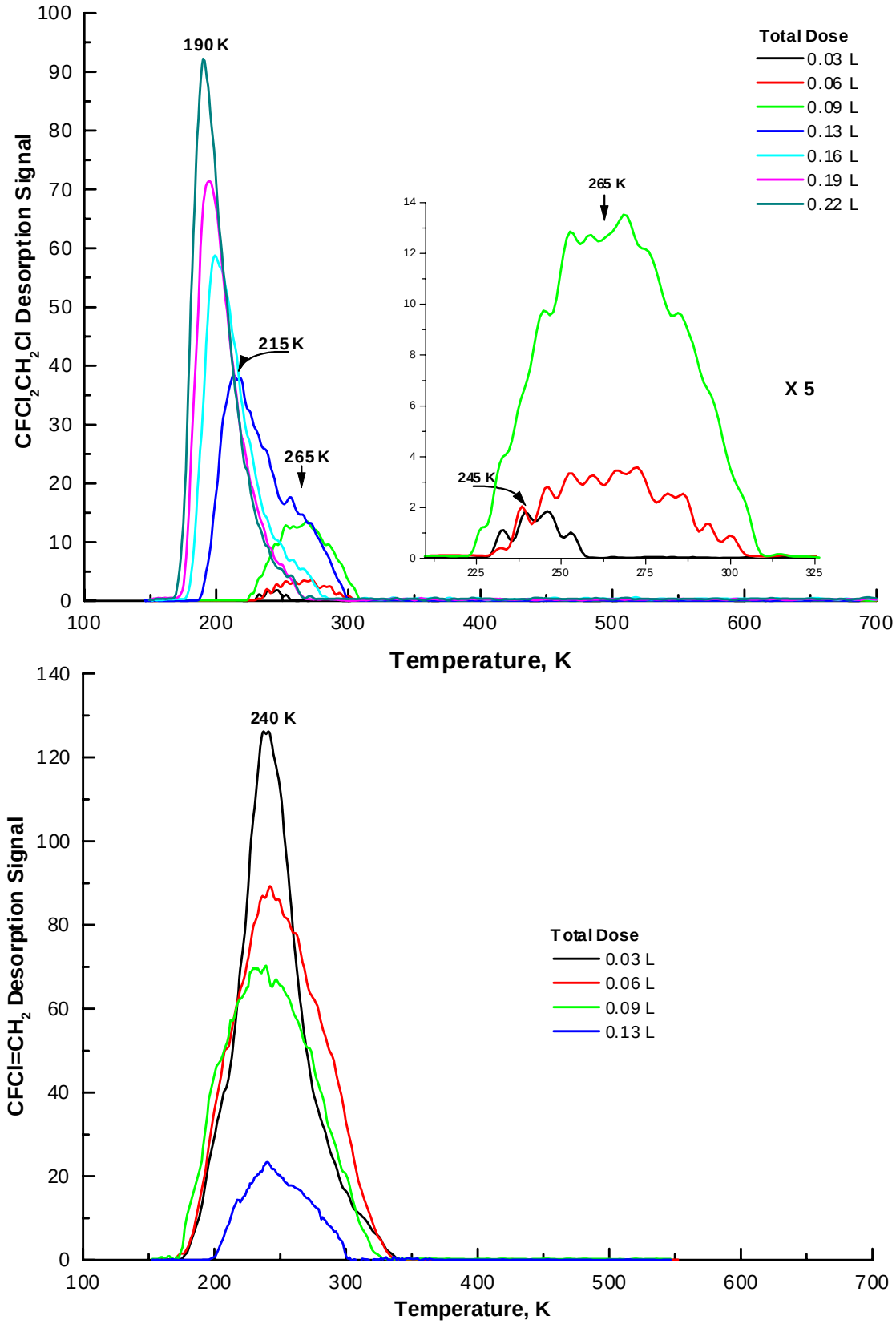

Figure 14. Desorption traces of the $CFCl_2CH_2Cl$ reactant (top) and the $CFCl{=}CH_2$ product (bottom) for a series of repeated 0.03L HCFC-131a doses over an ion-bombarded and annealed Cr_2O_3 (10$\underline{1}$2) surface.

decrease in product $CFCl=CH_2$ occurs in tandem with the increase in reactant ($CFCl_2CH_2Cl$) desorption discussed above. Additionally, the product $CFCl=CH_2$ desorption temperature is similar to that of the $CFCl_2CH_2Cl$ reactant via the high-temperature desorption channel, suggesting that these desorbing species originate from a common surface intermediate and share the same rate-limiting reaction step.

4.3.2 HC≡CH Product

Dosing $CFCl_2CH_2Cl$ onto nearly stoichiometric Cr_2O_3 (10$\underline{1}$2) yields an acetylene TDS spectrum containing two features, one around 350 K and the other around 470 K. Acetylene desorption spectra obtained from $CFCl_2CH_2Cl$ decomposition over a nearly stoichiometric surface are similar in both shape and peak desorption temperature to the acetylene formed from $CFCl=CH_2$ decomposition on a nearly stoichiometric surface (Chapter 3). However, the quantity of acetylene made from $CFCl_2CH_2Cl$ decomposition is small compared to product $CFCl=CH_2$, representing less than 10% of the total products made before the surface is deactivated.

4.3.3 Deposition of Surface Halogen

AES of the sample surface following the reaction of $CFCl_2CH_2Cl$ reveals a significant build-up of chlorine on the sample surface. The presence of product acetylene indicates that a small amount of surface fluorine should also be seen, but measuring fluorine with AES was not possible due to the rapid thermal and/or electron stimulated loss of surface fluorine. The rate of surface chlorine loss is, however, sufficiently slow to allow quantitative analysis. Figure 15 shows the AES spectrum of a Cr_2O_3 (10$\underline{1}$2) surface that has been deactivated by $CFCl_2CH_2Cl$ exposure. The spectrum gives an (AES) Cl/Cr ratio of 0.32 ± 0.01, and was collected at 800 K in order to avoid sample charging. No carbon is observed on the deactivated surface, and no evidence is seen for the replacement of lattice oxygen by halogen.

Figure 16 shows a graph of the thermal desorption product sum (right axis) and the surface Cl/Cr ratio (left axis) for a series of 0.03 L doses of $CFCl_2CH_2Cl$ initiated on a nearly stoichiometric Cr_2O_3 (10$\underline{1}$2) surface. The product sum was calculated by

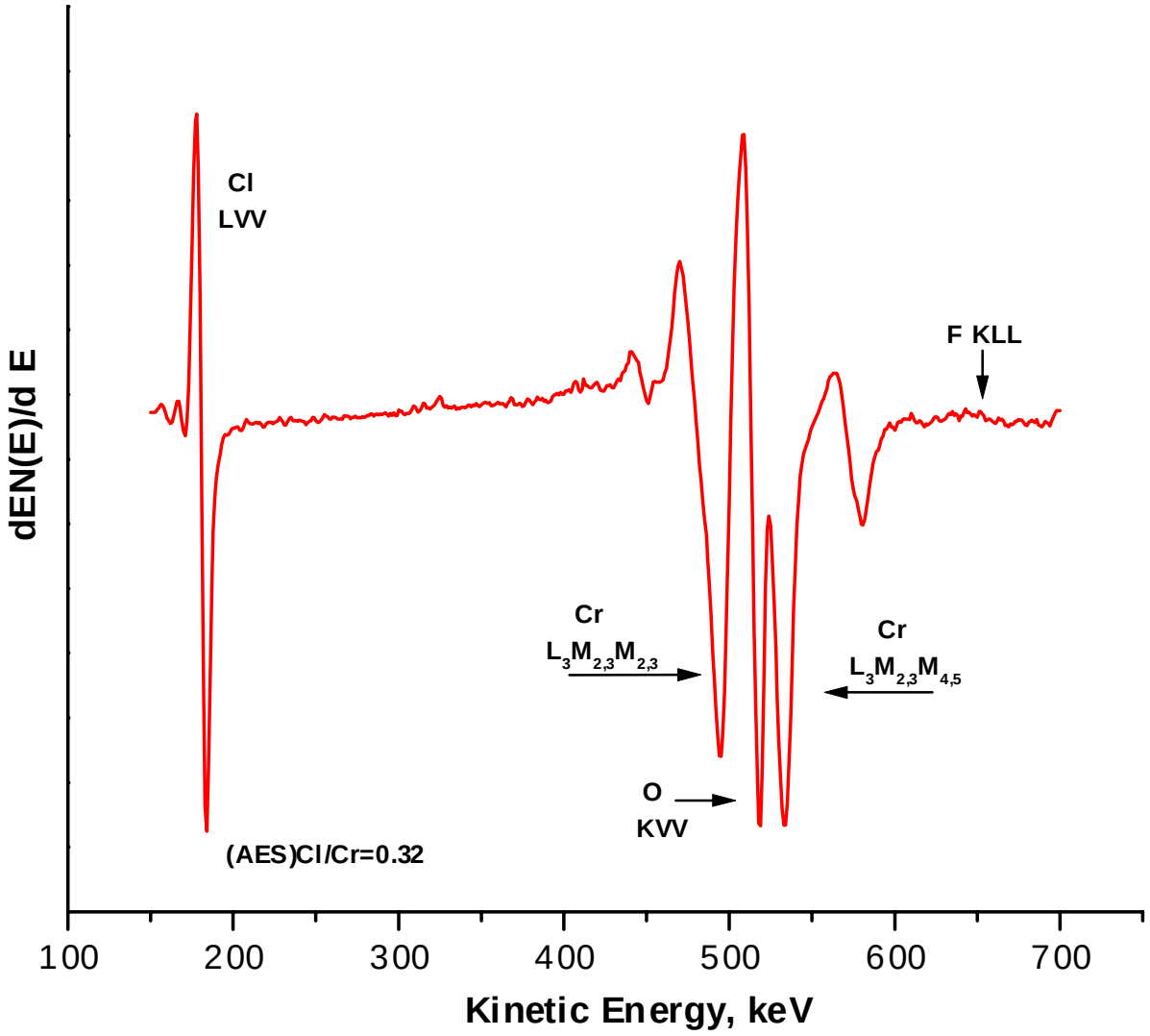

Figure 15. AES spectra of a Cr_2O_3 (10$\underline{1}$2) surface which has been deactivated by exposure to $CFCl_2CH_2Cl$ (HCFC-131a). The (AES) Cl/Cr ratio is calculated to be 0.32.

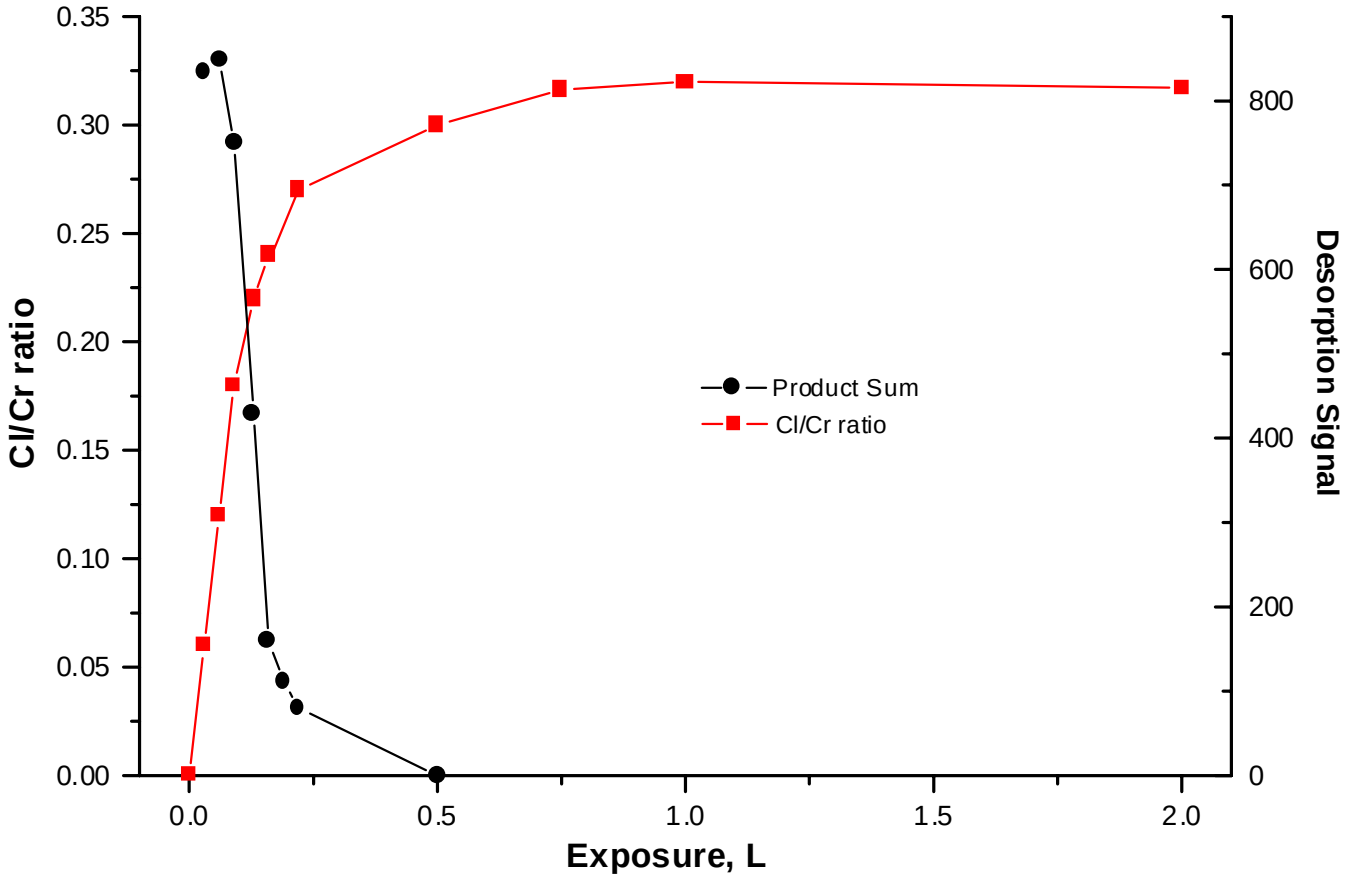

Figure 16. The quantity of products obtained from the surface ($CClF{=}CH_2$ and $HC{\equiv}CH$) and the changing surface (AES) Cl/Cr ratio are plotted versus exposure for a series of 0.03 L doses of $CFCl_2CH_2Cl$.

summing the integrated areas of the $CFCl=CH_2$ and $HC\equiv CH$ desorption curves, and correcting for mass spectrometer sensitivity [68, 69, 103]. AES spectra were collected following each TDS run. The surface Cl/Cr ratio rises rapidly and then levels off after a total exposure of around 0.75 L. The surface Cl/Cr ratio increases most rapidly for total $CFCl_2CH_2Cl$ exposures below 0.25 L, when the conversion to products is highest. As less product is made, the product sum declines and the surface Cl/Cr ratio levels off at about 0.32, suggesting that surface halogen is deposited directly by $CFCl_2CH_2Cl$ decomposition.

Due to molecular stoichiometry and product distribution, the halogen deposited onto the Cr_2O_3 (10$\underline{1}$2) surface from $CFCl_2CH_2Cl$ decomposition is overwhelmingly chlorine. Based upon the relative quantities of $CFCl_2CH_2Cl$ and $HC\equiv CH$ formed, as determined from the integrated desorption areas in TDS experiments and reaction stoichiometry, the fluorine deposited onto the surface is estimated to comprise only about 4% of the total surface halogen. Due to the small amount of fluorine present on the surface, disregarding the presence of fluorine at the halogen-saturated surface introduces an error of approximately 0.01 in the value of X/Cr. Therefore, (AES) Cl/Cr ratio of 0.32 may be regarded as an approximation of the total halogen content (X/Cr) of the halogen-saturated (deactivated) surface. Auger spectra of the sample surface following each run in a TDS series of consecutive $CFCl_2CH_2Cl$ 0.03 L doses demonstrate that the surface chlorine content progressively increases until product formation ceases. A surface deactivated by $CFCl_2CH_2Cl$ TDS yields an experimental Cl/Cr ratio of 0.32. An estimate of the Cl/Cr for a surface containing one adsorbed chlorine per five-coordinate surface cation was made by using an exponential AES signal decay model. An electron mean free path of 9 Å was used in this calculation and was estimated from a universal curve found in the literature [53]. Based on the (1x1) LEED pattern observed for a chlorinated surface, it was assumed that the chlorine adatoms are arranged on the surface in approximate registry with oxide anions found in the bulk, and the Cr^{3+}-Cl^- bond length was estimated using the combined ionic radii for chromium (III) (0.63Å) and chloride ion (1.32Å) obtained from the literature [104]. For a sample orientation normal to the axis of the spectrometer CMA, and based upon a signal collected in a solid angle emitted 42° off the surface normal, the expected Cl/Cr ratio for 100% coverage of surface cations by

chlorine is 0.325. This value is in good agreement with the Cl/Cr=0.32 measured from a halogen-saturated (deactivated) surface. Therefore, the deactivated (Cl/Cr=0.32) surface is assigned as having approximately one adsorbed chlorine atom per surface Cr^{3+} cation. Additional exposures at 163 K produce no increase in the Cl/Cr ratio of 0.32 and no additional product is made. $CFCl_2CH_2Cl$ exposures of up to 2.0 L at 773 K produced no increase in the (AES) Cl/Cr ratio beyond Cl/Cr=0.32. Deactivation of the Cr_2O_3 (10$\underline{1}$2) surface towards $CFCl_2CH_2Cl$ decomposition is directly attributed to site blocking due to halogen deposition onto the surface.

4.3.4 Thermal Loss of Surface Chlorine

It was found that chlorine is removed from the sample surface by heating to around 1100 K. AES spectra of a deactivated surface (Cl/Cr=0.32) following five minutes of heating at 1100 K show that all chlorine removed, and the nearly stoichiometric surface is returned. The desorption of halogen and halogen-containing species was exhaustively searched for with TDS, and no desorbing halogen or other halogen-containing products were detected. The lack of evidence for desorption of surface halogen or halogen-containing species (*i.e.* CrX_n) from heating a deactivated surface suggests that the thermal removal of chlorine from the sample surface occurs via migration into the sample bulk.

A series of AES experiments was conducted on deactivated surfaces, prepared by exposure to $CFCl_2CH_2Cl$, to determine the rate of Cl thermal migration. AES spectra were collected as a function of time to monitor the loss of chlorine for three different annealing temperatures. The Cl/Cr ratio was calculated from each AES spectra and the data is shown in Figure 17 (top). Variation in the (AES) Cl/Cr ratio with time is reasonably fit by first order kinetics at each temperature, as indicated by first-order plots shown in Figure 17. An Arrhenius analysis of the rate constant is shown in Figure 17 (bottom), and yields a first-order activation energy for chlorine migration of 173 kJ/mol.

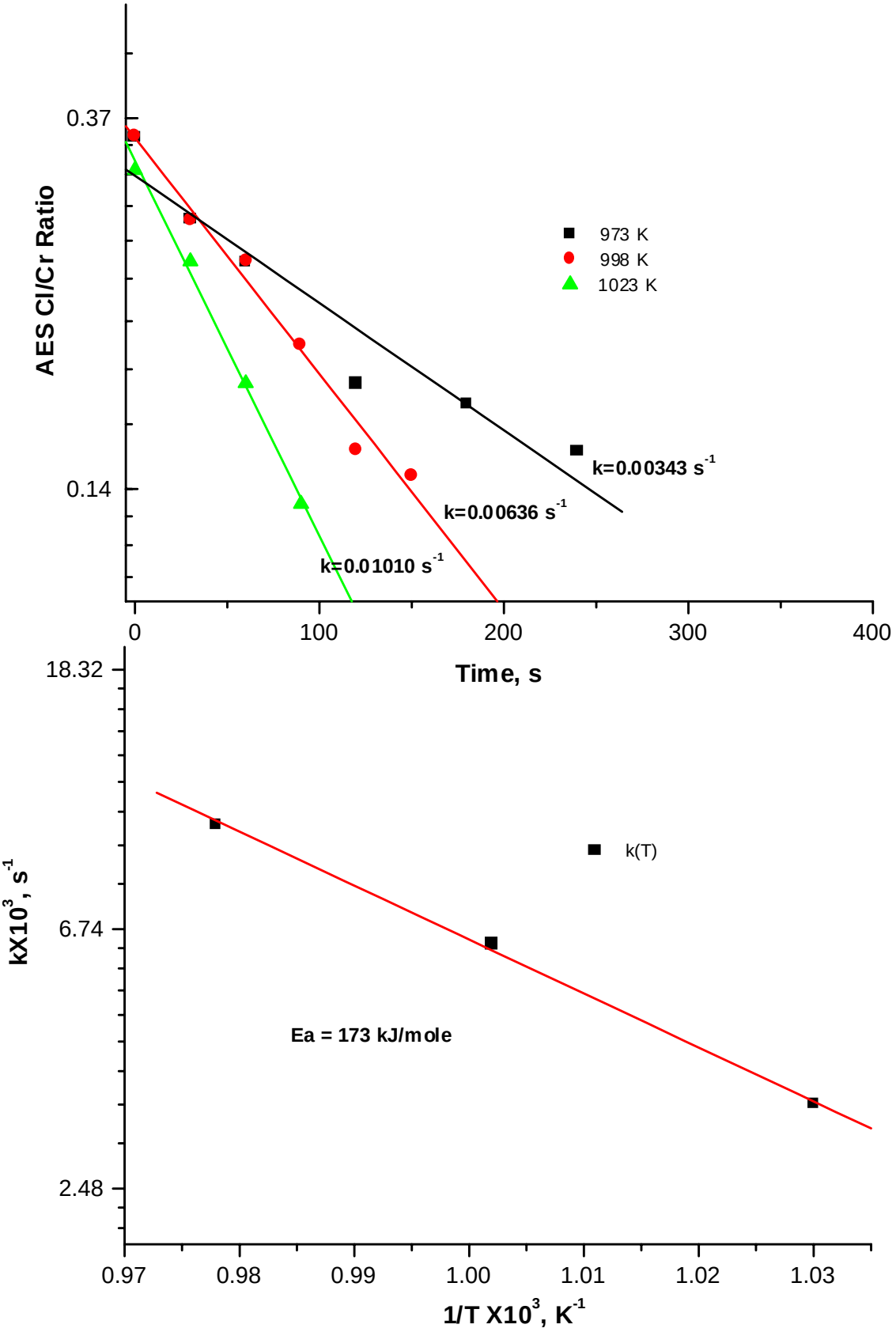

Figure 17. First-order rate analysis for Cl loss from the Cr_2O_3 (10$\underline{1}$2) surface. Determination of k as a function of T (top) and calculation of first-order E_a (bottom).

The manner that fluorine is removed from the surface cannot be directly addressed, though the deposition of a small amount of fluorine is indicated by the stoichiometry of $CFCl_2CH_2Cl$ decomposition to acetylene. The electron beam of the AES instrument was found to cause rapid loss of surface fluorine. Whether the electron stimulated loss of fluorine is due to desorption (ESD) or due to migration into the bulk is uncertain, but no fluorinated desorption products were observed. It does seem reasonable, however, to expect that the thermal loss of fluorine from the surface may occur via migration into the sample bulk, as suspected for thermal chlorine loss.

4.4 Discussion

The decomposition of $CFCl_2CH_2Cl$ over a nearly stoichiometric Cr_2O_3 (10$\underline{1}$2) surface yielded the major gas-phase product $CFCl{=}CH_2$ and a small quantity of acetylene. It was reported in Chapter 3 that acetylene is the only gas-phase product for $CFCl{=}CH_2$ decomposition over the same surface. Therefore, given the similarity in acetylene desorption traces for the two cases, it is reasonable to postulate a decomposition pathway for $CFCl_2CH_2Cl$ over the Cr_2O_3 (10$\underline{1}$2) surface that involves a series reaction through $CFCl{=}CH_2$ to acetylene, as represented below.

$$CFCl_2CH_2Cl_{(g)} \rightarrow CFCl{=}CH_{2(g)} + 2Cl_{(s)} \rightarrow HC{\equiv}CH_{(g)} + Cl_{(s)} + F_{(s)}$$

Formation of product $CFCl{=}CH_2$ appears to proceed via dissociative adsorption, followed by β-chlorine elimination, as discussed below. Acetylene is formed by carbon-chlorine bond cleavage and α-fluorine elimination, followed by a 2,1-hydrogen shift to form acetylene. Additional details of the formation of acetylene from $CFCl{=}CH_2$ may be found in Chapter 3. No thermal desorption evidence was found for the existence of other reaction products. AES of the deactivated surface reveals that only halogen is present on an inactive surface, and no carbon is detected. No evidence of halogen desorption is seen during TDS, indicating that halogen removed from the reactant molecule is strongly bound to the surface. HX abstraction is the most often reported reaction for $CFCl_2CH_2Cl$ and similar HCFC compounds over Cr_2O_3 powders [99, 105, 106], but was not observed

under the conditions of this study. The reaction of $CFCl_2CH_2Cl$ to $CFCl=CH_2$ most closely resembles the Zn-catalyzed dehalogenation of vicinal dihalides to alkenes [116].

4.4.1 210 K – 190 K $CFCl_2CH_2Cl$ Desorption

A large increase in $CFCl_2CH_2Cl$ desorption via the low temperature feature is observed as the formation of products declines. The low peak desorption temperature suggests a molecularly bound $CFCl_2CH_2Cl$ species is responsible for this low-temperature feature. The activation energy for desorption from this state (190 K) is estimated to be around 48 kJ/mol using the Redhead method and a normal, first-order pre-exponential factor of 10^{13} s^{-1} [52].

It is significant that the low-temperature $CFCl_2CH_2Cl$ desorption feature is not observed during initial TDS runs at small doses. AES spectra of the surface taken in conjunction with TDS experiments show that this feature grows in as the surface becomes progressively halogenated, suggesting that the low temperature desorption sites are created by halogen deposition. Desorption via the low temperature channel is proposed to originate from molecular $CFCl_2CH_2Cl$ bound at halogenated cation sites via a weak physical interaction. The total uptake ($CFCl_2CH_2Cl$ plus products) over a halogen saturated surface is observed to decrease by around 50%, relative to the nearly stoichiometric surface.

4.4.2 265 K Reaction Channel

Despite the high conversion to products a small $CFCl_2CH_2Cl$ desorption feature is observed during initial 0.03 L doses at high mass spectrometer sensitivity (Figure 14). The coincident desorption temperatures for both $CFCl_2CH_2Cl$ reactant and $CFCl=CH_2$ product molecules indicate that they arise via a common surface intermediate and share the same rate-limiting step. Additionally, the 265 K peak desorption temperature observed for product $CFCl=CH_2$ during $CFCl_2CH_2Cl$ TDS is around 50 K higher than the desorption temperature reported in section 3.3.1.1 for $CFCl=CH_2$ desorption from a molecular $CFCl=CH_2$ adsorbate. The higher desorption temperature for product $CFCl=CH_2$ indicates reaction-limited desorption kinetics for the 265 K reaction channel.

An activation energy for this process of 69 kJ/mol is calculated using the Redhead method [52] and assuming a normal first-order pre-exponential of 10^{13} s^{-1}.

The first step in the surface reaction mechanism is postulated to be the dissociative adsorption of $CFCl_2CH_2Cl$ at five-coordinate Cr^{3+} cations. The literature indicates the C-Cl bond on the more chlorinated carbon to be the weakest bond, and hence the most likely bond to break during dissociative adsorption [89, 107, 114, 115]. Gellman and coworkers [114] studied the rate constant for dechlorination of CH_2ClCH_2Cl versus CH_3CH_2Cl and found that the rate of dechlorination is reduced for haloethanes containing fewer chlorine atoms per carbon. They also found that the transition state for the above dechlorination reactions is not highly polarized, relative to the initial state, suggesting homolytic C-Cl bond cleavage. Therefore, dissociative adsorption of $CFCl_2CH_2Cl$ is thought to result in a surface alkyl group ($-CFClCH_2F$) and adsorbed chlorine ($Cl_{(s)}$), both bound at surface cation sites. Similar alkyl groups attached to transition metal cations are well known in the organometallic literature and a strong interaction between chlorine and microcrystalline Cr_2O_3 has been documented in the catalysis literature [38, 77, 88, 89].

Following the dissociative adsorption of $CFCl_2CH_2Cl$, two reaction pathways are possible.

1. The surface alkyl may recombine with chlorine on the surface to form the $CFCl_2CH_2Cl$ reactant molecule.
2. The surface alkyl may undergo a β-chlorine elimination step to form the $CFCl=CH_2$ product molecule and a second $Cl_{(s)}$.

Reactant molecules that are re-formed via the first pathway are expected to immediately desorb because the molecular desorption temperature (210 K) has already been exceeded. The second pathway is more favored initially, as evidenced in TDS by the much larger yield of $CFCl=CH_2$ compared to $CFCl_2CH_2Cl$ at 265 K. The organometallic literature contains many examples of β-halogen elimination from alkyl complexes [77, 76, 78].

As mentioned, pathways 1 and 2 (above) are likely to share a rate-limiting step because of the simultaneous desorption of both $CFCl=CH_2$ and $CFCl_2CH_2Cl$ at around 245 K. The combination of TDS and AES data demonstrates that as the surface becomes increasingly chlorinated, the recombination to $CFCl_2CH_2Cl$ becomes increasingly favored, but as the halogen content of the surface nears saturation both pathways become

unavailable due to a lack of exposed cations. Therefore, the common rate-limiting step is postulated to be the first-order β-chlorine elimination from the surface alkyl formed upon dissociative adsorption. It is postulated that chlorine liberated via β-elimination bonds to five-coordinate Cr^{3+} sites when they are available (*i.e.* low Cl/Cr ratio). As the surface becomes increasingly halogenated, bare cation sites become less available and recombination of chlorine with a surface alkyl becomes more likely, as evidenced by the increase in $CFCl_2CH_2Cl$ desorption. Consequently, the $CFCl_2CH_2Cl$ desorption intensity increases and the product $CFCl{=}CH_2$ intensity decreases as the surface halogen content increases. Eventually, surface deactivation results as nearly 100% of surface cations are capped by adsorbed halogen and the formation of $CFCl{=}CH_2$ is completely suppressed, as evidenced above using AES (section 4.3.3).

4.4.3 HC≡CH Product

The acetylene desorption features observed during $CFCl_2CH_2Cl$ TDS indicate that the desorption kinetics are similar to that discussed in Chapter 3 for acetylene formed from $CFCl{=}CH_2$ decomposition over a nearly stoichiometric surface. Both $CFCl_2CH_2Cl$ and $CFCl{=}CH_2$ TDS spectra contain two product acetylene desorption features having similar peak shapes and peak desorption temperatures. The similarity in TDS characteristics suggests that the kinetics and surface species involved in both desorption processes are the same. Therefore, based upon the arguments of sections 3.4.1 and 3.4.2, the 335 K feature is assigned as the first-order desorption of molecularly bound HC≡CH. Similarly, the 480 K peak is assigned as first-order and reaction-limited [78, 76].

4.4.4 Surface Chlorine

The uptake of halogen by Cr_2O_3 microcrystalline powder has been reported by various authors. Kemnitz *et al*. [102] used XPS to measure the amount of fluorine uptake by microcrystalline Cr_2O_3 powder exposed to $CFCl_2CH_2Cl$ at 673 K and atmospheric pressure. They reported a maximum F/Cr ratio of approximately 0.43. Blanchard and coworkers [61, 94, 97] studied the uptake of fluorine over microcrystalline Cr_2O_3 powder exposed to CF_3CH_2Cl at 653 K and atmospheric pressure and reported a F/Cr ratio of 0.36. Coulson and coworkers [98] report that exposures of CHF_3 and HF at 698 K over

microcrystalline Cr_2O_3 yielded F/Cr ratios of 0.22 and 0.30, respectively. The (AES) Cl/Cr=0.32 reported herein lies within the range of F/Cr values found in the literature is in approximate agreement with the literature values cited for halogen uptake over Cr_2O_3.

The deactivation of the Cr_2O_3 (10$\underline{1}$2) surface was coincident with a surface chlorine-to-cation ratio of approximately 1:1 (*i.e.* halogen-saturated). It is suggested that deactivation of the surface occurs by "capping" surface Cr^{3+} cations with chlorine, thereby preventing reaction by isolating the chromium cations from any surface adsorbate. It was suggested in section 4.3.2.2 that fluorine is also capable of the same type of site blocking. A similar argument was presented by Kemnitz *et al*. [102] to explain the deactivation of microcrystalline Cr_2O_3 powder samples toward fluorination reactions. The O/Cr ratio did not change from the nearly stoichiometric surface to the deactivated surface, suggesting that no replacement of lattice oxide by chloride ion occurred.

The absence of gas-phase desorption products during thermal treatments of a nearly chlorine-saturated surface suggests that surface chlorine loss occurs via migration into the sample bulk. A similar result was reported for fluorine in section 3.2.2. While no reports of halogen migration into Cr_2O_3 could be found in the literature, Freund and coworkers report that sodium adsorbed to Cr_2O_3 (0001) films also migrates into the sample bulk [63].

4.5 Conclusions

$CFCl_2CH_2Cl$ decomposes over a nearly stoichiometric Cr_2O_3 (10$\underline{1}$2) surface to $CFCl=CH_2$ and acetylene. The chlorine removed from the $CFCl_2CH_2Cl$ molecule was strongly bound to the surface. Eventually, the adsorption of halogen at five-coordinate surface Cr^{3+} sites terminates the decomposition reaction, presumably by site blocking. Fluorine could not be directly quantified using AES due to a rapid loss of fluorine from the surface induced by electron beam exposure.

The reaction is thought to proceed via dissociative adsorption of $CFCl_2CH_2Cl$ at the C-FCl_2 end of the molecule through homolytic C-Cl bond cleavage. TDS data suggests the presence of a common surface intermediate for $CFClCH_2Cl$ and $CFCl=CH_2$ desorption via the 265 K reaction channel. Based upon literature precedents, this intermediate is assigned as a surface alkyl and β-chlorine elimination from the alkyl is assigned as the common rate-limiting step. A small quantity of acetylene is also formed via $CFCl=CH_2$ decomposition. No carbon build up was observed on deactivated surfaces, and no evidence was seen for the replacement of lattice oxygen by halogen.

Chlorine deposited on the sample surface by the decomposition reaction is strongly bound. No evidence for desorption of surface chlorine was found, suggesting that chlorine (and presumably fluorine) are removed from the surface via migration into the sample bulk. The first-order activation energy for chlorine migration was estimated to be 173 kJ/mole [52].

Chapter 5

The Reactions of CF_2ClCH_2Cl and CF_2CH_2 over the Cr_2O_3 (10$\underline{1}$2) Surface

5.1 Introduction

The chlorofluorocarbon CF_2ClCH_2Cl (HCFC-132b) was investigated because of its importance as an intermediate in the production of CF_3CH_2F (HCFC-134a). CF_2ClCH_2Cl is the next stable intermediate, following $CFCl_2CH_2Cl$ (HCFC-131a), in the production of HCFC-134a from trichloroethylene (Chapter 1). Most HCFC compounds, especially alkane derivatives, are described as being increasingly reactive as the chlorine content increases [4, 60, 114]. Using this rule of thumb, CF_2ClCH_2Cl is expected to be somewhat less reactive than $CFCl_2CH_2Cl$, but somewhat more reactive than CF_3CH_2Cl.

Only a single study of the Cr_2O_3/ CF_2ClCH_2Cl system could be found in the literature. Kemnitz and coworkers [99] studied the reaction of CF_2ClCH_2Cl over Cr_2O_3 powder as part of a broader investigation of the manufacture of CF_3CH_2F (HFC-134a) from TCE. They reported that in the absence of added HF or HCl, the CF_2ClCH_2Cl molecule decomposes into CCl_2=CHF, CHCl=CF_2, and TCE. The formation of these products is attributed to a series of HX elimination and Markovnikov re-addition steps. A small amount of the halogen exchange product CF_3CH_2Cl (HCFC-133a) was also formed without added HF. In the presence of HF, the major reaction product was reported to be the thermodynamically stable HCFC-133a [4, 99].

5.2 Experimental

PCR Inc. 1,1-difluoro-1, 2-dichloroethane (CF_2ClCH_2Cl) (98%), PCR Inc. 1,1difluoroethene (CF_2=CH_2) (98%), and Matheson acetylene (HC≡CH) (99.6 %) were used as received. CF_2ClCH_2Cl is a liquid at room temperature and atmospheric pressure, therefore a stainless steel tube was filled with CF_2ClCH_2Cl liquid and attached to the gas

distribution manifold. The liquid was expanded into the gas-distribution manifold, and dosing was accomplished by backfilling the UHV chamber through a variable leak valve.

The reactions of both CF_2ClCH_2Cl and $CF_2=CH_2$ were investigated over a nearly stoichiometric, (1×1) Cr_2O_3 (10$\underline{1}$2) surface using thermal desorption spectroscopy (TDS), Auger electron spectroscopy (AES) and low energy electron diffraction (LEED). A stoichiometric surface was prepared by ion-bombardment followed by annealing to 900 K. LEED was used to verify the (1×1) periodicity at the sample surface. All doses for TDS experiments were conducted at 163 K, and all desorption quantities have been corrected for mass spectrometer sensitivity [69, 108, 109].

AES measurements were conducted at 800 K to avoid sample charging. Because of overlap between the primary oxygen and chromium Auger peaks, the Cl/Cr ratios were calculated using the peak-to-peak heights of the Cl LVV (190eV) and the Cr $L_3M_{2,3}M_{2,3}$ (490 eV) transitions. A sensitivity factor of 4.4 was applied to the Cr $L_3M_{2,3}M_{2,3}$ peak-to-peak height, as discussed in Chapter 2 [110].

5.3 Results

CF_2ClCH_2Cl decomposed on a (1×1), nearly stoichiometric Cr_2O_3 (10$\underline{1}$2) surface to form gas-phase $CF_2=CH_2$. Trace amounts of acetylene were also detected. Dosed $CF_2=CH_2$ decomposes on a nearly stoichiometric Cr_2O_3 (10$\underline{1}$2) surface to form acetylene as the only gas-phase product. The halogen atoms removed from $CF_2=CH_2$ and CF_2ClCH_2Cl during each surface reaction remain on the surface. The possibility of other gas-phase reaction products was eliminated by an exhaustive TDS search that included all mass (m/z) numbers from 2 – 200. The sequence of decomposition reactions observed for $CF_2=CH_2$ and CF_2ClCH_2Cl are very similar to the reactions of $CFCl=CH_2$ and $CFCl_2CH_2Cl$ discussed in Chapter 3 and Chapter 4, respectively.

5.3.1 $CF_2=CH_2$ Thermal Desorption from a Nearly Stoichiometric Surface

TDS experiments using $CF_2=CH_2$ (HFC-1132a) as the dosed molecule were initiated over an ion-bombarded and annealed (nearly stoichiometric) Cr_2O_3 (10$\underline{1}$2) (1×1) surface. Figure 18 shows the desorption spectra for the dosed molecule $CF_2=CH_2$ (top)

and product acetylene (bottom) for a series of 0.06 L doses. The parent mass (m/z=64) was used to monitor CF_2=CH_2 desorption and m/z=26 was monitored to follow acetylene desorption. No H_2, H_2O, CO, or CO_2 reaction products were observed during CF_2=CH_2 TDS. Additionally, no fluoroacetylene, HF, nor any fluorine containing desorption species was observed, other than the CF_2=CH_2 reactant molecule. The amount of fluorine deposited on the sample surface during CF_2=CH_2 TDS could not be quantified using AES because of electron stimulated loss of fluorine from the sample surface (see Chapter 4).

5.3.1.1 CF_2=CH_2 Desorption

Figure 18 (top) shows the desorption of the CF_2=CH_2 reactant molecule for a set of consecutive 0.06 L doses. A single feature at 170 K is observed. The desorption intensity of the CF_2=CH_2 peak gradually increased with each exposure without any significant change in the peak desorption temperature. The constant desorption temperature as a function of coverage is indicative of a first-order desorption process [52]. The low peak desorption temperature (170 K) and first-order desorption kinetics suggest that this feature results from the desorption of a molecularly bound CF_2=CH_2 species. The first-order activation energy for desorption is estimated to be around 45 kJ/mol, using the Redhead method and a normal first-order pre-exponential of 10^{13} s^{-1} [52].

Figure 19 shows the quantity of CF_2=CH_2 (black) desorbed from the surface for a series of 0.06 L CF_2=CH_2 doses. The amount of reactant desorbed increases throughout the TDS series. The sum of desorbing species shown in Figure 19 (blue) increases over the course of the TDS series, indicating that the CF_2=CH_2 sticking coefficient is increasing with total exposure.

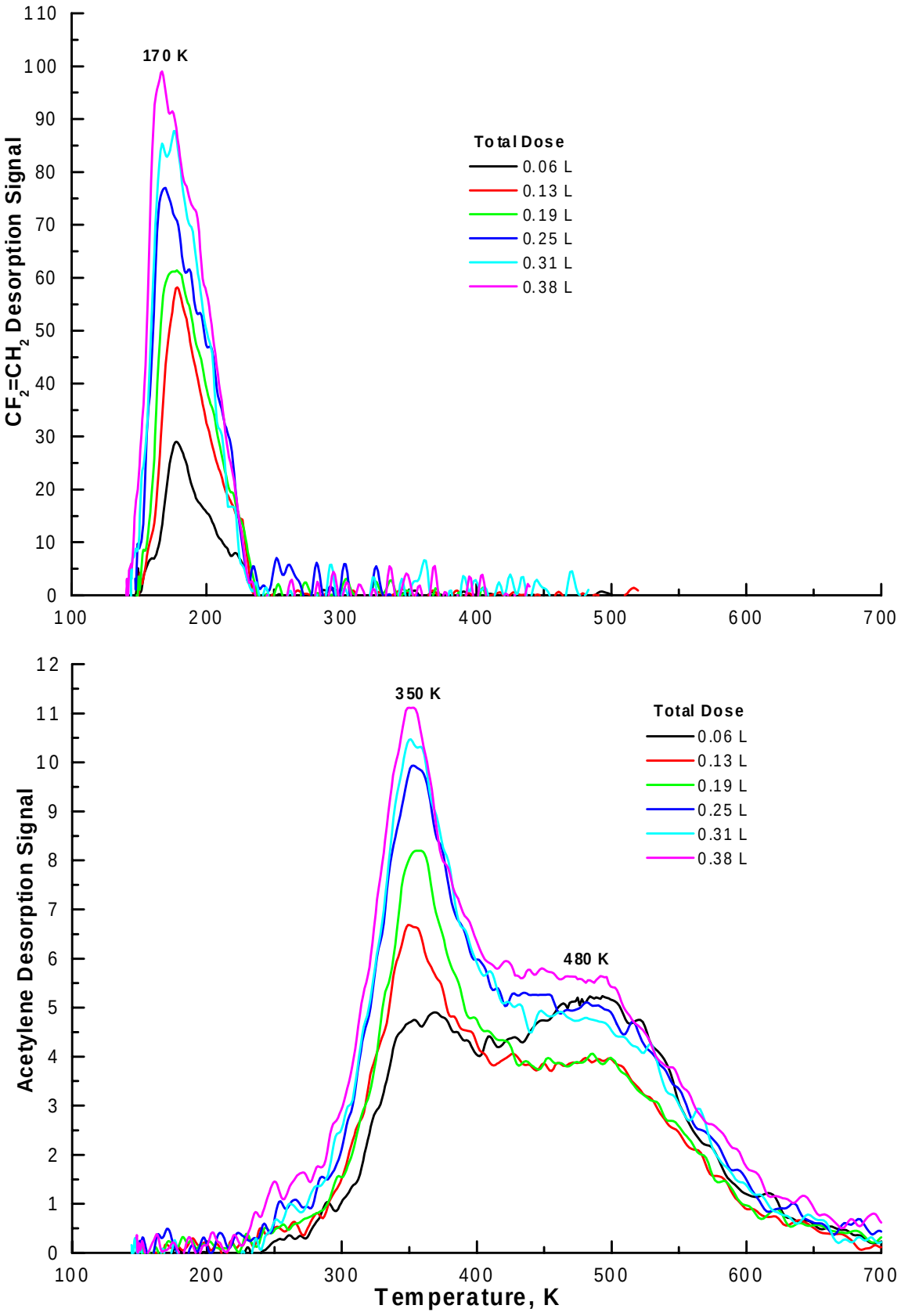

Figure 18. Desorption traces of the CF_2=CH_2 reactant (top) and the HC≡CH product (bottom) for a series of 0.06 L doses of CF_2=CH_2 over a nearly stoichiometric surface.

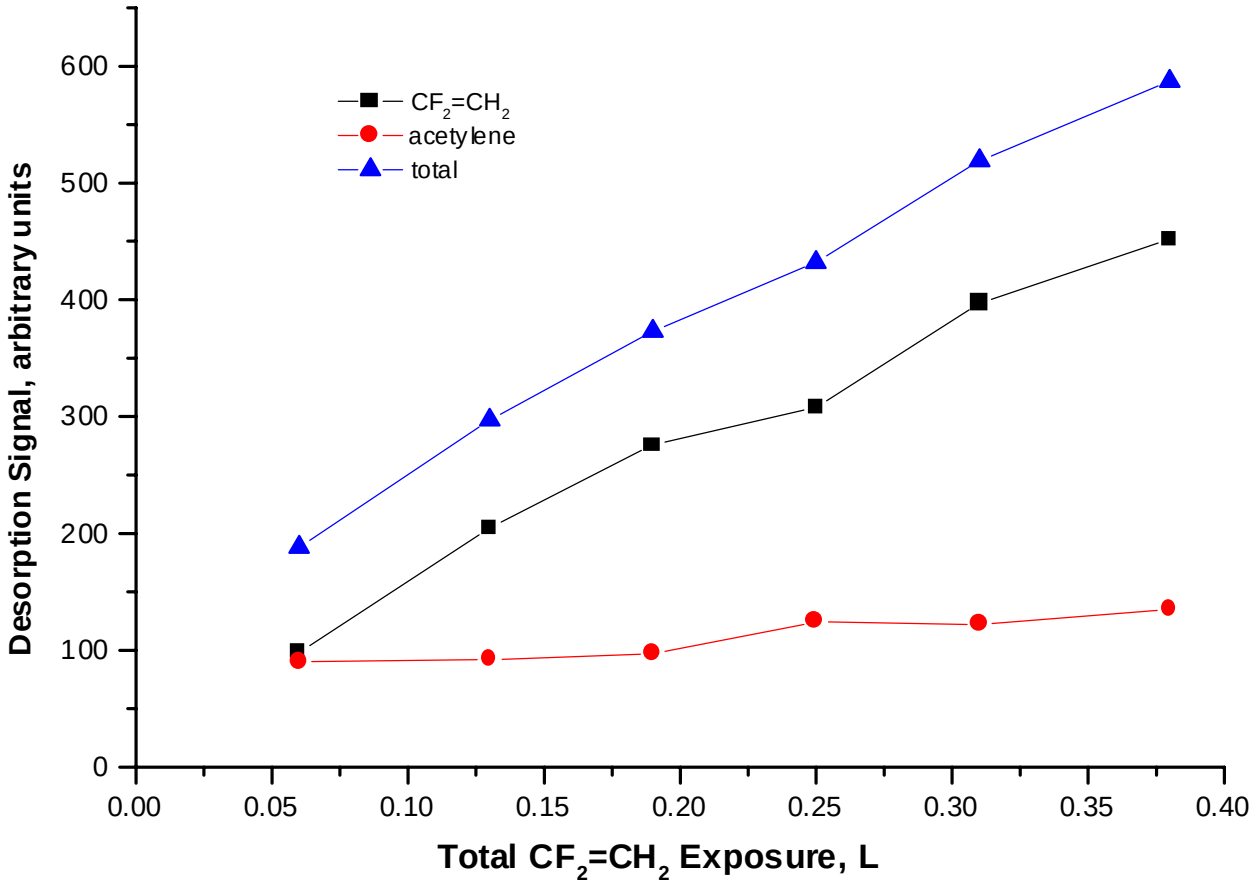

Figure 19. The relative quantities of $CFCl=CH_2$ (parent) and $HC\equiv CH$ desorbed from the sample surface during a series of 0.13 L doses. The total amount is also shown.

5.3.1.2 Product HC≡CH Desorption

Figure 18 (bottom) shows the desorption spectra for product acetylene in the same TDS series of 0.06 L CF_2=CH_2 doses discussed above. The acetylene product is desorbed in two features, a low temperature feature centered around 350 K and a high temperature feature around 480 K. The 350 K peak intensity increases following each 0.06 L dose and the 350 K desorption temperature remains constant over this exposure range, suggesting first-order desorption kinetics. The HC≡CH peak at 480 K does not change significantly in temperature or intensity during the TDS series.

The acetylene desorption features observed during CF_2=CH_2 TDS are similar to the desorption spectra discussed in Chapter 3 for product acetylene formed from CFCl=CH_2 decomposition on a nearly stoichiometric surface. Both reactants decompose to yield acetylene in two desorption features occurring at 350 K and around 470 K – 480 K. The similarity in TDS characteristics suggests that the reaction pathway and kinetics are the same for both reactions. Therefore, based upon the arguments of sections 4.4.1 and 4.4.2, the 350 K feature is assigned as the first-order desorption of a molecularly bound HC≡CH π-complex. Similarly, the 480 K peak is assigned as reaction limited, and the formation of acetylene likely proceeds via surface vinyl and vinylidene species [76, 78]. Assuming first-order processes and a pre-exponential of 10^{13} s^{-1}, an activation energy for desorption of 92 kJ/mol and 127 kJ/mol are calculated for the 350 K and 480 K peaks, respectively.

Figure 19 shows the relative amounts of HC≡CH, CF_2=CH_2, and the total desorbed from the surface for a series of consecutive 0.06 L doses of CF_2=CH_2. The amount of acetylene produced gradually increases throughout the 0.06 L TDS series. The increase in both reactant and product desorbed from the surface cause the total desorption amount to rise significantly over the course of the TDS series, indicating that the CF_2=CH_2 sticking coefficient increases over this exposure range. The increase in CF_2=CH_2 sticking coefficient is presumably the result of increasing fluorine concentration at the sample surface, but this could not be confirmed using AES.

The experimental set up limited the number of consecutive TDS runs that could be conducted in a single set of experiments. Therefore, the 0.06 L doses could not be continued until acetylene production ceased, assuming that surface deactivation would

eventually occur as observed for $CFCl=CH_2$ (Chapter 3). As shown in Figure 19, the quantity of product acetylene increases slowly over the entire range of exposure.

5.3.1.3 LEED and AES Following $CF_2=CH_2$ Thermal Desorption

Auger spectra of the sample surface following $CF_2=CH_2$ TDS confirm the presence of fluorine on the surface following TDS experiments. However, the electron-stimulated loss of fluorine from the sample surface occurred so rapidly as to make quantitative analysis impossible using AES (see Chapter 4). LEED experiments show that the surface retains its (1×1) periodicity following $CFCl=CH_2$ exposures of up to 1.0 L at 163 K. The surface O/Cr ratio was not found to change due to $CF_2=CH_2$ TDS, and no carbon was detected on the surface. No evidence was found for the replacement of lattice oxygen by fluorine following TDS experiments.

5.3.2 CF_2ClCH_2Cl Decomposition on Cr_2O_3 (10$\underline{1}$2)

CF_2ClCH_2Cl (HCFC-132b) reacted on a nearly stoichiometric Cr_2O_3 (10$\underline{1}$2) surface forming $CF_2=CH_2$ (HFC-1132a), and a small amount of HC≡CH (acetylene) as the only gas-phase products. Desorption of the CF_2ClCH_2Cl parent molecule was followed by monitoring m/z= 99. The presence of other gas-phase products having m/z from 2-200 was eliminated by an extensive TDS search. Specifically, no H_2, H_2O, CO, or CO_2 were observed. The halocarbon compounds CF_3CH_2Cl (HCFC-133a), CF_2ClCH_2Cl (HCFC-131a), $CFCl=CH_2$ (HCFC-1131a), CHF=CHCl (HCFC-1131), as well as fluoro- and chloro-acetylene were specifically searched for using TDS and were not observed. The fluorine and chlorine removed from the reactant molecule remained bound to the sample surface following TDS.

The $CF_2=CH_2$ product signal was obtained by following m/z= 64 and subtracting away the CF_2ClCH_2Cl contribution to the 64 signal. The relative intensities of three (subtracted) m/z signals (31, 45, 64) were used to positively identify $CF_2=CH_2$, and the relative intensities were in good agreement with mass spectrometer cracking patterns collected for $CF_2=CH_2$, and with published data [70]. The acetylene product signal was obtained by following m/z= 26 and correcting for both CF_2ClCH_2Cl and $CF_2=CH_2$ contributions to the 26 signal intensity. The acetylene product represented less that 1%

of the total amount desorbed from the surface and was only detected following small doses of CF_2ClCH_2Cl over nearly stoichiometric surfaces.

5.3.2.1 CF_2ClCH_2Cl Thermal Desorption from a Nearly Stoichiometric Surface

Figure 20 (top) shows the dosed molecule CF_2ClCH_2Cl (m/z=99) during a series of consecutive 0.06 L doses of CF_2ClCH_2Cl initiated on a nearly stoichiometric, (1×1) Cr_2O_3 (10$\underline{1}$2) surface. The CF_2ClCH_2Cl desorption feature is very broad and contains contributions from three separate desorption states. An intense, narrow peak occurs at around 220 K following the first 0.06 L dose of CF_2ClCH_2Cl. The 220 K peak losses intensity following every dose and is no longer visible as a separate feature by 0.38 L of total exposure. As the 220 K peak subsides, a second peak grows in at around 180 K. The 180 K contribution is first apparent as a distinct feature following 0.31 L of total CF_2ClCH_2Cl exposure and grows in intensity with increasing total exposure. Throughout the series of 0.06 L doses, and in TDS experiments conducted using 0.03 L and 0.13 L doses (not shown), a small feature is apparent at around 245 K in every CF_2ClCH_2Cl desorption trace. The amount of reactant obtained from the 245 K adsorbed state is small, but consistently appears in CF_2ClCH_2Cl TDS and is shown in the Figure 20 inset.

The amount of CF_2ClCH_2Cl desorbed from the surface, calculated by integrating the area under the desorption curve, for a series of 0.06 L CF_2ClCH_2Cl doses initiated over a nearly stoichiometric surface is shown in Figure 21. The amount of CF_2ClCH_2Cl desorbed from the surface shows a slight decreasing trend over the TDS series.

5.3.2.2 Product $CF_2=CH_2$ Desorption

The product $CF_2=CH_2$ desorption signal for the same series of 0.06 L doses of CF_2ClCH_2Cl as discussed above is shown in the bottom panel of Figure 20. After subtracting away the maximum possible reactant contribution, the $CF_2=CH_2$ trace shows a single desorption feature having a peak temperature of around 245 K. The $CF_2=CH_2$ signal broadens and increases in intensity following the first two 0.06 L doses. The product signal remains relatively constant from 0.13 L through 0.31 L, then begins to narrow and decrease in intensity beyond 0.31 L of total CF_2ClCH_2Cl exposure. The

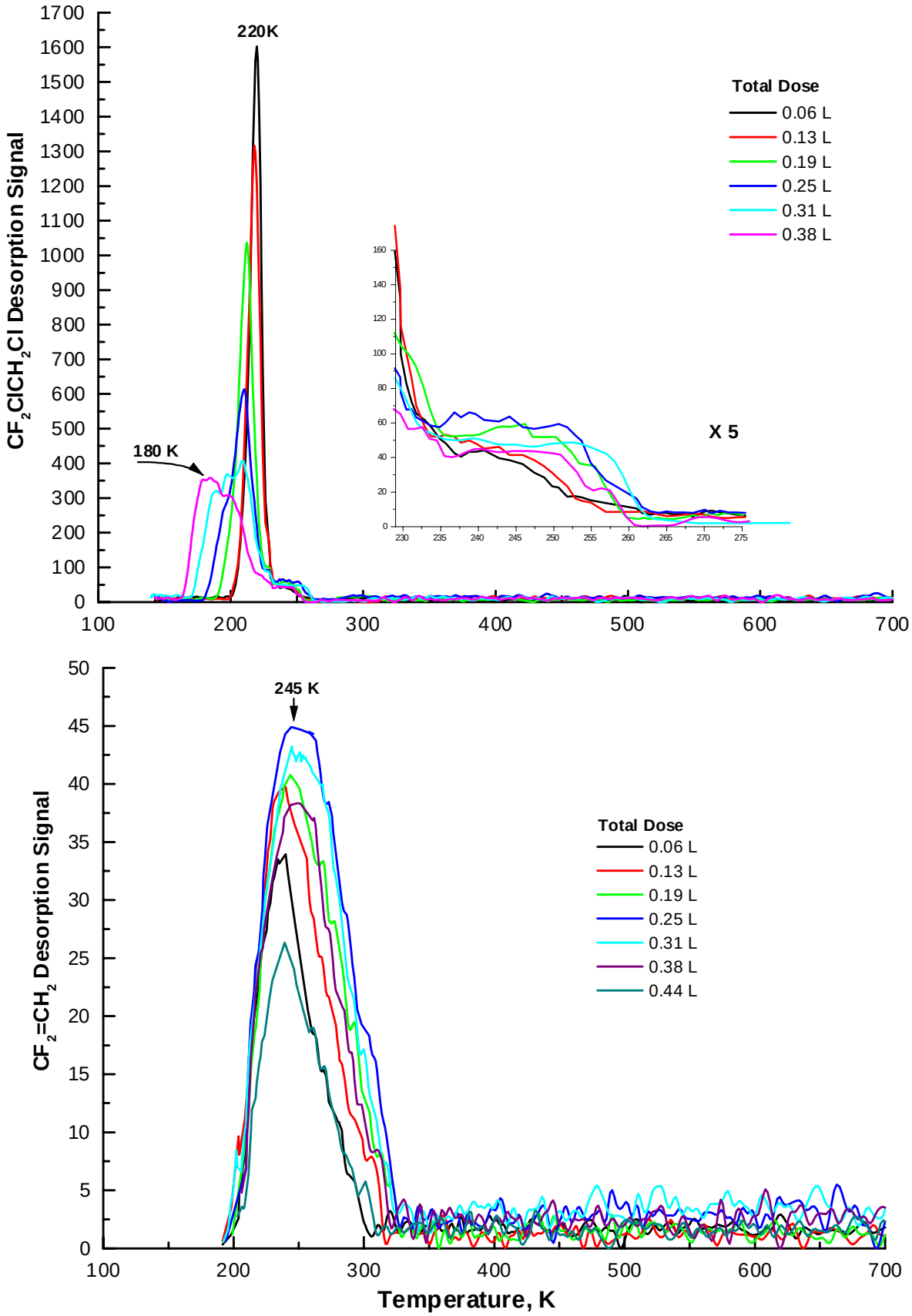

Figure 20. Desorption traces of the CF_2ClCH_2Cl reactant (top) and the $CF_2=CH_2$ product (bottom) for a series of 0.06 L doses of CF_2ClCH_2Cl over a nearly stoichiometric surface.

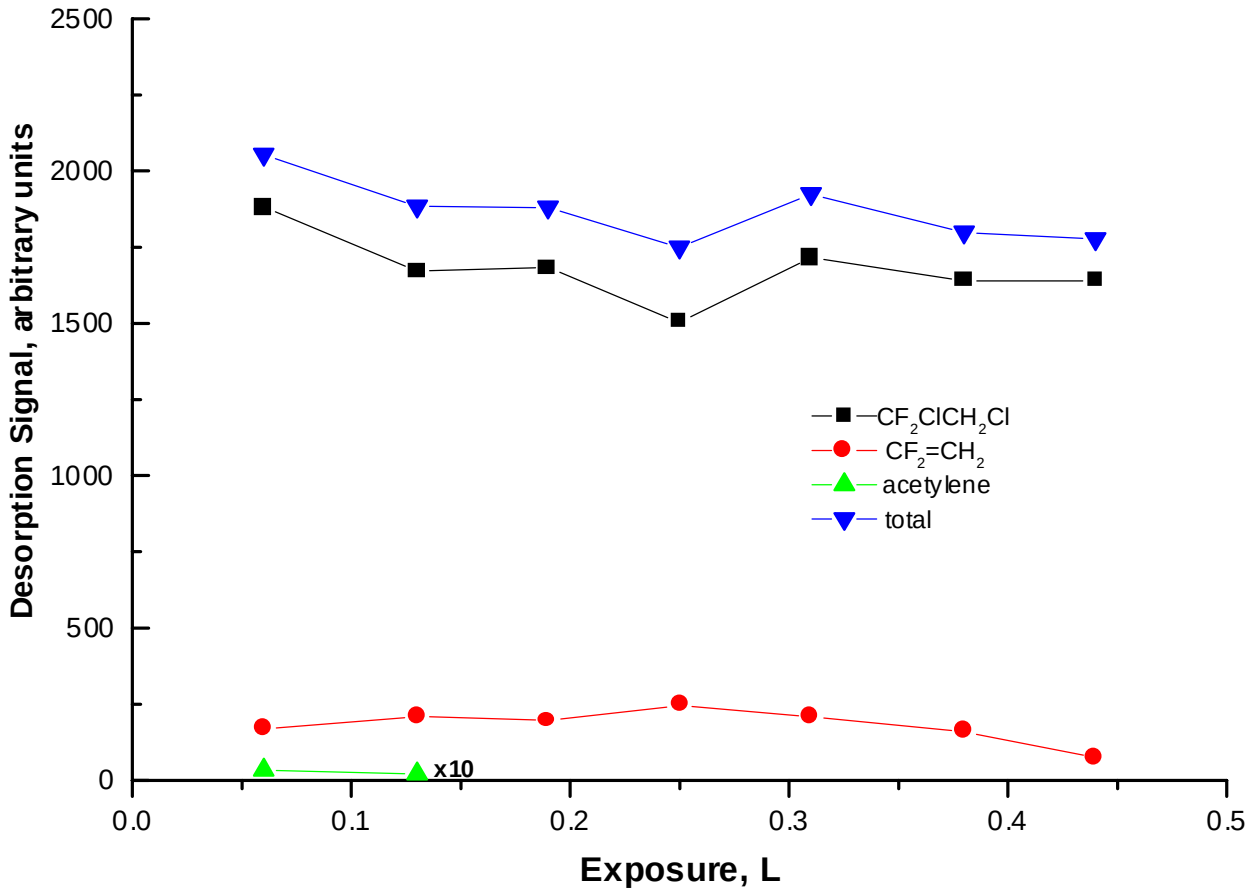

Figure 21. The relative quantities of CF_2ClCH_2Cl and $CF_2=CH_2$ desorbed from the sample surface during a series of 0.06 L doses. The total amount desorbed is also shown.

coincident desorption of both reactant and product at 245 K suggests that CF_2=CH_2 and CF_2ClCH_2Cl share a common surface intermediate and rate-limiting step.

In Figure 21, the integrated peak areas for product CF_2=CH_2 are plotted versus exposure, and illustrates only minor variations in the amount of CF_2=CH_2 formed, going through a slight maximum at 0.25 L. A small upward shift in the 240 K peak desorption temperature coincides with the increase in product CF_2=CH_2, suggesting an increase in the activation energy for desorption is coincident with initial halogenation of the surface. However, it should be noted that the subtraction necessary to obtain the product CF_2=CH_2 signal combined with the small CF_2=CH_2 contribution to m/z=64 signal intensity (around 25%) may give variations in the peak shape and temperature due to subtraction artifacts.

5.3.2.3 Product HC≡CH Desorption

Figure 21 shows the amounts of the products acetylene and CF_2=CH_2, and the reactant CF_2ClCH_2Cl desorbed from the surface for a series of 0.06 L doses of CF_2ClCH_2Cl initiated over a nearly stoichiometric surface. Acetylene comprised less than 1% of the total amount of products formed. Desorption traces of the acetylene product (not shown) showed two contributing features, one at 350 K and the second at around 470 K – 480 K. Because of the similarity in desorption characteristics between product acetylene formed from both CF_2ClCH_2Cl and CF_2=CH_2, the kinetics of acetylene formation are assigned as the same as from the CF_2=CH_2 reactant, and the reader is referred to section 5.3.1.2 for details of these assignments.

5.3.2.4 LEED and AES

AES spectra taken of the sample surface following CF_2ClCH_2Cl TDS confirm that the chlorine removed from the molecule is deposited on to the sample surface, and that no carbon remains on the surface after the desorption of gas-phase products. A series of consecutive TDS runs using CF_2ClCH_2Cl doses ranging from 0.13 L to 0.30 L generated surfaces having (AES) Cl/Cr ratios ranging from 0.11 to 0.14, with smaller total exposures yielding the lower values. The increasing Cl/Cr ratio as measured with AES during a TDS series of 0.03 L doses (black) is shown in Figure 22. Fluorine was not

quantifiable for the reasons discussed in Chapter 4. No evidence for the replacement of lattice oxygen by halogen was observed.

Figure 22 also shows the Cl/Cr ratio for a series of 4.0 L exposures (red) of CF_2ClCH_2Cl conducted at 773 K. The Cl/Cr ratio is seen to rise from zero through 20 L of total exposure and then levels off at around 0.22. Figure 23 shows the Auger spectra of the sample surface having a Cl/Cr=0.22, taken following 28.0 L of total CF_2ClCH_2Cl exposure (4.0 L doses) at 773 K.

5.3.2.5 CF_2ClCH_2Cl Thermal Desorption from an Oxygenated Surface

TDS experiments using CF_2ClCH_2Cl conducted over Cr_2O_3 (10$\underline{1}$2) surfaces that were pre-exposed to oxygen demonstrated that CF_2ClCH_2Cl decomposition does not occur on the oxide-terminated surface. TDS experiments using successive 0.03 L doses of CF_2ClCH_2Cl yielded no $CF_2{=}CH_2$ nor any other gas-phase reaction products. Specifically, no H_2, CO, CO_2, nor any other compound containing carbon, chlorine or fluorine (other than CF_2ClCH_2Cl) was detected. AES of the surface showed no indication of surface chlorine or carbon following CF_2ClCH_2Cl TDS on an oxide terminated surface.

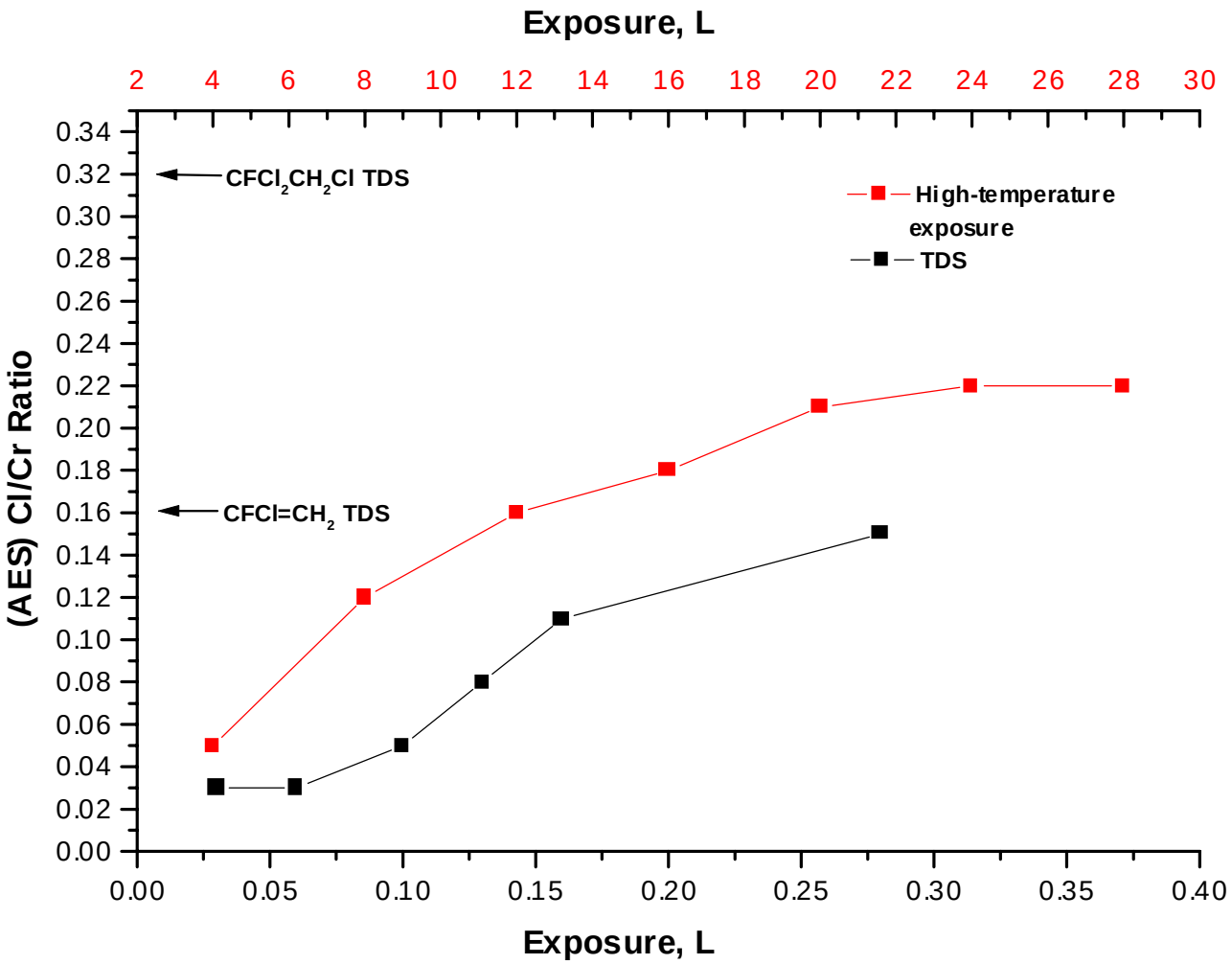

Figure 22. The (AES) Cl/Cr ratio at the sample surface following exposure to CF_2ClCH_2Cl. The red represents a series of 4.0 L exposures conducted at 773 K and the black represents a 0.03 L TDS series. The maximum Cl/Cr ratio for CF_2ClCH_2Cl TDS (Chapter 4) and $CFCl=CH_2$ TDS (Chapter 3) are also shown.

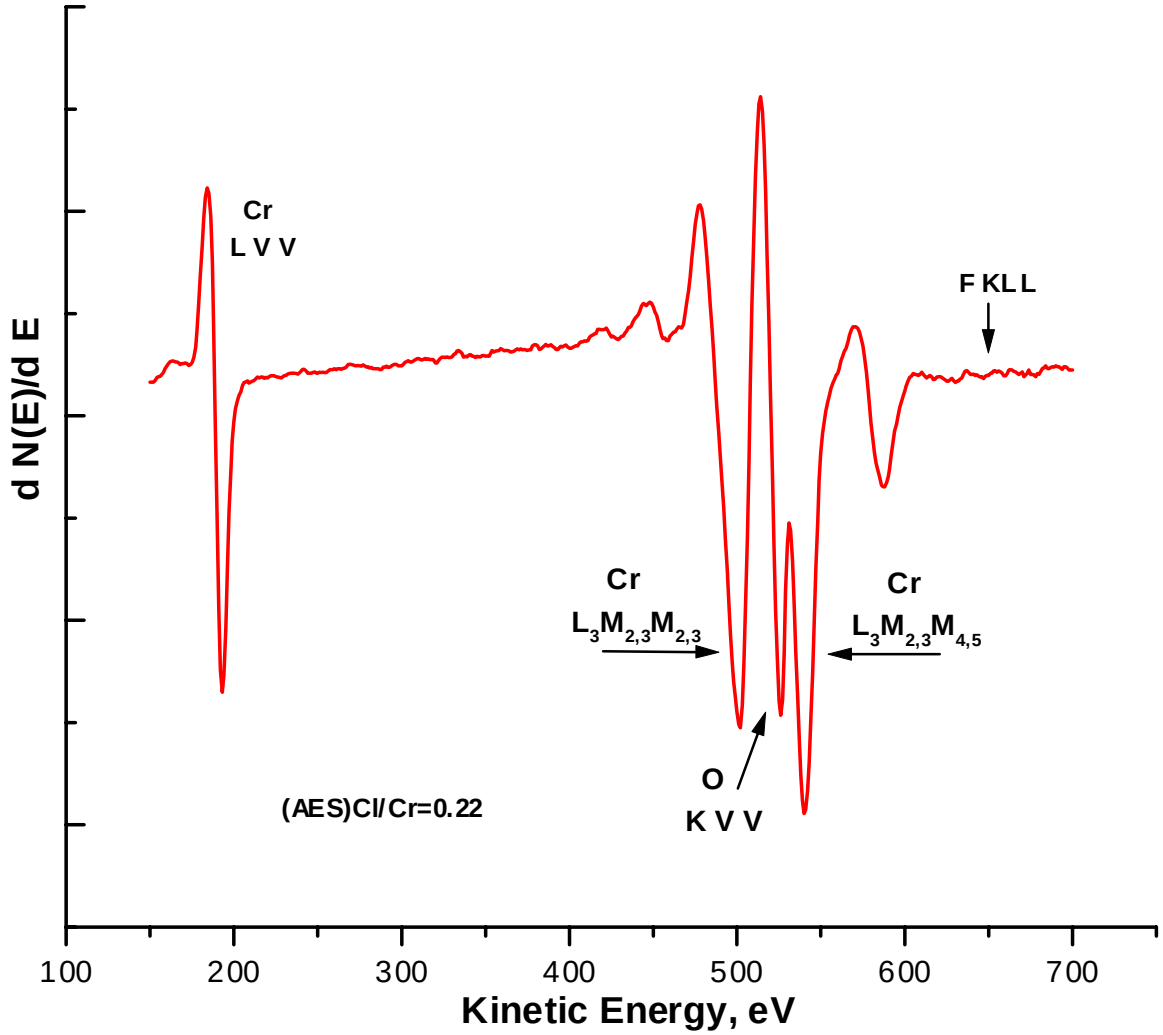

Figure 23. An AES spectrum of the Cr_2O_3 (10$\underline{1}$2) surface following 20 L of CF_2ClCH_2Cl exposure at 773 K. The (AES) Cl/Cr = 0.22 is the maximum that was obtainable using CF_2ClCH_2Cl as the treatment gas.

5.4 Discussion

The decomposition of CF_2ClCH_2F over a nearly stoichiometric Cr_2O_3 (10$\underline{1}$2) surface yielded the major gas-phase product $CF_2=CH_2$ and a small quantity of acetylene. The decomposition of $CF_2=CH_2$ over the same surface yielded acetylene as the only gas-phase product. The TDS data presented above is very similar to the TDS data for $CFCl=CH_2$ (HCFC-1131a) and $CFCl_2CH_2Cl$ (HCFC-131a) discussed in Chapters 3 and 4, respectively. Based upon the TDS data, it is reasonable to postulate a decomposition pathway for CF_2ClCH_2F that proceeds via a series reaction through $CF_2=CH_2$ to HC≡CH.

$$CF_2ClCH_2Cl_{(g)} \rightarrow CF_2=CH_{2(g)} + 2Cl_{(s)} \rightarrow HC{\equiv}CH_{(g)} + 2F_{(s)}$$

Formation of $CF_2=CH_2$ appears to proceed via direct dihalo-elimination, and the observed chemistry is most similar to the Zn-catalyzed reduction of vicinal dihalides to alkenes [116], as previously noted in Chapter 4. Acetylene is likely formed from $CF_2=CH_2$ through vinyl and vinylidene intermediates (as described below) followed by a 2,1-hydrogen shift to form acetylene. No evidence was found for the existence of other reaction products. AES of the surface following TDS shows that only halogen is present on the surface, no carbon is detected. No evidence of halogen desorption is observed during either CF_2ClCH_2F or $CF_2=CH_2$ TDS, indicating that halogen removed from the reactants is strongly bound to the surface.

5.4.1 CF_2ClCH_2Cl Decomposition to $CF_2=CH_2$

The first step in the decomposition of CF_2ClCH_2Cl over Cr_2O_3 (10$\underline{1}$2) is postulated to be the dissociative adsorption of CF_2ClCH_2Cl via carbon-chlorine bond cleavage at the number one carbon. This is the same initial step that was postulated for the decomposition of $CFCl_2CH_2Cl$ in Chapter 4. Gellman and coworkers [114, 115] found that the rate of dechlorination in halo-alkanes is higher for carbon atoms having a higher degree of chlorination. Other authors have also noted that more chlorinated HCFC compounds are generally more reactive [4, 99]. By analogy to similar HCFC compounds, the weakest bond in the CF_2ClCH_2Cl molecule should be the C-Cl bond on the number one carbon. Therefore, dissociative adsorption results in the formation of a

surface alkyl fragment ($-CF_2CH_2Cl$) and adsorbed chlorine $Cl_{(s)}$. Formation of the fluoro-alkene $CF_2=CH_2$ is postulated to occur via β-elimination of the remaining chlorine. Reaction steps involving β-halogen elimination from halocarbons are commonly cited in the organometalic literature [77, 78]. A small amount of the $CF_2=CH_2$ product decomposes to yield acetylene and two surface fluorides $F_{(s)}$.

CF_2ClCH_2Cl is much less reactive that its more chlorinated analog $CFCl_2CH_2Cl$. For an initial 0.06 L dose, only about 10 % of CF_2ClCH_2Cl is converted to products over a nearly stoichiometric surface compared to virtually 100% reaction of $CFCl_2CH_2Cl$ over the same surface. This finding is in agreement with anecdotal evidence from numerous literature sources [4, 60, 99], though a complete ranking of HCFC and HFC reactivity that includes halo-alkanes and halo-alkenes could not be found. Generally, haloalkane reactivity is cited as proportional to the number of C-Cl bonds contained in the compound.

5.4.1.1 240 K Reaction Channel

It is significant that the 240 K desorption temperature for product $CF_2=CH_2$ coincides with the small high temperature shoulder for the reactant CF_2ClCH_2Cl. The 240 K desorption temperature of product $CF_2=CH_2$ is 90 K above the 170 K desorption temperature observed for $CF_2=CH_2$ dosed directly on a nearly stoichiometric surface, demonstrating that the desorption of product $CF_2=CH_2$ is reaction-limited. The coincident desorption of both reactant and product suggests that $CF_2=CH_2$ and CF_2ClCH_2Cl share a common surface intermediate and rate-limiting step at 240 K.

The formation of reaction-limited $CF_2=CH_2$ from CF_2ClCH_2Cl decomposition is analogous to the reaction-limited formation of $CFCl=CH_2$ from $CFCl_2CH_2Cl$ that was reported in Chapter 4. The proposed alkyl intermediate ($-CF_2CH_2Cl$) formed by dissociative adsorption undergoes β-chlorine elimination at 240 K to form product $CF_2=CH_2$. Some of the chlorine recombines with the $-CF_2CH_2Cl$ surface intermediate to reform CF_2ClCH_2Cl, comprising the reactant contribution to desorption via the 240 K reaction channel. Based upon the discussion presented in Chapter 3, the 240 K desorption of both CF_2ClCH_2Cl and $CF_2=CH_2$ are assigned as first-order. Elimination of β-chlorine is the likely rate-limiting step. Assuming first-order kinetics and a pre-

exponential of 10^{13} s^{-1}, the activation energy for desorption at 240 K is 67 kJ/mol, using the Redhead method [52]. The chlorine liberated by β-elimination may become bound at an available five-coordinate Cr^{3+} site or may recombine with an adsorbed -CF_2CH_2Cl alkyl fragment to yield the CF_2ClCH_2Cl contribution to desorption at this temperature. The mechanism through the formation of $CF_2=CH_2$ is represented below.

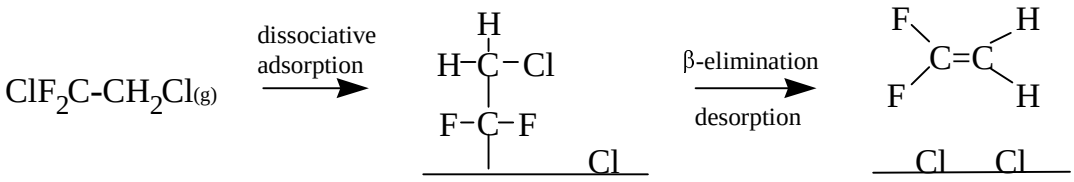

5.4.1.2 CF_2ClCH_2Cl Desorption at 180 K – 220 K

Desorption of the CF_2ClCH_2Cl reactant molecule arises from three adsorbed states of CF_2ClCH_2Cl. Initially, only five-coordinate Cr^{3+} cations are exposed on the nearly stoichiometric surface. The narrow desorption feature occurring at 220 K following initial TDS runs on a nearly stoichiometric surface is assigned as originating from molecular CF_2ClCH_2Cl desorption from these sites. As total CF_2ClCH_2Cl exposure increases, the amount of chlorine on the sample surface increases, as evidenced by AES. The shift in the CF_2ClCH_2Cl desorption temperature from 220 K to 180 K is attributed to a decrease in the activation energy for desorption caused by the presence of adsorbed chlorine on the Cr_2O_3 (10$\underline{1}$2) surface. Assuming first order kinetics and a normal, first-order pre-exponential of 10^{13} s^{-1} the activation energy for desorption from the 180 K and 220 K states is calculated to be 46 kJ/mol and 57 kJ/mol, respectively [52].

Following 0.44 L of total CF_2ClCH_2Cl exposure, the Cl/Cr ratio is measured around 0.13, and the surface is found to remain active for CF_2ClCH_2Cl decomposition. Similar exposures of a nearly stoichiometric surface to the more chlorinated molecule $CFCl_2CH_2Cl$ (Chapter 4) resulted in a Cl/Cr ratio of 0.32, and a complete loss of surface activity. Comparison of product amounts and halogen deposition for CF_2ClCH_2Cl versus $CFCl_2CH_2Cl$ TDS show that the more chlorinated $CFCl_2CH_2Cl$ is much more reactive, as suggested in the literature [4, 99, 115].

5.4.1.3 Surface Halogen following CF_2ClCH_2Cl Exposure

Auger of the sample surface following exposure to CF_2ClCH_2Cl verifies that chlorine is deposited on the sample surface, but successive TDS runs could not be continued until deactivation (halogen saturation) of the surface was observed. A high temperature series of 4.0 L exposures of HCFC-1132a at 773 K eventually resulted in a maximum obtainable surface (AES) Cl/Cr ratio of 0.22, corresponding to approximately 70 % coverage of surface cations by chlorine.

Based upon the CF_2ClCH_2Cl reaction stoichiometry discussed above, it is expected that each molecule of $CF_2{=}CH_2$ formed from CF_2ClCH_2Cl will result in the adsorption of two chlorine atoms by the surface. As reported in Chapter 4, a surface that is completely deactivated by chlorine (*i.e.* each cation capped by a chlorine) has a Cl/Cr ratio of 0.32. Because acetylene is a minor product of CF_2ClCH_2Cl decomposition, any halogen deposited is expected to be nearly 100% chlorine. AES performed following CF_2ClCH_2Cl TDS experiments consistently yielded (AES) Cl/Cr values around 0.13, indicating the surface has around 40% of its cations capped by chlorine.

High-temperature exposures of CF_2ClCH_2Cl did not indicate a clear connection between the number of cations on a nearly stoichiometric surface and the reaction stoichiometry at 773 K. By analogy to the high temperature $CFCl{=}CH_2$ experiments discussed in Chapter 3, it may be expected that a sufficient number of 4.0 L CF_2ClCH_2Cl exposures at 773 K would result in an eventual Cl/Cr ratio of 0.32, as observed in similar experiments with $CFCl_2CH_2Cl$ and $CFCl{=}CH_2$. However, Figure 28 shows the maximum obtainable (AES) Cl/Cr ratio to be around 0.22 L. A cause for this lower Cl/Cr ratio following high temperature CF_2ClCH_2Cl exposures can not be offered, but it is suggested that the low reactivity of CF_2ClCH_2Cl may limit the amount of CF_2ClCH_2Cl which reacts with the Cr_2O_3 (10$\underline{1}$2) surface, under these conditions. Additionally, the formation of products can not be followed by TDS during the high-temperature exposures, therefore, other reaction processes such as HX abstraction that are reported in the literature over powdered Cr_2O_3 may become important under these conditions [99].

5.4.2 $CF_2=CH_2$ Decomposition on Cr_2O_3 (10$\underline{1}$2)

Thermal desorption experiments using $CF_2=CH_2$ yielded acetylene as the only gas-phase product. The proposed mechanism for $CF_2=CH_2$ decomposition is essentially identical to the mechanism proposed for $CFCl=CH_2$ decomposition in Chapter 3; dissociative adsorption followed by α-elimination to form a vinylidene. Acetylene is likely formed via intramolecular rearrangement of the vinylidene intermediate (below). The rate-limiting step is postulated to be the rearrangement/desorption of vinylidene, as discussed in Chapter 3. The overall process is represented below.

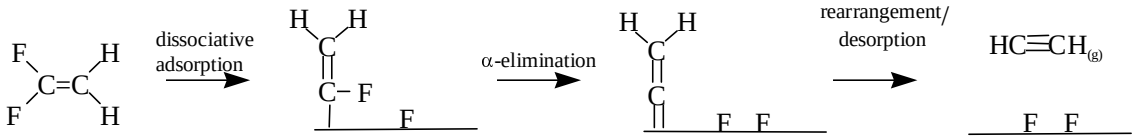

A direct measure of the amount of fluorine deposited on to the sample surface via $CF_2=CH_2$ TDS can not be offered because of the limitations of AES in measuring surface fluorine, as discussed previously. The lack of any fluorine containing desorption product in TDS demonstrates that fluorine removed from the molecule remains on the surface, and evidence for fluorine adsorption has been presented previously (section 3.4.4).

5.5 Conclusions

CF_2ClCH_2Cl and $CF_2=CH_2$ both decompose over a nearly stoichiometric (1×1) Cr_2O_3 (10$\underline{1}$2) surface. The major CF_2ClCH_2Cl reaction product is the alkene $CF_2=CH_2$, formed by an overall 1,2-dichloroelimination reaction, with β-chlorine elimination as the likely rate limiting step. The halogen atoms removed from both CF_2ClCH_2Cl and $CF_2=CH_2$ remain on the sample surface following reaction.

TDS experiments using $CF_2=CH_2$ as the dosed molecule showed acetylene to be the single gas-phase product formed. The $CF_2=CH_2$ reaction sequence is postulated to proceed through a surface vinylidene. The rate-limiting step is thought to be the rearrangement/desorption of the surface vinylidene intermediate. The reactions discussed in this chapter are analogous to the series of reaction steps proposed for $CFCl=CH_2$ and $CFCl_2CH_2Cl$ on Cr_2O_3 (10$\underline{1}$2) discussed in Chapters 3 and 4, respectively.

The reactivity of $CF_2=CH_2$ and CF_2ClCH_2Cl were lower than their counterparts discussed in Chapters 3 and 4. The reduced activity is the result of fewer C-Cl bonds in these molecules, as suggested in the literature [4, 60, 99].

Chapter 6
CF_3CH_2Cl and CF_3CH_2F Adsorption on the Cr_2O_3 (10$\underline{1}$2) Surface

6.1 Introduction

Studies of both CF_3CH_2Cl (HCFC-133a) and CF_3CH_2F (HFC-134a) reactions over Cr_2O_3 powders may be found in the literature [100, 102, 105, 111]. CF_3CH_2Cl is the final, stable intermediate in the production of the chlorine free refrigerant HFC-134a from trichloroethylene (TCE) [4]. CF_3CH_2Cl is very stable, and the last chlorine-for-fluorine exchange required to manufacture HFC-134a is often cited as being equilibrium-limited and difficult to carry out [4, 100]. Much of the relevant literature has been generated by interest in facilitating this reaction.

Kohne and Kemnitz [100] report that CF_3CH_2Cl is stable over Cr_2O_3 powders up to 673 K, even in the presence of HF. Extended residence time and a large excess of HF are required to obtain even small amounts of the fluorinated product CF_3CH_2F. Kohne and Kemnitz also report CF_3CH_2Cl as the major product of $CFCl_2CH_2Cl$ (HCFC-131a) and CF_2ClCH_2Cl (HCFC-132b) reactions with HF over Cr_2O_3 powders. They postulate that Cl/F exchange for the halo-alkanes above occurs via direct halogen exchange with the surface. Kavanagh *et al.* [62] reported similar results for the reaction of TCE to HCFC-134a over Cr_2O_3 catalyst in the presence of HF.

Brunet and coworkers [105, 111] studied the CF_3CH_2Cl to CF_3CH_2F fluorination reaction over Cr_2O_3 powders. They report that, in the absence of added HF, HF elimination to form CF_2=CHCl produces sufficient HF to drive the reaction to form some CF_3CH_2F product. Brunet and coworkers suggest that the fluorination reaction occurs via a HF oligomer species present on the Cr_2O_3 surface, in agreement with earlier proposals by Webb and coworkers [89, 91]. It is also suggested by Brunet *et al.* [111] that the activity for HCFC fluorination of powdered Cr_2O_3-based catalysts is directly dependent upon the number of reversibly oxidizable chromium cations at the catalyst surface. Coulson and coworkers [98] also noted the importance of cation reduction in the

formation of active fluorination sites on Cr_2O_3 powder, and suggested the presence of complexed HF on the catalyst surface.

Kemnitz and Niedersen [106] studied the isomerization of CHF_2CHF_2 (HCF-134) to the asymmetric isomer CF_3CH_2F (HFC-134a) over pre-halogenated Cr_2O_3 powder. They postulated that the reaction proceeds via HF elimination followed by Markovnikov HF addition. They also reported that if HCl was used as the pretreatment gas or if chlorine-containing halocarbons were introduced into the reacting system, then a complicated and unresolved set of side-reactions ensued. Additionally, Kemnitz and Niedersen [106] report that the introduction of chlorine in to the system leads to the eventual deactivation of the catalyst, leaving behind an inactive chlorine residue on the surface.

No studies of CF_3CH_2Cl or CF_3CH_2F adsorption over Cr_2O_3 single crystals in UHV are known, however Gellman and coworkers [114, 115] have studied UHV adsorption of several similar HCFC compounds over Pd (111) [114, 115]. They investigated the kinetics of carbon-chlorine bond cleavage for compounds having different degrees of chlorine substitution. In TDS experiments, they reported adsorption of CF_3CFCl_2, CH_3CFCl_2, CH_2FCFCl_2, CH_3CHCl_2, and CH_2ClCH_2Cl at 100 K resulted in molecular adsorption without reaction. The peak desorption temperature from molecular surface states is reported to be inversely related to the number of fluorine atoms in the molecule. Gellman and coworkers [115] followed the rate of dechlorination at higher temperatures (250 K – 325 K) by monitoring the rate of surface chlorine deposition with XPS. They reported that C-Cl bond cleavage is homolytic and that the apparent activation barrier to C-Cl bond cleavage ranges from 7.7 kJ/mol to 18.7 kJ/mol [115].

The work reported herein on the halo-alkanes $CFCl_2CH_2Cl$ (Chapter 4) and CF_2ClCH_2Cl (Chapter 5) has demonstrated that these molecules undergo dihalo-elimination reactions on Cr_2O_3 (10$\underline{1}$2) well below room temperature. Based upon the similarity of $CFCl_2CH_2Cl$ and CF_2ClCH_2Cl to CF_3CH_2Cl and CF_3CH_2F, similar reaction pathways may be expected for these molecules. However, based upon the relative reactivity observed for the halo-alkanes discussed in Chapters 4 and 5 and the consensus from the literature that less chlorinated molecules tend to be more stable, little or no

reactivity under TDS conditions might be expected for CF_3CH_2Cl and CF_3CH_2F relative to the previously studied (more chlorinated) halo-alkanes.

6.2 Experimental

PCR Inc. 1,1,1-trifluoro-2-chloroethane (CF_3CH_2Cl) (99% min), and PCR 1,1,1,2-tetrafluoroethane (CF_3CH_2F) (99% min) were used as received. Gas dosing was accomplished by backfilling the chamber through a variable leak valve. All dose sizes have been corrected for ion gauge sensitivity, and TDS data has been corrected for mass spectrometer sensitivity [41, 112, 113]. All TDS doses were conducted at a sample temperature of 163 K.

The adsorption of CF_3CH_2Cl and CF_3CH_2F over a nearly stoichiometric, (1×1) Cr_2O_3 (10$\underline{1}$2) surface was investigated using thermal desorption spectroscopy (TDS), Auger electron spectroscopy (AES), and low-energy electron diffraction (LEED). A nearly stoichiometric surface was prepared by ion-bombardment followed by annealing to 900 K. A (1×1) surface periodicity was confirmed using LEED following sample annealing.

AES of the sample surface was conducted at 800 K to avoid sample charging. Due to overlap of the primary oxygen and chromium Auger signals, the (AES) Cl/Cr ratios reported have been calculated by measuring the peak-to-peak height of the Cr $L_{2,3}M_{2,3}M_{2,3}$ (490 eV) signal and then applying a corrected sensitivity factor of, as described in Chapter 2 [110].

6.3 Results

Thermal desorption experiments demonstrated that both CF_3CH_2Cl and CF_3CH_2F do not react on a nearly stoichiometric Cr_2O_3 (10$\underline{1}$2) surface under TDS conditions. All TDS doses were conducted at 163 K. Acetylene (HC≡CH), fluoroacetylene (FC≡CH), CF_2=CHF, and the isomers CF_2=CH_2 and CHF=CHF were considered the most likely gas-phase products based upon previous results (Chapters 4 and 5) and literature precedents [4, 99]. These products were specifically searched for and were not detected.

Additionally, no HF, HCl, CO_2, CO, F_2, or H_2 was observed. Other products ranging in m/z from 2-200 were searched for with mass spectrometry and none were indicated. AES of the surface before and after TDS experiments demonstrated that no chlorine, fluorine, or carbon is deposited, and there is no change in the surface O/Cr ratio following CF_3CH_2Cl or CF_3CH_2F exposures conducted at or below 773 K. LEED observations showed no change in the (1×1) periodicity of the surface following any CF_3CH_2Cl or CF_3CH_2F exposures at 773 K or below.

6.3.1 CF_3CH_2Cl

Figure 24 shows the TDS traces for series of 0.03 L through 0.25 L doses of CF_3CH_2Cl over a nearly stoichiometric Cr_2O_3 (10$\underline{1}$2) surface. The dosed molecule CF_3CH_2Cl (m/z=118) is the only desorbing species detected, having a peak desorption temperature of 185 K. The peak intensity increases with dose size until reaching saturation at around 0.13 L. Doses up to 1.0 L produced no additional CF_3CH_2Cl adsorption. The 180 K peak desorption temperature does not change as coverage increases, indicating a first-order desorption process. The low desorption temperature and first-order desorption kinetics suggest simple molecular CF_3CH_2F adsorption and desorption. AES of the sample surface following CF_3CH_2Cl TDS shows no carbon or chlorine on the surface, and no change in the O/Cr ratio. The nearly stoichiometric surface is apparently unchanged by CF_3CH_2Cl TDS experiments.

In addition to the 185 K desorption feature observed in CF_3CH_2Cl TDS there is a small, high temperature shoulder around 230 K. This portion of the desorption trace is small, and remains relatively unchanged as dose size increases from 0.03 L to 0.25 L. The small quantity of CF_3CH_2Cl adsorbed in this state suggests that the feature may be the result of adsorption at surface defect sites.

While no reactivity is indicated under TDS conditions, Auger spectra of the surface following CF_3CH_2Cl exposures at 773 K indicate that CF_3CH_2Cl does react on Cr_2O_3 (10$\underline{1}$2) at this temperature. Figure 25 shows the Cl/Cr ratios from AES experiments conducted in tandem with a series of high-temperature (773 K) CF_3CH_2Cl exposures. Each dose of CF_3CH_2Cl consisted of 4.0×10^{-8} Torr [112] of CF_3CH_2Cl exposure for 250 s (~10 L), and an AES spectrum was taken of the surface following

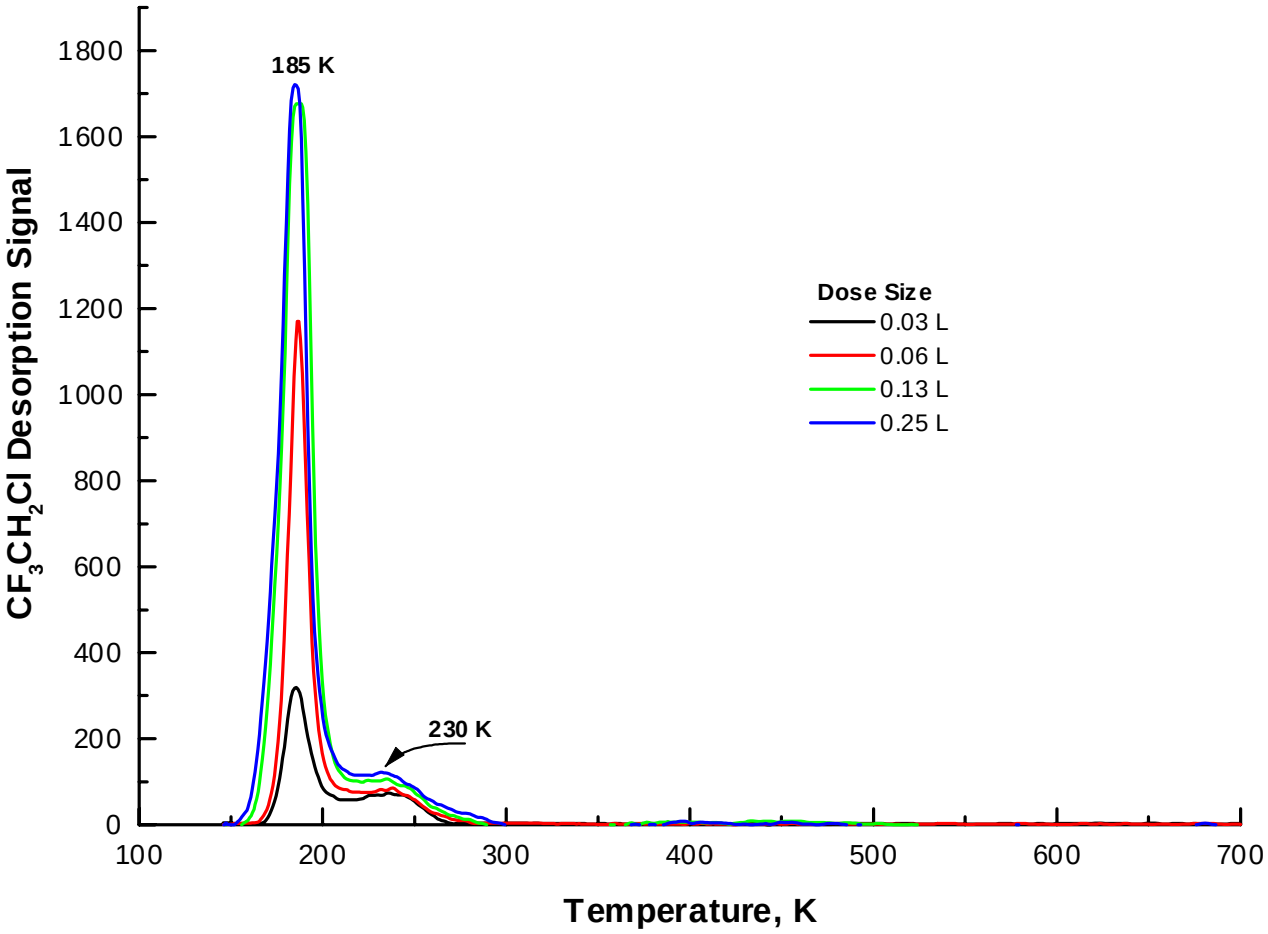

Figure 24. TDS traces from a series of increasing doses of CF_3CH_2Cl initiated over a stoichiometric Cr_2O_3 (10$\underline{1}$2) surface. The parent molecule was the only desorbing species observed.

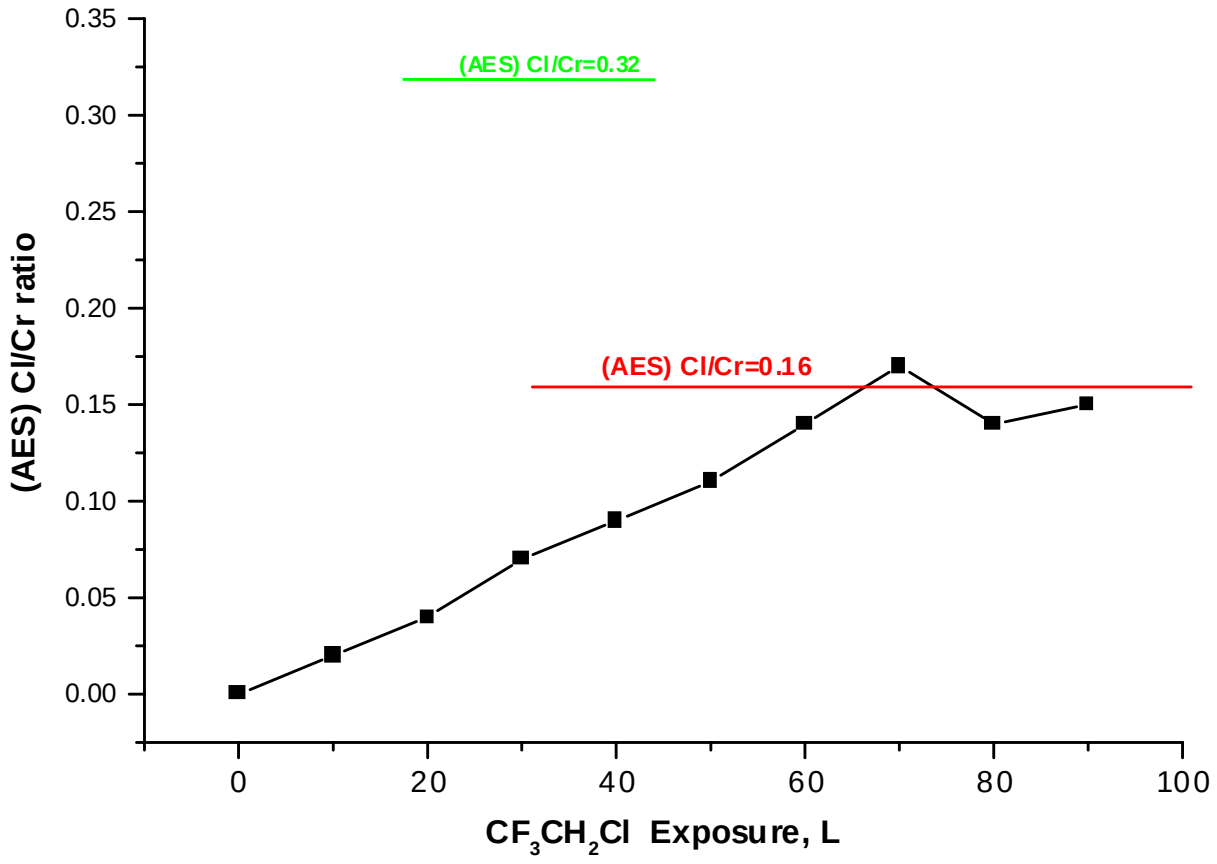

Figure 25. The (AES) Cl/Cr ratio for a series of 10 L exposures of CF_3CH_2Cl at 773 K. The chlorine signal represents half of the total amount of halogen on the surface.

each exposure. As shown in Figure 25, chlorine is deposited onto the surface at 773 K, demonstrating that a surface reaction does occur at this higher temperature. The Cl/Cr ratio rises linearly following each exposure until leveling off at around 0.16, following 70 L of total CF_3CH_2Cl exposure at 773 K. A Cl/Cr ratio of 0.32 has been demonstrated to correspond to a chlorine-saturated surface (section 4.3.3), and is shown in Figure 25 for comparison

6.3.2 CF_3CH_2F

Adsorption of CF_3CH_2F on the nearly stoichiometric Cr_2O_3 (10$\underline{1}$2) surface is completely reversible under TDS conditions. Figure 26 shows the TDS traces for a series of 0.03 L through 0.50 L doses of CF_3CH_2F (HFC-134a) on a nearly stoichiometric Cr_2O_3 (10$\underline{1}$2) surface. The dosed molecule CF_3CH_2F (m/z=83) is the only desorbing species detected. The peak desorption temperature occurs at 210 K following a 0.03 L dose, with a small low temperature shoulder evident. As dose size increases, the 210 K feature remains unchanged, and the shoulder at 180 K grows in while shifting to lower temperature. Saturation of the low temperature feature is still not indicated by 0.50 L, suggesting the CF_3CH_2F sticking coefficient is small for this adsorbed state as compared with CF_3CH_2Cl. However, as dose size increases the peak desorption temperature approaches the CF_3CH_2F adsorption temperature, which demonstrates that the dose temperature of 163 K is not low enough to fully sample this TDS feature. The 210 K feature maintains the same temperature, intensity, and shape throughout the TDS series in Figure 26, indicating saturation upon the first 0.03L dose. The small uptake associated with the 210 K desorption feature suggests that it is defect-related.

High-temperature (773 K) exposure of the surface to 2.0×10^{-8} Torr [113] of CF_3CH_2F for 17 minutes indicated that no reaction occurs at this temperature. AES of the surface following the exposure showed no indication of surface fluorine or carbon, although fluorine detection is problematic as previously reported (Chapter 4). The lack of any chlorine in CF_3CH_2F makes AES detection of halogen deposition particularly difficult for this molecule. All indication from TDS, AES, and LEED data are that no reaction of CF_3CH_2F (HFC-134a) occurs over a nearly stoichiometric Cr_2O_3 (10$\underline{1}$2) surface in UHV for temperatures at or below 773 K.

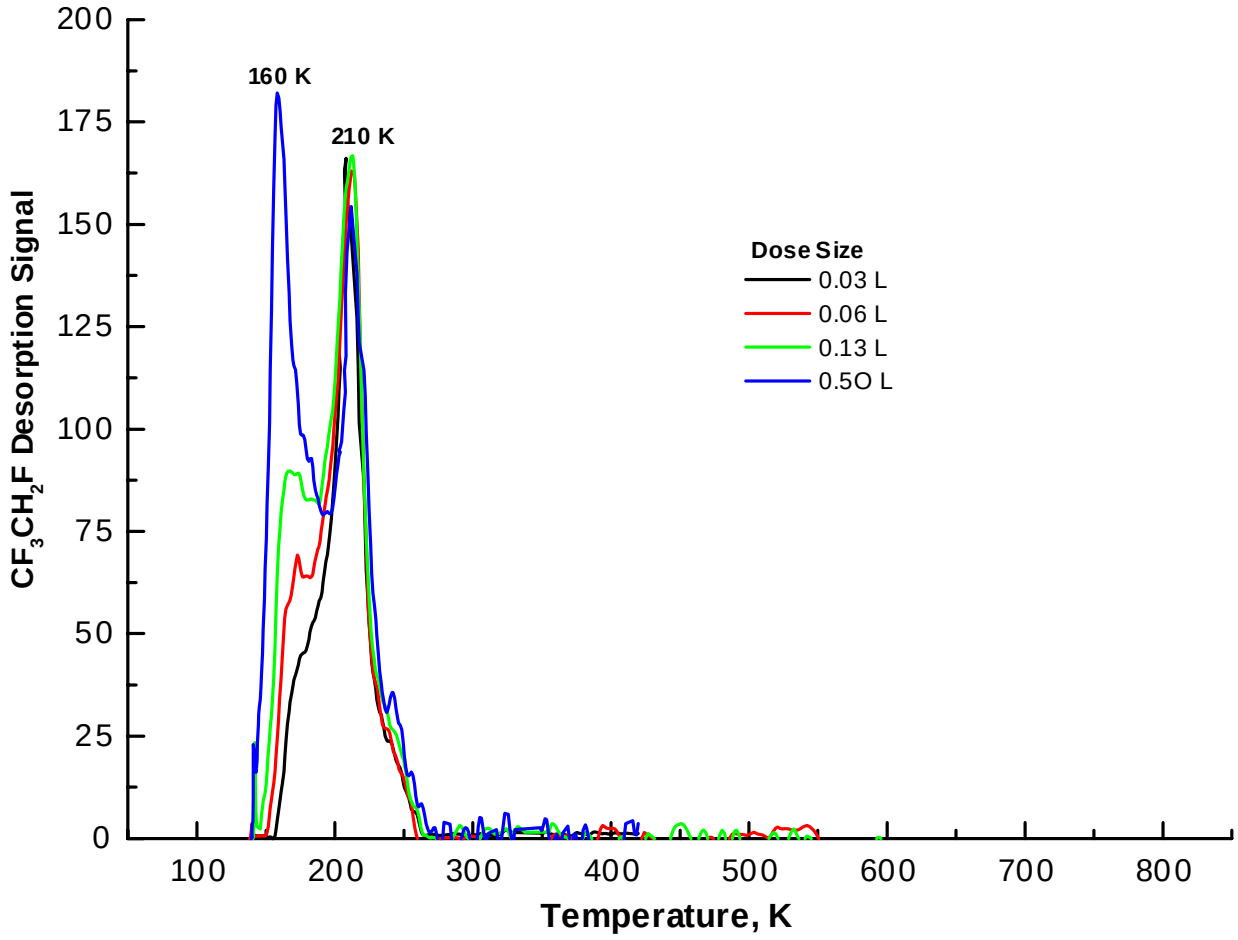

Figure 26. TDS traces from a series of CF_3CH_2F doses at 163 K. TDS indicates that no reaction occurs.

6.4 Discussion

Neither CF_3CH_2Cl nor CF_3CH_2F were found to react with the Cr_2O_3 (10$\underline{1}$2) surface under TDS conditions. Both molecules were molecularly adsorbed at 163 K. CF_3CH_2Cl was found to react with the surface at 773 K, as evidenced by detection of surface chlorine following high-temperature exposures.

6.4.1 CF_3CH_2Cl

The low desorption temperature and constant peak temperature for CF_3CH_2Cl are consistent with the desorption of molecular halo-alkanes previously described in Chapters 4 and 5. Gellman and coworkers [114, 115] have studied the adsorption of several halo-alkanes in UHV on the Pd (111) surface. They report that CH_3CFCl_2 and CH_3CHCl_2 have (molecular) peak desorption temperatures of 202 K and 207 K, respectively [115]. Based upon the low desorption temperature, and analogy to other compounds in the literature and in this work, the 185 K desorption feature for CF_3CH_2Cl is assigned as the first-order desorption of a molecularly bound CF_2CH_2Cl species. Assuming a first-order pre-exponential of 10^{13} s^{-1}, an activation barrier to desorption of 47 kJ/mol is calculated using the Redhead method [52].

For exposures conducted at 773 K, the reaction of CF_3CH_2Cl to $CF_2{=}CH_2$ is suggested by the surface Cl/Cr ratio of 0.16, and by analogy to the reactions reported for $CFCl_2CH_2Cl$ and CF_2ClCH_2Cl in Chapters 4 and 5, respectively. The surface chemistry apparently ceases following 70 L of exposure, as the Cl/Cr ratio levels off at around 0.16. The stoichiometry of CF_3CH_2Cl decomposition to $CF_2{=}CH_2$ requires that $Cl_{(s)}$ and $F_{(s)}$ are deposited onto the surface at the same rate. It was previously shown (section 3.3.2) that a Cl/Cr ratio of 0.16 corresponds to a surface having half of its cations "capped" by adsorbed chlorine. Assuming a 1:1 ratio between chlorine and fluorine on the surface, the Cl/Cr=0.16 represents a surface that is halogen saturated (deactivated) by exposures at 773 K. This suggests that the surface reaction is CF_3CH_2Cl decomposition to $CF_2{=}CH_2$ via 1,2-dihalo elimination as seen for $CFCl_2CH_2Cl$ and CF_2ClCH_2Cl. The Cl/Cr=0.16 suggests that half of the surface cations are covered by adsorbed chlorine and half by adsorbed fluorine, and that site blocking is the reason for surface deactivation.

The same mode of surface deactivation was seen with the halo-alkanes $CFCl_2CH_2Cl$ and CF_2ClCH_2Cl.

Unfortunately, the products made during large exposures conducted at high temperature can not be followed using mass spectrometry, and a reaction pathway for CF_3CH_2Cl cannot be substantiated based solely upon post-reaction AES data. The inability to quantify surface fluorine further complicates an assignment because halogen saturation of the surface can not be assured. However, based upon analogy to the previous HCFC compounds discussed in this work a dihalo-elimination reaction of CF_3CH_2Cl to form $CF_2=CH_2$ is a reasonable hypothesis.

6.4.2 CF_3CH_2F

Two distinct molecular adsorption states are indicated for CF_3CH_2F TDS. An initial desorption peak is observed at 210 K and a low temperature peak grows in at 175 K and shifts to 155 K as coverage increases. The 210 K feature is apparently saturated by a 0.03 L dose, and the small uptake suggests defect-related adsorption. The 175 K feature slowly grows in and shifts to lower temperature with larger exposures. The amount of CF_3CH_2F uptake by the surface is small in comparison to CF_3CH_2Cl, indicating a low sticking coefficient for CF_3CH_2F over Cr_2O_3 (10$\underline{1}$2). For CF_3CH_2F dose sizes of 0.5 L, the peak desorption temperature approaches the dose temperature of 163 K, which results in the immediate desorption of CF_3CH_2F upon sample heating. A lower CF_3CH_2F dosing temperature is necessary to properly sample this adsorbed state.

Using the Redhead method [52] and assuming a normal, first-order pre-exponential of 10^{13} s^{-1}, the activation energy for desorption from the 210 K state is 54 kJ/mol. The low temperature feature has a desorption energy that ranges from around 40 kJ/mol to 45 kJ/mol [52].

6.4.3 Summary of HCFC Properties

Using conversion to products to rank reactivity, the compounds CF_3CH_2Cl (HCFC-133a) and CF_3CH_2F (HFC-134a) are the least reactive of the halo-alkanes studied in this work. As predicted by the literature, the halo-alkanes having the highest chlorine content were found to be the most reactive [99, 105, 107]. For a dose size of 0.03 L on a nearly stoichiometric Cr_2O_3 (10$\underline{1}$2) surface, $CFCl_2CH_2Cl$ was virtually 100% converted to products. A CF_2ClCH_2Cl dose of the same size on a nearly stoichiometric surface leaves approximately 90% of the dosed molecule unreacted. The halo-alkane CF_3CH_2Cl was found to react only at elevated temperature, and CF_3CH_2F did not react under any of the conditions investigated. The halo-alkanes are ranked below in the order of increasing reactivity.

$CFCl_2CH_2Cl$	>	CF_2ClCH_2Cl	>	CF_3CH_2Cl	>	CF_3CH_2F
HCFC-131a		HCFC-132b		HCFC-133a		HFC-134a

Thermal desorption experiments showed that the molecularly adsorbed states of the above compounds do differ in energy from one another, but not greatly. Gellman and coworkers [114, 115] demonstrated that for CF_3CFCl_2, CH_2FCFCl_2, CH_3CFCl_2 and CH_3CHCl_2, the molecular desorption temperature is inversely related to the amount of fluorine in the molecule. This trend is confirmed for the halo-alkanes studied in this work if adsorption at defects is neglected. As shown in Figure 27, more chlorinated compounds were more reactive and have higher molecular desorption temperatures on the Cr_2O_3 (10$\underline{1}$2) surface.

CF_3CH_2F is the most fluorinated of the compounds in this study, and is shown (blue) in the top panel of Figure 27. CF_3CH_2F has the lowest molecular desorption temperature (160 K) of the halo-alkanes studied (the 210 K feature is attributed to adsorption at defect sites). The low desorption temperature and small sticking coefficient of this molecule prevented the complete characterization of molecular CF_3CH_2Cl adsorption. The compounds CF_3CH_2F and CF_3CH_2Cl did not react with the

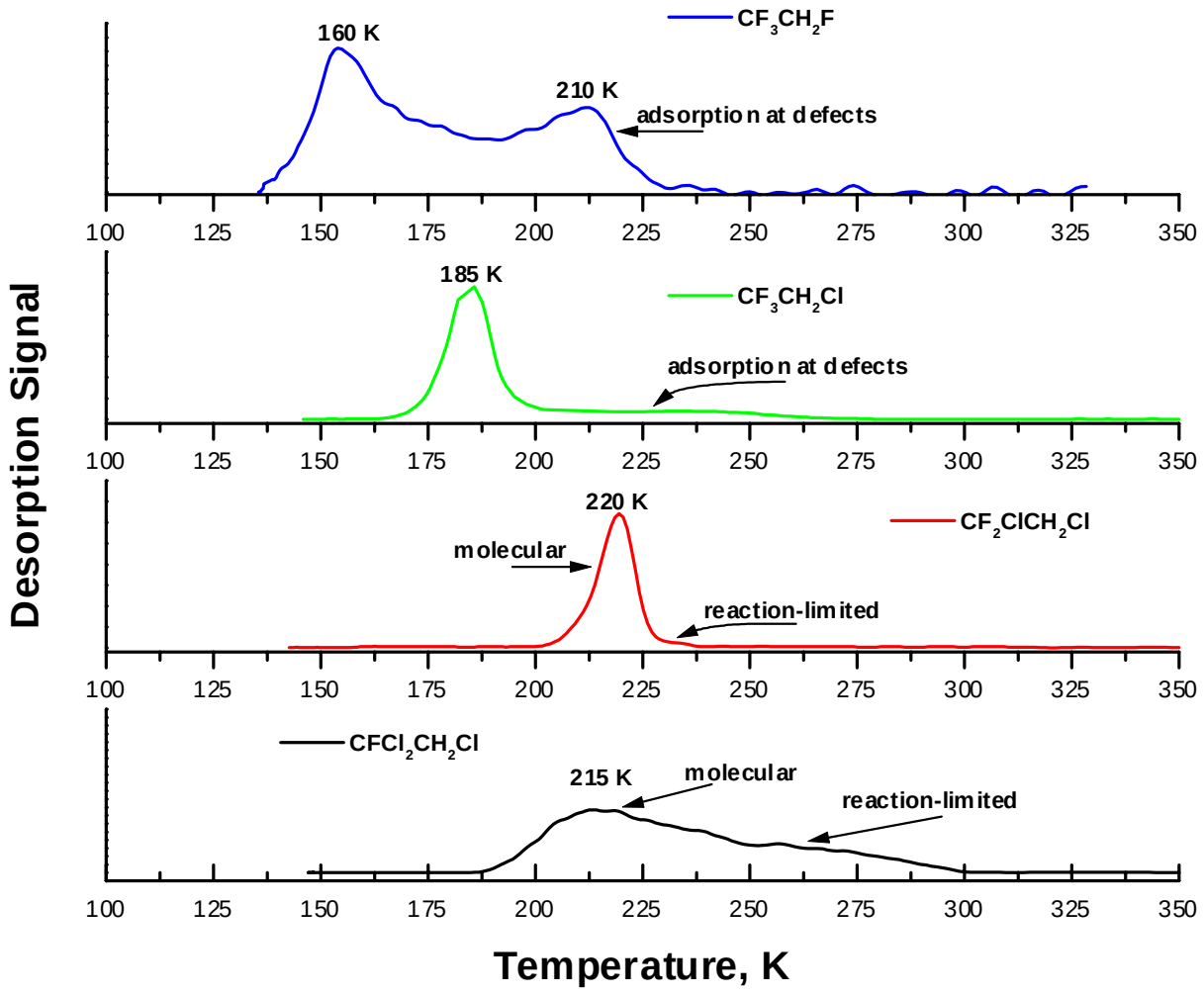

Figure 27. Comparason of molecular desorption temperatures for the halo-alkanes $CFCl_2CH_2Cl$ (blue), CF_2ClCH_2Cl (green), CF_3CH_2Cl (red), and CF_3CH_2F (black).

Cr_2O_3 (10$\underline{1}$2) surface under TDS conditions. However, the single chlorine in CF_3CH_2Cl (green) does enhance the surface-adsorbate interaction as evidenced by the increased molecular desorption temperature (185 K) compared to CF_3CH_2F.

The CF_2ClCH_2Cl molecule (red) has a molecular desorption feature at 220 K on a nearly stoichiometric Cr_2O_3 (10$\underline{1}$2) surface, as shown in Figure 27. The $CFCl_2CH_2Cl$ molecule (black) is so reactive that molecular desorption is only observed after partial chlorination of the surface has occurred. The presence of chlorine on the surface may act to shift the $CFCl_2CH_2Cl$ desorption temperature lower, as seen with CF_2ClCH_2Cl TDS (section 5.3.2.1). The observation that molecular desorption temperature is lower for more fluorinated compounds is consistent with the findings of Gellman and coworkers [114, 115] for similar halo-alkanes, and their reactivity is consistent with the "rule of thumb" found in the literature [4, 99] that more chlorinated HCFC's are more reactive.

6.5 Conclusions

Under TDS conditions, both CF_3CH_2Cl (HCFC-133a) and CF_3CH_2F (HFC-134a) are reversibly adsorbed to the nearly stoichiometric Cr_2O_3 (10$\underline{1}$2) surface. The adsorbed state is assigned as molecular in each case. CF_3CH_2Cl yields a single desorption peak having an activation barrier to desorption of 47 kJ/mol, and reacted with the nearly stoichiometric surface at 773 K. The more fluorinated CF_3CH_2F exhibits desorption peaks at 210 K and around 160 K – 170 K, and no reactivity is indicated. It is suggested that the 210 K adsorbed state for CF_3CH_2F is defect related, and the low temperature feature (160 K) represents CF_3CH_2F adsorption at five-coordinate Cr^{3+} sites on the nearly stoichiometric surface.

Comparison of the data collected for $CFCl_2CH_2Cl$, CF_2ClCH_2Cl, CF_3CH_2Cl, and CF_3CH_2F suggests that the reactivity and molecular desorption temperatures of these compounds is directly related to the chlorine content of the molecule, and to the degree of surface halogen coverage. More chlorinated molecules are more reactive and have higher molecular desorption temperatures over the nearly stoichiometric surface. In each case where halocarbon reactivity is observed, site blocking due to a build up of adsorbed halogen is postulated to be the mode of surface deactivation.

Chapter 7

Summary and recommendations for future work

7.1 Summary and conclusions

The (1×1) Cr_2O_3 (10$\underline{1}$2) surface has been reproducibly prepared from a single crystal sample via ion bombardment followed by annealing to 900 K in UHV. XPS, AES, and LEED were used to demonstrate that the surface stoichiometry and periodicity are reasonably explained as a nearly stoichiometric, non-polar termination of the surface. A (1×1) oxygen terminated surface may also be prepared via dissociative oxygen adsorption on the nearly stoichiometric surface. Dissociatively adsorbed oxygen adatoms form a terminal chromyl species that is stable on the Cr_2O_3 (10$\underline{1}$2) surface up to 1100 K.

A primary focus of this work was to investigate the surface-adsorbate interaction of $CFCl_2CH_2Cl$, CF_2ClCH_2Cl, CF_2ClCH_2Cl, and CF_3CH_2F on the Cr_2O_3 (10$\underline{1}$2) surface. Molecules with higher chlorine content had higher conversion to products. TDS experiments show that the halo-alkanes $CFCl_2CH_2Cl$ and CF_2ClCH_2Cl undergo a 1,2-dichloro-elemination reaction to form the halo-ethenes $CFCl=CH_2$ and $CF_2=CH_2$, respectively. Halo-alkane surface reactions are initiated by dissociative adsorption via homolytic C-Cl bond cleavage, forming an alkyl fragment and adsorbed chlorine. The halo-alkenes are formed via β-chlorine elimination in a reaction-limited step occurring around 245 K for both $CFCl_2CH_2Cl$ and CF_2ClCH_2Cl over a nearly stoichiometric Cr_2O_3 (10$\underline{1}$2) surface. The chemistry of $CFCl_2CH_2Cl$ and CF_2ClCH_2Cl reaction to their respective halo-alkenes most closely resembles the Zn-catalyzed dehalogenation of vicinal dihalides to alkenes found in the organic chemistry literature [116]. Acetylene is formed as a minor product of both $CFCl_2CH_2Cl$ and CF_2ClCH_2Cl decomposition. All halogen removed from reactant molecules remains bound to the surface following TDS experiments.

CF_2ClCH_2Cl reacted only at elevated temperatures (773 K), and no reaction of CF_3CH_2F was indicated at or below 773 K. The halo-ethane reactivity observed for the compounds investigated supports the “rule-of-thumb” cited in the catalysis literature that HCFC reactivity increases with increasing chlorine content [4, 60, 99].

The unsaturated compounds $CFCl=CH_2$ and $CF_2=CH_2$ were found to decompose to form acetylene and adsorbed halogen. As detailed in Chapter 4, the reaction mechanism is postulated to proceed from a surface fluoro-vinyl fragment, formed by dissociative adsorption, through a vinylidene intermediate via α-elimination. A 2,1-hydrogen shift then forms the acetylene product prior to desorption. In TDS experiments, both compounds yielded desorption and reaction limited acetylene product features at around 350 K and 475 K, respectively. Formation of the minor product acetylene from $CFCl_2CH_2Cl$ and CF_2ClCH_2Cl decomposition is postulated to occur via a series reaction through the halo-alkenes $CFCl=CH_2$ and $CF_2=CH_2$, respectively.

Thermal desorption experiments on a nearly stoichiometric surface yielded molecular desorption temperatures of 220 K for $CFCl=CH_2$ and 170 K for $CF_2=CH_2$, suggesting that increased fluorine content also lowers the desorption temperature for halo-alkenes, as Gellman and coworkers [114, 115] noted for halo-alkanes. Table 7.1 lists the halo-alkanes and halo-alkenes investigated, and summarize the TDS products and desorption temperatures for each.

Table 7.1. Comparison of reactivity and desorption temperatures.

Compound	**Thermal Desorption from a Nearly Stoichiometric Surface (163 K doses)**
$CFCl_2CH_2Cl$ HCFC-131a	major product: $CFCl=CH_2$ at 245 K – 265 K molecular desorption at 215 K
CF_2ClCH_2Cl HCFC-132b	major product: $CF_2=CH_2$ at 245 K molecular desorption at 220 K
CF_3CH_2Cl HCFC-133a	reacts at 773 K molecular desorption: 185 K
CF_3CH_2F HFC-134a	no reaction molecular desorption:155 K – 210 K.
$CFCl=CH_2$ HCFC-1131a	major product: HC≡CH at 350K & 475 K molecular desorption: 220 K
$CF_2=CH_2$ HFC-1132a	major product: HC≡CH at 350K & 475 K molecular desorption: 170 K

The active site for all surface chemistry observed is five-coordinate Cr^{3+} cations contained in the second atomic layer of the nearly stoichiometric Cr_2O_3 (10$\underline{1}$2) surface. Surface activity was found to vary with halogen coverage. Initially, a through-surface effect enhanced the surface-adsorbate interaction at neighboring cations. This effect was evident for CF_2ClCH_2Cl, $CFCl=CH_2$, and $CF_2=CH_2$, and suggests an optimal surface ensemble of halogenated and bare cation sites for dehalogenating these molecules. $CFCl_2CH_2Cl$ was most reactive on a clean, nearly stoichiometric Cr_2O_3 (10$\underline{1}$2) surface. As halogen coverage approaches a 1:1 ratio with surface cations, site blocking by adsorbed halogen begins to shut down the surface chemistry and causes the eventual deactivation of the surface.

AES of the surface following TDS experiments and 773 K exposures demonstrated that no carbon was deposited onto the sample surface for any of the halocarbons investigated. Additionally, no evidence was seen for the replacement of lattice oxygen by halogen. Dissociatively adsorbed oxygen also blocked cation sites and caused surface deactivation for most of the halocarbons studied. However, $CFCl_2CH_2Cl$ does react with the terminal chromyl oxygen on the oxide-terminated Cr_2O_3 (10$\underline{1}$2) surface, and is capable of displacing oxygen from the terminating oxide layer with chlorine.

7.2 Recommendations for future work

The greatest obstacle encountered during this work was the inability to detect fluorine on the sample surface. XPS should be investigated as an alternative to AES, which proved ineffective for fluorine analysis. XPS may be capable of detecting both chlorine and fluorine on the sample surface. Fluorine detection would be useful in confirming the reaction pathways proposed herein, and allow investigation of surface fluorine loss as a function of sample temperature.

Additional supporting evidence for the migration of fluorine and chlorine into the sample bulk is needed before bulk migration can be fully accepted as an explanation for halogen loss at the surface. Large $CFCl_2CH_2Cl$ and/or $CFCl=CH_2$ exposures at elevated temperatures could be used to introduce chlorine and fluorine into the crystal bulk.

Migration into the bulk may be investigated by depth profiling, using a technique such as secondary ion mass spectroscopy (SIMS), or by monitoring the decay of radioactively labeled halogen.

The presence of pre-adsorbed oxygen on the Cr_2O_3 (10$\underline{1}$2) surface was found to deactivate the surface towards reaction with CF_2ClCH_2Cl and $CFCl{=}CH_2$, but not for $CFCl_2CH_2Cl$. The reaction of $CFCl_2CH_2Cl$ (HCFC-131a) on an oxygen-saturated surface and the behavior of O_2 on surfaces that have been deactivated by chlorine adsorption indicated a complex interaction between chlorine and oxygen on the surface that was not fully investigated in this work. An extensive TDS investigation of O_2 adsorption over halogen-saturated surfaces, and $CFCl_2CH_2Cl$ adsorption over oxygen-saturated surfaces is needed to explain this chlorine-oxygen exchange process. Higher-temperature exposures of $CFCl{=}CH_2$ over an oxygen-saturated surface should also be investigated to determine if fluorine can also participate in this process.

The use of vibrational spectroscopy in tandem with halo-alkene TDS would be useful in the confirmation of the proposed vinyl and vinylidene surface intermediates, and help to determine the rate-limiting step in acetylene formation. Identification of a stable surface vinyl species would indicate that α-elimination is rate-limiting, while identification of a stable vinylidene would suggest that hydrogen rearrangement is rate-limiting. Vibrational spectroscopy could also be useful in identification of alkyl intermediates formed by dissociative adsorption of $CFCl_2CH_2Cl$ and CF_2ClCH_2Cl, and confirm β-fluorine elimination as the rate-limiting step in halo-alkene formation.

The 1,2-dihalo elimination reactions reported in this work are very different from the HX elimination reactions that are often cited in the literature [4, 89, 100]. Investigation of the surface reactions reported herein at atmospheric pressure could help attribute the different activities to differences in reaction conditions and/or surface preparation. Additionally, if other, low-index surfaces of Cr_2O_3 can be successfully prepared, then repetition of these experiments on such surfaces could yield insight into the structure sensitivity of these reactions. Preferably, the surface investigated would expose Cr^{3+} cations having a different coordination environment than the (10$\underline{1}$2) surface, thus broadening the database on Cr_2O_3 chemistry. The ideal, non-polar stoichiometric Cr_2O_3 (0001) surface contains three-coordinate Cr^{3+} cations. If this surface can be

successfully prepared from a single crystal, then it should be possible to create halogenated cation sites that are not coordinately saturated. This would allow the chemistry of coordinately unsaturated, halogenated cation sites to be investigated, which was not possible with the Cr_2O_3 (10$\underline{1}$2) surface. Additionally, there is available literature on Cr_2O_3 (0001) films [63, 64, 65, 66] that would allow direct comparison between single crystal and thin film data.

References

1. F.Wholer and F. Mahala, *Analytical. Chemistry*, **81** (1852) 255.
2. S. W. Weller and S. E. Voltz, *Journal of the American Chemical Society*, **76** (1954) 4695.
3. J. L. G. Fierro and J. F. G. La Banda, *Catalysis Reviews*, **28** (1986) 265.
4. L. E. Manzer and V. N. M. Rao, *Advances in Catalysis*, **39** (1993) 329.
5. G. Webb and J. Winfield, *Chemistry in Britain*, November (1992) 998.
6. V. E. Henrich, *Progress in Surface Science*, **50** (1995) 77.
7. D. P. Woodruff and T. A. Delchar, *Modern Techniques of Surface Science*, 2nd Edition (Cambridge: Cambridge University Press, 1994).
8. W. Gopel, *Progress in Surface Science*, **20** (1985) 9.
9. G. Pacchioni and P. S. Bagus, *Adsorption on Ordered Surfaces of Ionic Solids and Thin Films* (Springer-verlag, Berlin, 1993).
10. W. Göpel, G. Rocker, and R. Feierabend, *Physical Review B*, **28** (1983) 3427.
11. K. Hadjiivanova and G. Busca, *Langmuir*, **9** (1993) 1492.
12. R. Fahim, M. Zaki, and N. Yacoub, *Journal of the Chemical Society, Faraday Transactions 1*, **78** (1982) 2721.
13. V. E. Henrich and P. A. Cox, *The Surface Science of Metal Oxides* (Cambridge: Cambridge University Press, paperback edition,1996).
14. D. Adler, *Solid State Physics*, **21** (1968) 83.
15. R. E. Newnham and Y. M. de Haan, *Zeitschriftr fur Kistallographie*, **27** (1962) 235.
16. P. J. Lawrence, S. C. Parker, and P. W. Tasker, *Communications of the American Ceramic Society*, **42** (1988) 389.
17. R. J. Lad and V. E. Henrich, *Surface Science*, **193** (1988) 81.
18. J. B. Malherbe, S. Hofmann, and J. M. Sanz, *Applied Surface Science*, **27** (1986) 355.
19. V. E. Henrich, *Solid State Communications*, **98** (1996) 711.
20. V. E. Henrich, *Reports of Progress in Physics*, **48** (1985) 1481.
21. N. S. McIntyre and D. G. Zetaruk, *Journal of Vacuum Science and Technology*, **14** (1977) 181.
22. K. S. Kim, W. E. Baitinger, J. W. Amy, and N. Winograd, *Journal of Electron Spectroscopy and Related Phenomena*, **64** (1993) 307.
23. R. L. Burwell, Jr., L. Haller, K. C. Taylor, and J. F. Read, *Advances in Catalysis*, **19** (1969) 2.
24. S. R. Morrison, *Journal of Catalysis*, **47** (1977) 69.
25. P. J. M. Carrott and N. Sheppard, *Journal of the Chemical Society, Faraday Transactions 1*, **79** (1983) 2425.
26. A. Zecchina, S. Coluccia, L. Cerruti, and E. Borello, *Journal of Physical Chemistry*, **75** (1971) 2783.
27. D. Scarano, G. Spoto, S. Bordiga, G. Ricchiardi, and A. Zecchina, *Journal of Electron Spectroscopy and Related Phenomena*, **64** (1993) 307.
28. A. Zecchina, S. Coluccia, E. Guglielminotti, and G. Ghiotti, *Journal of Physical Chemistry*, **75** (1971) 2790.

29. A. Zecchina, S. Coluccia, E. Guglielminotti, and G. Ghiotti, *Journal of Physical Chemistry*, **75** (1971) 2774.
30. D. Scarano, G. Spoto, S. Bordiga, L. Carnelli, G. Ricchiardi, and A. Zecchina, *Langmuir*, **10** (1994) 3094.
31. S. R. Ely and R. L. Burwell, Jr., *Journal of Colloid and Interface Science*, **65** (1978) 244.
32. D. Scarano, A. Zecchina, and A. Reller, *Surface Science*, **198** (1988) 11.
33. D. Scarano and A. Zecchina, *Spectrochimica Acta*, **43** (1987) 1441.
34. M. P McDaniel and R. L. Burwell, Jr., *Journal of Catalysis*, **36** (1975) 394.
35. D. Klissurski, K. Hadjiivanoy, and A. Davydov, *Journal of Catalysis*, **111** (1988) 421.
36. A. Davydov, *Journal of the Chemical Society, Faraday Transactions*, **87** (1991) 913.
37. A. Davydov, Y. M. Shchekochikhin, and N. P. Keirer, *Kinetics and Catalysis*, **13** (1972) 980.
38. J. S. Foord and R. M. Lambert, *Surface Science*, **169** (1986) 327.
39. M. Iwamoto, Y. Yoda, N. Yamazoe, and T. Seiyama, *Journal of Physical Chemistry*, **82** (1978) 2564.
40. E. S. R. Winter, *Advances in Catalysis*, **10** (1958) 196.
41. R. L. Brainard and R. J. Madix, *Journal of the American Chemical Society*, **111** (1989) 3826.
42. C. D. Wagner, W. M. Riggs, L. E. Davis, J. F. Moulder, and G. E. Muilenberg, *Handbook of X-Ray Photoelectron Spectroscopy* (Perkin-Elmer, Eden Prairie, MN, 1979).
43. J. F. Moulder, W. F. Stickle, P. E. Sobol, K. D. Bomben, J. Chastain, *Handbook of X-Ray Photoelectron Spectroscopy* (Perkin-Elmer, Eden Prairie, MN, 1992).
44. S. Hofmann, *Journal of Electron Spectroscopy and Related Phenomena*, **59** (1992) 15.
45. J. Cazaux and P. Lehuede, *Journal of Electron Spectroscopy and Related Phenomena*, **59** (1992) 49.
46. Q. Guo, L. Gui, P. J. Moller, and K. Binau, *Applied Surface Science*, **92** (1996) 513.
47. M C. Kung and H. H. Kung, *Surface Science*, **104** (1981) 253.
48. D. de Cogan and G. A. Lonergan, *Solid State Communications*, **15** (1974) 1517.
49. Y. Fukuda and A. Ignatiev, *Solid State Communications*, **41** (1982) 597.
50. L. E. Davis, N. C. MacDonold, P. W. Palmberg, G. E. Riach, R. E. Weber, *Handbook of Auger Electron Spectroscopy* (Perkin-Elmer, Eden Prairie, MN, 1976).
51. A. G. Schrott, G. S. Frankel, A. J. Davenport, H. S. Isaacs, C. V. Jahnes, and M. A. Russak, *Surface Science*, **250** (1991) 139.
52. P.A. Redhead, *Vacuum*, **12** (1962) 203.
53. W. M. Riggs and M. J. Parker in *Methods of Surface Science Analysis*, edited by A. W. Czanderna (Elsevier, Amsterdam, 1975) 103.
54. Estimates of the expected XPS O/Cr ratios were calculated assuming (1) an exponential decay of signal intensity with distance for normal emission, (2) no diffraction effects, and (3) inelastic mean free paths of 10.0 Å for Cr 2p (E_{kin}=670 eV) and 10.1 Å for O1s (E_{kin}=720 eV) photoelectrons. Mean free paths were estimated from the "universal" curve in reference 53.

55 J. M. McKay and V. E. Henrich, *Surface Science*, **137** (1984) 463.
56. K. Wandelt, *Surface Science Reports*, **2** (1982) 20.
57. F. A. Cotton and G. Wilkinson, *Advanced Inorganic Chemistry*, 4th Edition (NewYork, John Wiley & Sons, 1980).
58. K. Jagannathan, A. Srinivasan, and C. N. R. Rao, *Journal of Catalysis* **69** (1981) 418.
59. I. Ikemoto, K. Ishii, S. Kinoshita, H. Kuroda, M. A. A. Franco, and J. Thomas, *Journal of Solid State Chemistry* **17** (1976) 425.
60. M. Vecchio, G. Gropelli, and J. C. Tatlow, *Journal of Fluorine Chemistry*, **4** (1974) 117.
61. M. Blanchard, L. Wendlinger, and P. Canesson, *Applied Catalysis*, **59** (1990) 123.
62. D. M. C. Kavanagh, T. A. Ryan, and B. Mile, *Journal of Fluorine Chemistry*, **64** (1993) 167.
63. B. Dillmann, F. Rohr, O. Seiferth, G. Klivenyi, M. Bender, K. Homann, I. Yakovkin, D. Ehrlich, M. Baumer, H. Kuhlenbeck, and H. Freund. *Faraday Discussions*, **105** (1996) 295.
64. I. Hemmerich, F. Rohr, O. Seiferth, B. Dillmann, and H. Freund, *Zeitschrift fur Physikalische Chemie*, **202** (1997) 31.
65. H. Kuhlenbeck, C. Xu, B. Dillmann, M, HaBel, B. Adam, D. Ehrlich, S. Wohlrab, H. –J. Freund, U. A. Ditzinger, H. Neddermeyer, M. Neuber, M. Neumann, *Ber. Bunsenges. Phys. Chem.*, **96** (1992) 15.
66. H. –J. Freund, B. Dillmann, D. Erlich, M. HaBel, R. M. Jaeger, H. Kuhlenbeck, C. A. Ventrice Jr., F. Winkelmann, S. Wohlrab, C. Xu, Th. Bertrams, A. Brodde, and H. Neddermeyer, *Journal of Molecular Catalysis*, **82** (1993) 143.
67. D. Scarano, G. Spotto, S. Bordiga, L. Carnelli, G. Ricchiardi, and A. Zecchina, *Langmuir*, **10** (1994) 3094.
68. An ion guage sensitivity of 5.9 was used for $CFCl=CH_2$. This value was calculated using a correlation by S. George reported in reference [41]. A mass spectrometer sensitivity factor of 1.45 was determined experimentally for m/z=80.
69. An ion guage sensitivity of 2.2 was used for acetylene. This value was calculated using a correlation by S. George reported in reference [41]. A mass spectrometer sensitivity factor of 5.34 was determined experimentally for acetylene for m/z=26.
70. *Eight Peak Index of Mass Spectra*, 3rd Edition (Royal Society of Chemistry, United Kingdom, 1983).
71. M. Albert and J. Yates, *The Surface Scientists Guide to Organometallic Chemistry* (Americam Chemical Society, Washington, DC, 1987).
72. J. M. Vohs and M. A. Barteau, *Journal of Physical Chemistry*, **91** (1987) 4766.
73. W. A. Herman, *Advances in Organometallic Chemistry*, **20** (1982) 159.
74. K. Minachev, Y. Khodakov, and V. Nakhshunov, *Russian Chemical Reviews*, **45** (1976) 142.
75. Gaussian 94, Revision C.2, M. J. Frisch, G. W. Trucks, H. B. Schlegel, P. M. W. Gill, B. G. Johnson, M. A. Robb, J. R. Cheeseman, T. Keith, G. A. Petersson, J. A. Montgomery, K. Raghavachari, M. A. Al-Laham, V. G. Zakrzewski, J. V. Ortiz, J. B. Foresman, J. Cioslowski, B. B. Stefanov, A. Nanayakkara, M. Challacombe, C. Y. Peng, P. Y. Ayala, W. Chen, M. W. Wong, J. L. Andres, E. S. Replogle, R.

Gomperts, R. L. Martin, D. J. Fox, J. S. Binkley, D. J. Defrees, J. Baker, J. P. Stewart, M. Head-Gordon, C. Gonzalez, and J. A. Pople, Gaussian, Inc., Pittsburgh PA, 1995.
76. M. Bruce and A. Swincer, *Advances in Organometallic Chemistry*, **22** (1983) 59.
77. J. P. Collman, L. S. Hegedus, J. R. Norton, and R. G. Fink, *Principals and Applications of Organometalic Chemistry* (University Science Books, Mill Valley, CA, 1987).
78. P. Stang, *Chemical Reviews*, **78** (1978) 383.
79. E. Boyles, D. Coulson, G. Coulston, M. Diebold, P. Gai, G. Jones, C. Kellner, J. Lerou, L. Manzer, P. Mills, and V. Rao, *Americam Chemical Society Symposium on Chemistry and Characterization of Supported Metal Catalysts*, **38** (1993) 847.
80. R. M. Ormerod, R. M. Lambert, H. Hoffman, F. Zaera, L. P. Wang, D. W. Bennett, and W. T. Tysoe, *Journal of Physical Chemistry*, **98** (1994) 2134.
81. L. L. Kesmodel, L. H. Dudois, and G. A. Somorjai, *Journal of Chemical Physics*, **70** (1979) 2180.
82. G. Vacek, J. Thomas, B.DeLeeuw, Y. Yamaguchi, and H. Schaefer, *Journal of Physical Chemistry*, **98** (1993) 4766.
83. G. H. Hatzikos and R. I. Masel, *Surface Science*, **185** (1987) 479.
84. J. A. Gates and L. L. Kesmodel, *Surface Science*, **124** (1983) 68.
85. M. M. Hills, J. E. Parmeter, and W. H. Weinberg, *Journal of the American Chemical Society*, **109** (1987) 597.
86. S. York, unpublished results.
87. H. Onishi, C. Egawa, T. Aruga, and Y. Iwasawa, *Surface Science*, **191** (1987) 479.
88. A. Wiersma, E. J. A. X. van de Sant, M. Makkee, H. van Bekkum, and J. A. Moulijn, *Studies in Surface Science and Catalysis*, **101** (1996) 369.
89. L. Rowley, G. Webb, J. M. Winfield, and A. McCulloch, *Applied Catalysis*, **52** (1989) 69.
90. J. Kijowski, G. Webb, and J. M. Winfield, *Applied Catalysis*, **27** (1986) 181.
91. L. Rowley, J. Thomson, G. Webb, J. Winfield, and A. McCulloch, *Applied Catalysis A*, **79** (1991) 89.
92. J. Kijowski, G. Webb, and J. M. Winfield, *Journal of Fluorine Chemistry*, **27** (1985) 213.
93. L. E. Manzer, U. S. Patent 5,051,537 (1991).
94. D. Bechadergue, M. Blanchard, and P. Canesson, *Studies in Surface Science and Catalysis*, (New York, Elsevier, 1988).
95. D. Bechadergue, M. Blanchard, and P. Canesson, *Applied Catalysis*, **20** (1986) 179.
96. M. Blanchard, L. Wendlinger, and P. Canesson, *Applied Catalysis*, **59** (1990) 123.
97. J. Barrault, S. Brunet, B. Requieme, and M. Blanchard, *Journal of the Chemical Society, Chemical Communications*, **35** (1993) 374.
98. D. R. Coulson, P. W. J. G. Wijnen, J. J. Lerou, and L. E. Manzer, *Journal of Catalysis*, **140** (1992) 103.
99. A. Kohne and E. Kemnitz, *Journal of Fluorine Chemistry*, **75** (1995) 103.
100. E. Kemnitz and K.-U. Niedersen, *Journal of Catalysis*, **155** (1995) 111.
101. K. –U. Niedersen, E. Schreier, and E. Kemnitz, *Journal of Catalysis*, **167** (1997) 210.

102. E. Kemnitz, A. Kohne, I. Grohmann, A. Lippitz, and W. E. S. Unger, *Journal of Catalysis*, **159** (1996) 270.
103. An ion guage sensitivity of 5.9 was used for $CFCl_2CH_2Cl$ (m/z=. This value was calculated using a correlation by S. George reported in reference [31]. A mass spectrometer sensitivity factor of 1.00 was arbitrarily set for m/z=115.
104. A. F. Wells, *Structural Inorganic Chemistry* (Clarendon Press, Oxford, 1984).
105. S. Brunet, B. Requieme, E. Colnay, J. Barrault, and M. Blanchard, *Applied Catalysis B: Environmental*, **5** (1995) 305.
106. E. Kemnitz and K. U. Niedersen, *Journal of Fluorine Chemistry*, **79** (1996) 111.
107. L. Marangoni, C. Gervasutti, and L. Cone, *Journal of Fluorine Chemistry*, **19** (1981/82) 21.
108 An ion guage sensitivity of 4.6 was used for $CF_2=CH_2$. This value was calculated using a correlation by S. George reported in reference [31]. A mass spectrometer sensitivity factor of 2.24 was determined experimentally for m/z=64.
109 An ion guage sensitivity of 10.1 was used for CF_2ClCH_2Cl. This value was calculated using a correlation by S. George reported in reference [41]. A mass spectrometer sensitivity factor of 2.32 was determined experimentally for m/z=99.
110. An AES sensitivity factor of 4.4 was calculated for the Cr $L_{2,3}M_{2,3}M_{2,3}$ peak by scaling the Cr $L_{2,3}M_{2,3}M_{4,5}$ sensitivity factor found in reference [41] to adjust for differences in peak-to-peak height.
111. S. Brunet, B. Requieme, E. Matouba, and M. Blanchard, *Journal of Catalysis*, **152** (1995) 70.
112. An ion guage sensitivity of 8.8 was used for CF_3CH_2Cl. This value was calculated using a correlation by S. George reported in reference [41]. A mass spectrometer sensitivity factor of 1.22 was determined experimentally for m/z=118.
113. An ion guage sensitivity of 7.5 was used for CF_3CH_2F. This value was calculated using a correlation by S. George reported in reference [41]. A mass spectrometer sensitivity factor of 1.71 was determined experimentally for m/z=83.
114. C. W. Chan and A. J. Gellman, *Catalysis Letters*, **53** (1998) 139.
115. G. Zhou, C. Chan, and A. J. Gellman, *Journal of Physical Chemistry*, **103** (1999) 1134.
116. Morrison an Boyd, *Organic Chemistry* (Allyn and Bacon, Inc., Boston, 1983).

VITA

Steve and Francene York reside in Floyd county Virginia. Steve has a B. S. in chemistry and a Ph.D. in chemical engineering. His work experience ranges from steeplejack to rocket scientist. Steve and Francene also volunteer their time to raise dogs for Canine Companions for Independence.